UNIVERSITÀ DEGLI STUDI DI MILANO - BICOCCA
Scuola di Dottorato di Scienze

Dottorato in Fisica e Astronomia, Ciclo XXII
Coordinatore: Prof. Claudio Destri

INTERACTION OF PULSED ELECTRIC FIELDS WITH CELL MEMBRANE

Tutore: Prof. Marco Paganoni

Tesi di: Marco Pizzichemi
Matricola n. 025855

Anno Accademico 2008 -2009

Contents

List of Figures

List of Tables

Abstract

Pulsed Electric Fields (PEF) allow non-thermal pasteurization and sterilization of liquids, involving the application of high intensity electric field pulses (20-80 kV/cm) of short duration (1-10 μs). The electric field interacts with microorganisms at the level of plasma membrane, through the mechanism of electroporation, but, although many theories have been proposed to describe this phenomenon, a satisfactory explanation has not been found yet. An extensive description of the state of the art of the knowledge on this field is given, along with the current research needs and the main obstacles to a wide diffusion of PEF applications.

The time course of cell transmembrane voltage is studied, developing an analytical expression for planar, spherical, cylindrical and prolate spheroidal membranes, with the aim to evaluate the charging time constants and the steady state intensity upon variation of treatment conditions. The results of this approach are used to investigate the impact of the electric field in rod-like bacteria. The electric field distribution in test chamber is studied by means of computer simulations for various electrode geometries, optimizing the shape for intensity and uniformity of electric field. The impact on PEF treatment of a normal distribution of cell dimensions in a microbial population and the rotational movement of bacteria inside treatment chambers are also investigated. Computer simulations are used to obtain a possible explanation to the deviations from first order inactivation kinetics, and to the intrinsic variability of microbial laboratory results.

PEF inactivation experiments of *Escherichia Coli* are carried out in a test system under different conditions of treatment duration and microbial concentration. Inactivation kinetics is compared to theories of electroporation and computer simulations previously carried out. Experimental evidence of a variation in the effectiveness of PEF as a function of bacterial concentration is discovered and a possible explanation proposed. The application of high permittivity ceramics materials to PEF is also studied, with the aim of increasing the volumes of treatment chambers, improving the duration of electrodes, and allowing the use of the most energy efficient square wave

pulses to large volumes of liquid. These materials can also be used to test the possibility of a relation between energy deposited in treatment chambers and microbial inactivation, in order to acquire more insight on the interaction between Pulsed Electric Fields and cell membranes. A novel chamber is prepared with the use of a high permittivity non-toxic material (Sodium Potassium Niobate) and it is ready to be tested in PEF applications.

Chapter 1

Introduction

Pulsed electric fields (PEF) is a new method for sterilization and pasteurization involving the application of high electric field pulses of short duration to inactivate microorganisms in a fluid. Field intensities are typically in the 15-50 $kVcm^{-1}$ range, while the pulse duration is in the order of some microseconds. The electric field interacts with microorganisms at the level of cytoplasmatic membrane, through the mechanism of electroporation, but, although many theories have been proposed to describe this phenomenon, a satisfactory explanation has not been found yet. PEF is considered a non-thermal alternative to pasteurization, since it does not require high temperatures, and the treatment can therefore preserve nutritional, functional and sensory characteristics of foods. In this chapter, a brief description of the relevant biological issues related to PEF is given, followed by an extensive analysis of the most important publications regarding this technique, a short introduction to pulsed power technology and a description of the main research needs.

1.1 Relevant microbiological issues

The major causes of death at the beginning of the twentieth century were infectious diseases, caused by microorganisms called pathogens [1]. Today, the impact of infectious diseases is lower, at least in western countries, but microorganisms can still be a major threat to survival. Microorganisms play an important role in the food industry where spoilage alone results in huge economic losses each year, and could be cause of serious illness and death. However, several microorganisms have benefic effects on food products or those who eat them. Many dairy products depend on microbial transformations, like for example cheese and buttermilk. Furthermore, baked goods

and alcoholic beverages rely on the fermentative activities of yeast for the production of carbon dioxide and alcohol. The control of microorganism population in food is usually achieved through heat, in a process generically called pasteurization (see section 1.1.5).

1.1.1 The cell

The cells are the fundamental units of life, and can be divided in eukaryotic and prokaryotic. Prokaryotic cells are simpler, lacking a proper nucleus, and are divided in Eubacteria (or Bacteria) and Archeabacteria (or Archea). Eukaryotic cells, probabily developed from these two groups, can be classified in Protozoa, Algae, Fungi, higher plants and animals. In nature many different morphologies of bacteria exist. For example, a spherical bacterium is called a *coccus*, a cylindrical one a *rod*. Some rods twist into spiral shapes and are called *spirilla*. Prokaryotes vary in size from cells as small as 0.2 μm to those more than 700 μm in diameter. The vast majority of rod shaped Prokaryotes that have been grown in laboratory are between 0.5 and 4 μm wide and less than 15 μm long. There are significant advantages in small dimensions for a cell. Small cells contain more surface area relative to cell volume than large cells, and the surface to volume ratio affects many aspects of cell biology. For example, the cell's growth rate depends, among other things, on the rate of nutrient exchange, and the higher surface to volume ratio of smaller cells supports greater nutrient exchange per unit cell volume in comparison with larger cells. Because of this, smaller cells in general grow faster than larger cells. In addition, a given amount of resources will support a larger number of small cells. This is important because the larger the number of cells in a population, the greater the number of replication of DNA that will occur, and hence mutations. Thus in a population of small cells, the total number of mutations is greater if compared to the number of mutations in a population of large cells in the same environmental conditions, and therefore small cells have a greater ability to adapt to external conditions.

1.1.2 Cell membrane

The cytoplasmatic membrane is a thin structure that surrounds the cell. Although very thin, this vital structure is the barrier separating the inside of the cell (cytoplasm) from its environment. If the membrane is broken, the integrity of the cell is destroyed, the cytoplasm leaks into the environment, and the cell dies. The cytoplasmatic membrane is also a highly selective permeability barrier, enabling a cell to concentrate specific metabolites and excrete waste materials.

The general structure of biological membranes is a phospholipid bilayer. Phospholipids contains both hydrophobic (fatty acids) and hydrophilic (glycerol phosphate) components and can exist in many different chemical forms. As a consequence of this, phospholipids aggregate in water solutions to naturally form bilayer structures. This membrane, 6 - 8 nm wide, is embedded with proteins, and its overall structure is stabilized by hydrogen bonds and hydrophobic interactions. Although in a diagram the cytoplasmatic membrane can appear rather rigid, in reality it is somewhat fluid, having a viscosity approximating that of a light grade oil. As mentioned before, the cytoplasmatic membrane plays a critical role in cell function. First of all, the membrane functions as a permeability barrier, preventing the passive leakage of substances into or out of the cell. Secondly, the membrane is an anchor for many proteins, among which are enzymes that catalyze bioenergetic reactions and transport substances in and out of the cell. The interior of the cell consists in an aqueous solution of salts, sugars, aminoacids, nucleotides, vitamins, coenzymes and other soluble materials. The hydrophobic internal portion of the membrane is a tight barrier to diffusion. Although a small hydrophobic molecule can pass through the membrane, polar and charged molecules do not pass and must be specifically transported.

Because of the activities of transport systems, the cytoplasm of bacterial cells maintains a high concentration of dissolved solutes. This causes significant osmotic pressures to develop, about 2 atmospheres in a bacterium such as *Escherichia coli*. To withstand this pressure and prevent bursting, bacteria have cell walls, that also give them shape and rigidity. Species of bacteria can be divided in two main groups, as regards to their cell walls, called Gram-positive and Gram-negative. Gram-positive cell walls contain a thick layer of peptidoglycan and teichoic acids, while gram-negative cells contain a thin layer of peptidoglycan and have an outer lipo-polysaccharide layer (see fig. 1.1 and 1.2). The cell wall of a gram-positive cell has a thickness varying from 20 to 80 nm, while gram-negative cells have a layer of peptidoglycan with a thickness from 7 to 8 nm. Peptidoglycan is a polymer net consisting of sugar and amino acid linear chains bounded together by cross-links, resulting in a three-dimensional structure that is strong and rigid. This structure gives shape to the bacterium and, as mentioned before, protects it. For this reason, gram-positive cells are usually more resistant to hostile environments than gram-negative ones. On the other hand, peptidoglycan can be destroyed by lysozyme, an enzyme abundantly present in a number of secretions, such as tears, causing the death of the cell. Gram-negative cells have an external phospholipid membrane protecting peptidoglycan (see fig. 1.1), so lysozyme does not affect them, while gram-positive cells are highly sensitive to this enzyme and for the same reason more sensitive to the action of antibiotics.

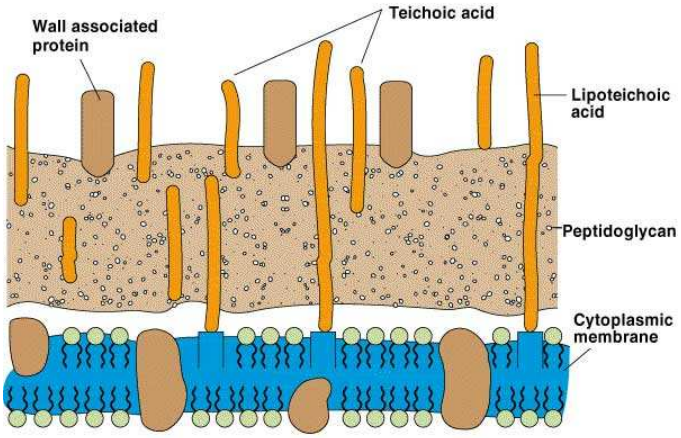

Figure 1.1: A Gram-positive cell membrane.

1.1.3 Bacterial growth

In a laboratory, under favorable conditions, a growing bacterial population doubles at regular intervals. Growth is by geometric progression and therefore usually referred to as exponential growth. In reality, exponential growth is only part of the bacterial life cycle, made of four characteristic phases:

Lag phase When bacteria are inoculated into fresh medium, their population remains temporarily unchanged. The length of this phase is dependent on a wide variety of factors including the size of the inoculum, the time necessary to recover from physical damage or shock in the transfer, the time required for synthesis of essential co-enzymes or division factors and the time required for synthesis of new enzymes that are necessary to metabolize the nutrient materials present in the medium.

Exponential phase During this phase of growth the cells divide at a constant rate depending upon the composition of the growth medium and the conditions of incubation. Different bacteria can have very different growth rates in optimal conditions. A common criterion to measure these rates is the *generation time*, the time interval required for the cells to divide. We can see in table 1.1 the value of this parameter in optimal conditions for a few bacteria.

Stationary Phase The exponential growth cannot go on forever in a batch culture, that is a closed system like a Petri dish or a flask, because of

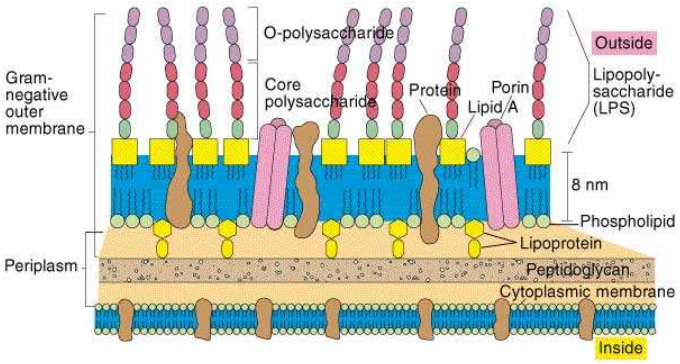

Figure 1.2: A Gram-negative cell membrane.

exhaustion of available nutrients, accumulation of inhibitory metabolites or exhaustion of space. During the stationary phase the bacterial population can usually reach 10^9 cells per ml.

Death phase If the available nutrient material runs out, a death phase follows. During the death phase, the number of viable cells decreases exponentially, essentially the reverse of growth during the exponential phase.

Colony Forming Units (CFU) and Log Reductions

Bacterial populations are evaluated by measuring changes in number of cells or changes in the level of some cellular component. The first method is a direct cell count, while the second, an example of which is the measure of turbidity, is a measure of cell mass. The most direct way to count bacteria in a sample is the use of a microscope to observe and enumerate the cells. Although this method is simple, results can be unreliable, for many different reasons among which the most important, for the purpose of this study, is the impossibility, at least without special staining techniques, to distinguish between dead and alive cells. A way to measure only viable cells consists in spreading a precise amount of liquid on a nutrient medium and let bacteria growth into colonies, a big cluster of cells usually visible to naked eye. An example of this procedure is shown in fig. 1.3. Since the real count is not performed directly on the liquid sample but on the number of colonies grown from a given portion of this sample, bacterial concentrations are usually

Bacterium	**Medium**	**Generation Time [minutes]**
Escherichia coli	Glucose-salts	17
Bacillus megaterium	Sucrose-salts	25
Streptococcus lactis	Milk	26
Streptococcus lactis	Lactose broth	48
Staphylococcus aureus	Heart infusion broth	27-30
Lactobacillus acidophilus	Milk	66-87
Rhizobium japonicum	Mannitol-salts-yeast extract	344-461
Mycobacterium tuberculosis	Synthetic	792-932
Treponema pallidum	Rabbit testes	1980

Table 1.1: Generation time for a few types of bacteria.

referred to as *Colony Forming Units* per ml, CFU/ml. In principle this procedure could be a source of errors (two or more bacteria could grow into a single colony, for example), but the process of spreading bacteria on a Petri dish can be done by very accurate machines able to spread very small amounts of liquid on a relatively long spiral line. In this case it is usually assumed that each bacterium is far enough from the next one to grow undisturbed into a single colony.

The great concentration of bacteria usually involved in experiments suggests the use of a logarithmic scale to evaluate the modifications of population. Thus when discussing about bacterial inactivation, rather then considering the simple concentration, *Log Reductions* (Log) are used, defined as

$$Log = \log_{10} \frac{C_i}{C_f} \tag{1.1}$$

where C_i and C_f are the initial and final bacterial concentration, measured in CFU/ml.

1.1.4 Effect of temperature on bacteria

The activities of microorganisms are greatly affected by the chemical and physical state of their environment. The main factors can be considered temperature, pH, water availability and oxygen. Temperature, in particular, can affect microorganisms in two opposite ways. As temperature rises, chemical and enzymatic reactions in the cell proceed at more rapid rates and growth becomes faster. However, above a certain temperature, cell components may be irreversibly damaged. Each microorganisms have its own

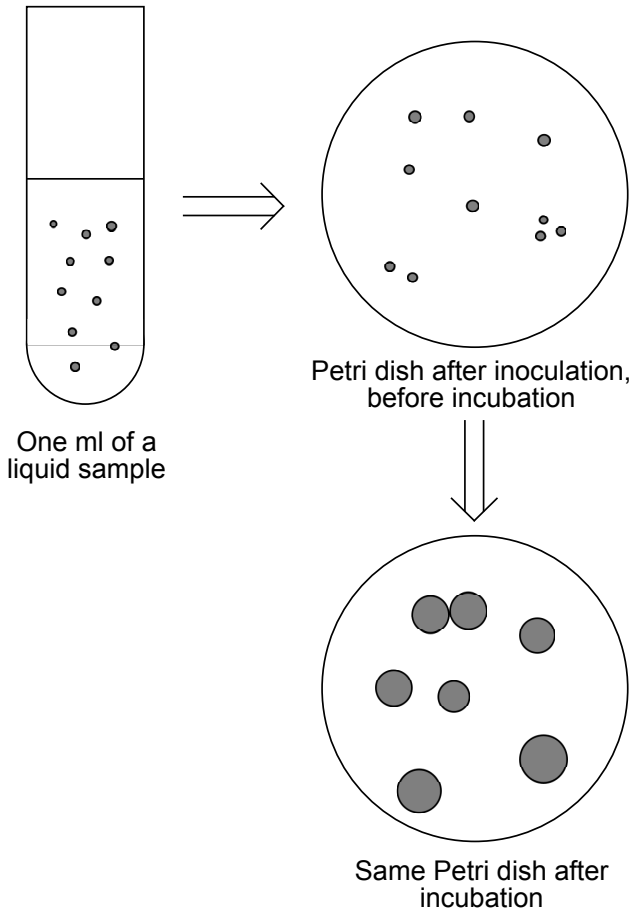

Figure 1.3: Example of bacterial colony growth.

minimum temperature, below which growth is not possible, an optimum temperature at which growth is most rapid, and a maximum temperature above which growth is inhibited. *Escherichia coli*, a bacterium particularly important in this study, has a minimum temperature of $8°C$, an optimum temperature of $39°C$ and a maximum temperature of $48°C$. Above maximum temperature, in general, denaturation of proteins occurs, and if the temperature rises above a certain limit, the cell dies. Below the minimum temperature the cytoplasmatic membrane stiffens at the point that it no longer functions properly, and the bacterium cannot grow.

1.1.5 Pasteurization

Pasteurization uses precisely controlled heat to reduce the microbial load in milk and other heat sensitive liquids. It does not kill all the organisms, but it is used to control commonly encountered pathogens, including *Listeria monocytogenes*, *Campylobacter* species, *Salmonella* and *Escherichia coli* O157:H7 that can be found in foods such as dairy products and juices. In addition, pasteurization retards the growth of spoilage organisms, increasing the shelf life of liquids. Pasteurization of liquids is usually achieved by passing the liquid through heat exchangers. The milk temperature is risen to $71°C$ for 15 seconds, and the milk is then rapidly cooled. This process is called flash pasteurization. Milk can also be heated in large vats to 63 - $66°C$ for 30 minutes, however this bulk pasteurization method is less satisfactory because the liquid must be held at higher temperatures for longer times. In both the cases, however, pasteurization causes loss of flavor and nutritional values.

1.2 Review of literature

PEF (Pulsed Electric Fields) technology has been applied to a variety of liquid substrates. The most common laboratory tests have been performed on dairy products, fruit juices and liquid eggs. In the following we give an extensive description of the most important results of PEF treatments on this liquids achieved so far.

1.2.1 PEF applications to dairy products

A work from Dunn and Pearlman [2] tested PEF for the inactivation of both *Escherichia coli* and *Salmonella Dublin* in milk with a 156 ml cylindrical chamber. In the first experiment, *E. coli* was treated with 20 pulses with a peak voltage of 42.84 kV, after which three test pulses were delivered to the chamber to test its correct functioning. The initial temperature was 25°C and, though the pulse frequency was not particularly high, it increased during the experiment to reach 43°C. After the treatment the sample of milk was quickly cooled down and stored at 7° - 9°C, to analyze the growth of bacteria over almost 6 days. The biological results in tab. 1.2 underline how the PEF treatment reduced the number of bacteria of more than 3 Logs and that the population of *E. coli* did not restart its growth in the first four days after the treatment. The same chamber was used to treat Salmonella Dublin in milk, this time delivering 40 pulses at a peak voltage of 36.7 KV, reaching a final temperature of 63°C. The same refrigeration procedure as before was carried

Time after treatment (hours)	Not treated milk [CFU/ml]	Treated milk [CFU/ml]
0	$8.1 \cdot 10^6$	$7.4 \cdot 10^3$
19	$7.6 \cdot 10^6$	$5.8 \cdot 10^3$
45	$9.1 \cdot 10^6$	$3.6 \cdot 10^3$
96 (4 days)	$4.7 \cdot 10^7$	$3.1 \cdot 10^3$
140 (5.8 days)	$6.2 \cdot 10^8$	$1.4 \cdot 10^5$

Table 1.2: The biological results of PEF treatment of *E. coli* in milk [2].

Time after treatment (hours)	Not treated milk [CFU/ml]	Treated milk [CFU/ml]
0	3800 S	20 B, 0 S
24	4600 (S + B)	6 B, 0 S
72	$1.2 \cdot 10^6$ (S + B)	100 B, 0 S
144	$2.7 \cdot 10^7$ B S too many to count	100 B, 0 S
192	10^7 B S too many to count	400 B, 0 S

Table 1.3: The biological results of PEF treatment of Salmonella Dublin in milk. S = Salmonella Dublin, B = milk bacteria [2].

out immediately after the experiment to measure bacterial concentration during a long period in standard storage conditions. Results from table 1.3 show the possibility of selective treatment of bacteria. Salmonella Dublin was completely inactivated by PEF treatment, and even after 8 days it was impossible to find any trace of it in the treated sample. The usual bacteria of milk (B in table 1.3), are reduced by PEF treatment but not completely inactivated, and they are able to grow again after a short period of time.

Qin et al. [3] analyzed the shelf life of fresh milk after a PEF treatment of 20 pulses, with an electric field of 40 KV/cm, reaching a two weeks extension, without noticing apparent changes in its physical and chemical properties and any significant difference in sensory attributes between heat pasteurized and PEF treated milk. The aspect of extending shelf life of milk has been studied also by Fernandez-Molina et al. [4], with particular attention to the combined effects of heat and PEF. The authors compared the effects on raw skim milk of 30 pulses at 40 KV/cm, at a temperature of 28°C, with a similar treatment following a 6 seconds 80°C pasteurization. In the second case the

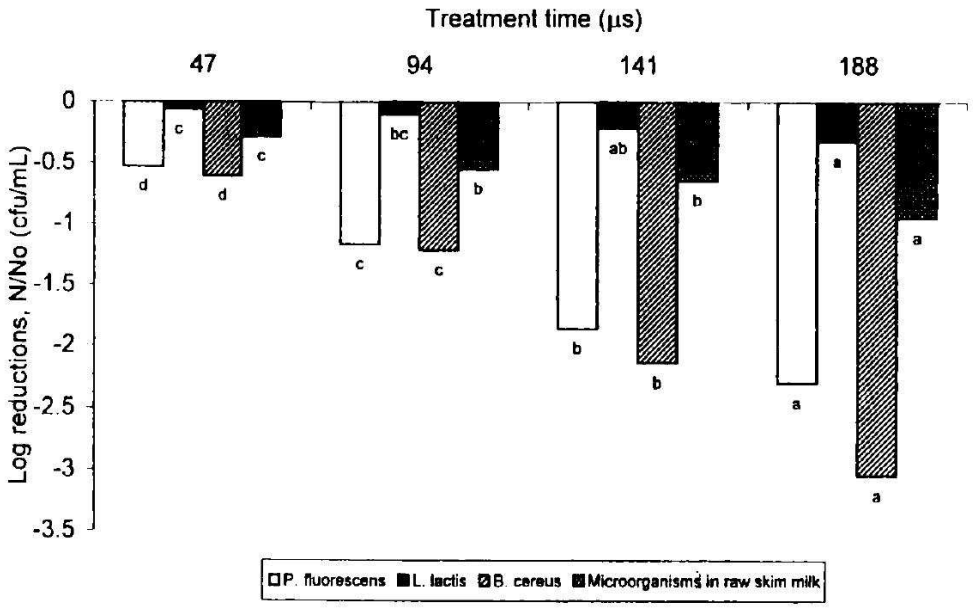

Figure 1.4: Inactivation on *Pseudomonas Fluorescens, Lactococcus Lactis* and *Bacillus Cereus* in inoculated UHT skim milk and total microorganisms in raw skim milk after PEF treatment [5].

shelf life of milk was extended from 14 to 22 days.

A comparison between standard pasteurization (73°C for 30 s) and PEF as been analyzed by Michalac et al. [5]. A total number of 64 pulses, 35 $kVcm^{-1}$, with a duration of 2.8 μs each, was applied to raw skim milk and ultra high temperature (UHT) skim milk. The repetition rate was 500 Hz, and the UHT milk was inoculated with *Pseudomonas Fluorescens, Lactococcus Lactis* and *Bacillus Cereus*. The effectiveness of both treatments was compared to the inactivation of raw skim milk total microorganisms, and results are reported in fig. 1.4 and 1.5. *B. Cereus* is the largest cell among the three inoculated, and exhibits the highest level of inactivation under PEF, which is expected from theory, since the potential developed across the membrane at the application of a pulse in proportional to cell dimensions (see eq. 2.1). Gram positive bacteria are more resistant to electric fields than Gram negative bacteria [6]. Similar results were observed on Gram positive *L. lactis* and Gram negative *P. Fluorescens*, but not with Gram positive *B. cereus*. These results suggest that the size of the microorganism could have greater influence than its type for microbial inactivation by PEF processing. Pasteurization was more effective than PEF in inactivating *P. fluorescens* and

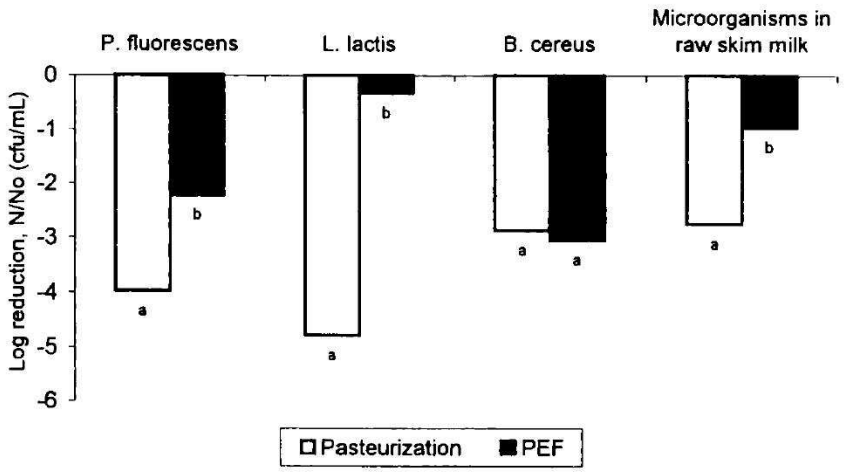

Figure 1.5: Comparison of effectiveness of PEF treatment and pasteurization on the inactivation of microorganisms in inoculated UHT milk and raw skim milk [5].

L. lactis, but achieved a similar inactivation effect on B. cereus. A comparison of the effects of PEF and pasteurization on proteins, vitamins and taste was conducted, and PEF was found not to significantly modify any of them, while pasteurization has been reported to cause protein denaturation, vitamin destruction and taste deterioration [7].

Interaction between PEF and other pasteurization techniques is often referred to as hurdle approach, and has been studied in a variety of publications. The work from Calderon-Miranda et al. [8] shows the effects of PEF and nisin, a polycyclic peptide antibacterial, on the morphology of cellular membranes through the use of transmission electron microscopy. Fig. 1.6 shows the damages inflicted by the combined action of PEF and nisin to the cell membrane. The treated cell was subjected to 32 exponentially decaying pulses ($\tau = 2\mu$s), at a rate of 3.5 Hz, in a coaxial chamber with 0.6 cm gap between electrodes, charged to 50 KV, and the solution was inoculated with 37 IU nisin/ml. The opening of a large pore results in the leakage of cytoplasmatic material, with loss of functionality of the cell. Unusual membrane roughness and cytoplasmatic clumping even in not-inactivated cells was also reported. Smith et al. [9] tested the interaction of PEF, mild heat (52 °C), nisin and lysozyme to the treatment of raw skim milk. PEF conditions consisted in 50 squared pulses of 2 μs, 80 KV/cm. Results are reported in table 1.4. The combination of these techniques results in a higher microbial

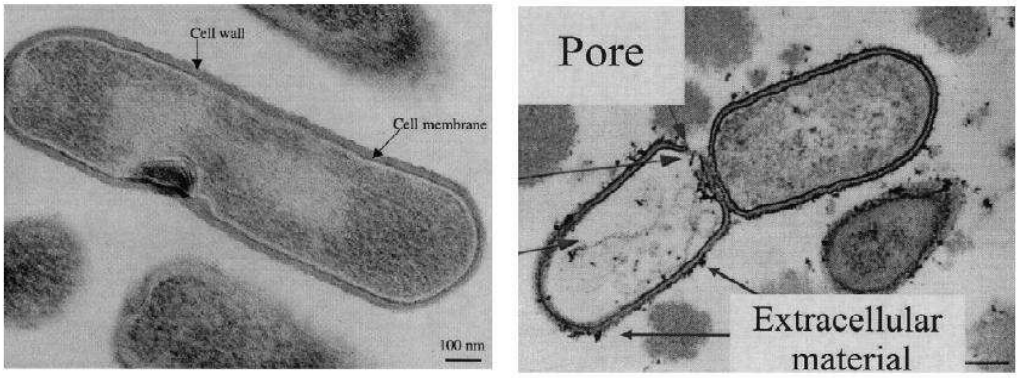

Figure 1.6: Untreated cell (left) and a cell treated by PEF and nisin (right), where it is possible to see a large pore and a clear leakage of cytoplasmatic material [8].

Antimicrobial	$\mathbf{N}_0$	$\mathbf{N}_a$	$\mathbf{N}_{PEF}$
None	3.10×10^8	3.10×10^8	1.55×10^7
Nisin (100 IU/ml)	3.65×10^8	5.78×10^6	7.00×10^1
Lysozyme (4150 IU/ml)	1.36×10^8	8.58×10^7	8.90×10^4
Lyso:Chrisin (38 IU/ml nisin 1638 IU/ml lysozyme)	1.38×10^8	8.71×10^6	1.26×10^1

Table 1.4: Combined effect of PEF, mild heat nisin and lysozyme, where N_0 is the initial population, N_a the final population without the application of PEF and N_{PEF} the final population with the application of PEF. Concentrations are reported in CFU/ml [9].

inactivation than the sum of the individual reduction achieved from each treatment alone, indicating a synergistic effect. This can be explained by the weakening of cell membrane caused by antimicrobial agents combined with the additional stress given by the PEF treatment, as PEF as been shown to be more effective against gram-negative than gram-positive bacteria, while nisin and lysozyme are more effective against gram-positive bacteria [10]. Synergistic effects between nisin and PEF on *Bacillus Cereus* have also been reported by Pol et al. [11], as shown in fig. 1.7. Here nisin concentration was 0.06 μg/ml, while PEF conditions are 50 pulses of 16.7 kVcm^{-1}, each of 100 μs duration, spread along 11.5 minutes. Other examples of synergistic effects of PEF and antimicrobials are reported, for example, in [12].

PEF (30 kVcm^{-1} for a total treatment time of 32 μs) and mild heat

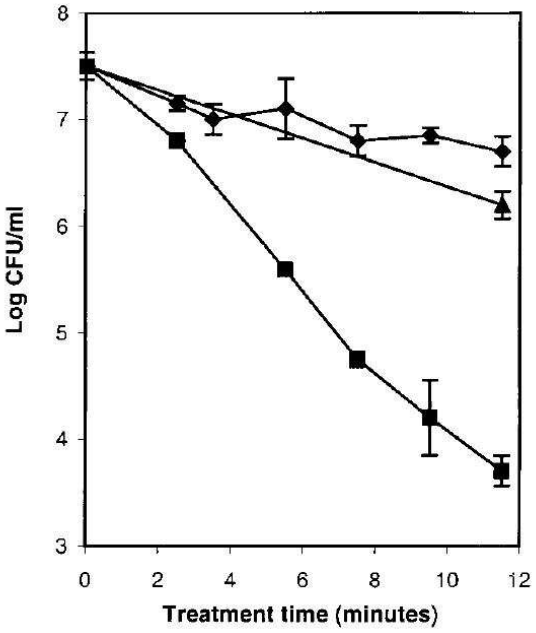

Figure 1.7: Kinetics of combined action of nisin and PEF on *B. Cereus*. ▲, PEF treatment. ♦, nisin treatment. ■ combined treatment [11].

(60°C for 30 s) treatment of yogurt-based drinks has been investigated by Yeom et al. [13], where a microbial, sensory and physical evaluation was conducted, and a comparison between bacterial population over a long period (3 months) in different storage conditions. As it is clear from fig. 1.8 and 1.9, combination of PEF and mild heat allows the storage of this product at higher temperatures (22°C) maintaining a bacterial population similar or inferior to the standard storage conditions (4°C). This aspects can lead to a great improvement in preservation of taste and nutritional values of the treated food, as reported in this study, and could also greatly reduce the problems arising from the necessity to keep storage temperatures at a low level. No significant loss of sensory and physical quality was observed in the processed products.

Tables 1.5 and 1.6 provide a summary of other important publications and their results on the application of PEF to diary products.

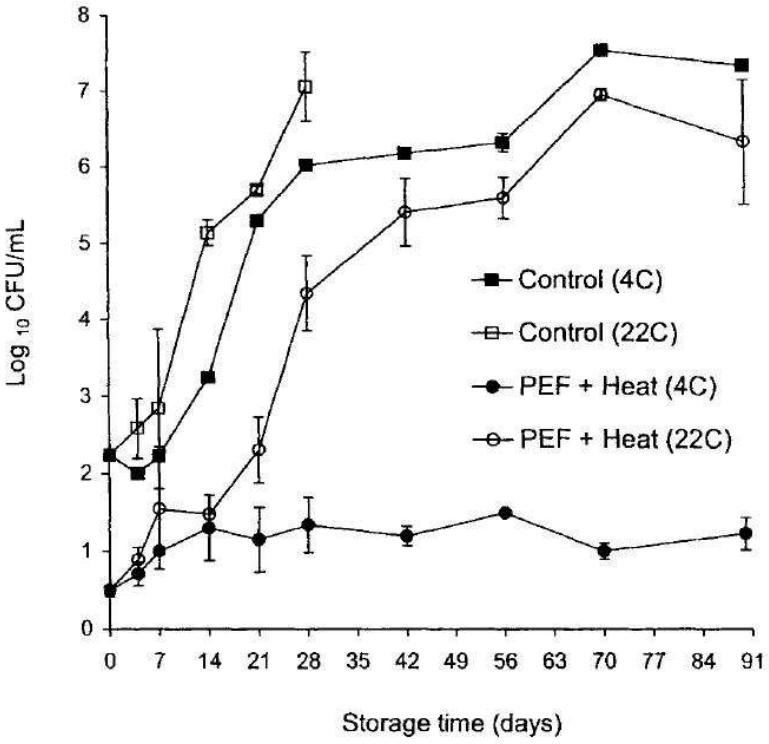

Figure 1.8: Combined mild heat and PEF treatment on total numbers of viable aerobic bacteria present at 4°C and 22°C [13].

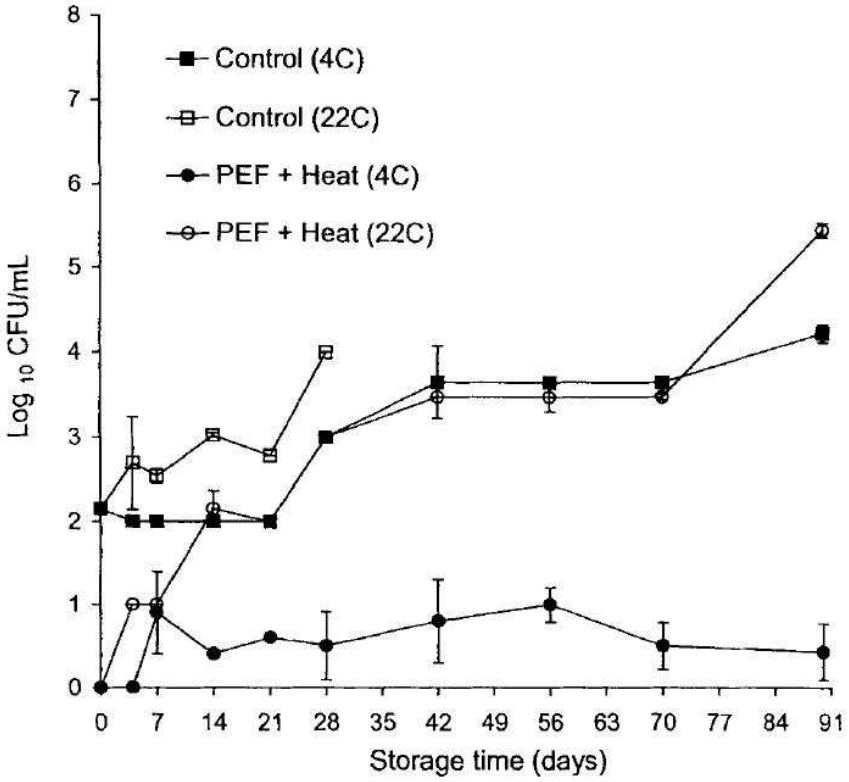

Figure 1.9: Combined mild heat and PEF treatment on total numbers of yeast and mold present at 4°C and 22°C [13].

PEF treatments of dairy products				
Microorganisms	Process condition	Log or % reduction (max)	Treatment Vessel	Source
E. coli and L. innocua	17°C, 120L/h, 41kV cm^{-1}, 2.5 μs, 10Hz, 63 pulses	4.0	Continuous, 28.6 ml, d=0.6 cm	[14]
E. coli	29°C, 24-31kV cm^{-1}, 2.8 and 4 μs of Bi or monopolar square wave, 700 Hz, t= 141-202 μs	1.96	6 Co-field chambers, 0.137 cm gap, D = 0.29 cm, $\nu = 0.0209\ cm^3$	[15]
E. coli	17°C, 120 L/h, 41kV cm^{-1}, 2.5 μs, 10 Hz, 63 pulses	4.0	Continuous, 28.6 ml, d=0.6 cm	[16]
S. Dublin	15-40 kV cm^{-1}, $10^\circ - 50$°C, t= 12 - 127 μs	~ 3.0	Co-field treatment chamber	[17]
B. Cereus *P. Fluorescens* *Lactococcus lactis*	$22^\circ - 55$°C, 35 kVcm^{-1}, 64 pulses, 3 μs bipolar square wave form, 500 Hz, t=188 μs, 1 L/min, 0.53 S/m	3.0 2.5 0.5	4 co-field treatment chambers, 0.19 cm gap, D = 0.23 cm	[18]
L. innocua	22° *to* 34°C, 0.5 L/min, 2μs, 3.5 Hz, 32 pulses, 50 kV, Exponential decay	2.4	Continuous, 25 ml, d = 0.6 cm	[19]

Table 1.5: Summary of PEF treatments of milk in literature, taken from [20].

PEF treatments of dairy products				
Microorganisms	Process condition	Log or % reduction (max)	Treatment Vessel	Source
L. innocua	15° *to* 28°C, 0.5 L/min, 100 pulses, 50 $kVcm^{-1}$, 2 μs, 3.5 Hz, Exponential decay	2.6	Coaxial, 29 ml d= 0.63 cm	[12]
L. monocytogenes	10° *to* 50°C, 0.07 L/s, 30 $kVcm^{-1}$, 1.5μs, 1700 Hz, Bipolar pulses, t=600μs	3.0-4.0	Co-field flow, 20 ml	[21]
L. monocytogenes	5-55 pulses, 15-30 $kVcm^{-1}$, 0° *to* 66°C	4.5	Static chamber, D = 8.4 mm 3.4 mm gap	[22]
S. Aureus	40°C, 36 $kVcm^{-1}$, exponential decay pulses, 2-3 μs pulse width	5.0	Co-axial treatment chamber, V = 29 ml, 0.6 cm gap	[23]
S. Aureus	40°C, 35 $kVcm^{-1}$, bipolar square wave of 3.7 μs pulse duration, 250 Hz, 1 ml/s, t=460μs	3.0	6 co-field treatment chambers, D = 2.3 mm, 1.0 mm gap	[24]
Total microorganisms	52°C, 80 $kVcm^{-1}$, 50 pulses instant charge reversal pulse wave form of 2μs, nisin (38 IU/ml), lysozyme (1638 IU/ml), pH 6.7 and 5	7.0	circular treatment chamber, D = 16.5 cm, 3 mm gap, V = 49.5 ml	[25]

Table 1.6: Summary of PEF treatments of milk in literature (Continued), taken from [20].

1.2.2 PEF applications to fruit juices

Fruit juices can undergo quality degradation due to microbiological and enzymatic activities and chemical reactions [26]. Spoilage microorganisms and native enzymes can be inactivated by thermal treatment, but this causes the irreversible loss of fresh flavor [27] as well as a reduction of nutrients and the initiation of undesirable browning reactions in the juices [26].

A work by Sen Gupta et al. [28] investigated the effectiveness of PEF on inactivation of *E. coli* K12 in apple juice, using two different values of applied electric field, 20 KV/cm and 40 KV/cm. Results are reported in tab. 1.7.

N° of pulses	**Log red. at 20 kVcm^{-1}**	**Log red. at 40 kVcm^{-1}**
0	0	0
20	0.606	1.762
40	0.940	1.735
60	1.326	2.143
80	1.354	2.178
100	1.511	5.398

Table 1.7: Comparison between PEF treatment of *E. coli* K12 at 20 KV/cm and 40 kVcm^{-1} [28].

The work demonstrated that the only way to achieve an inactivation of 5 Logs, the regulatory requirement for food safety, was to use 100 pulses of 40 KV/cm electric field. The experiment was carried out at 20°C and the maximum temperature rise was 2°C, so the possible interaction with heat was not investigated. The authors, anyway, reported no significant modifications in natural taste and aroma of the treated juice.

Qin et al. [29] investigated the inactivation by PEF in apple juice and simulated milk ultra-filtered (SMUF) of *Escherichia coli*, *Saccharomyces Cerevisea* and *Bacillus Subtilis*, under different pulse waveforms. Monopolar and bipolar square pulses, monopolar and bipolar exponentially decaying pulses and oscillatory decaying were tested at 30 °C. Square pulses were found to be more effective in inactivating bacteria than exponentially decaying pulses, with an average of 60% more inactivation, keeping an identical peak value of voltage applied to the food and the same amount of energy delivered. Oscillatory decaying pulses were found to be the least effective and not suitable for non-thermal pasteurization of food. Bipolar pulses provided more efficient inactivation of microorganisms compared to monopolar pulses. Undesirable

electrolysis of liquid foods was minimized and solid deposits on electrode surfaces were reduced by more than 80%.

A comparison between heat pasteurization, 94.6 °C for 30 s, and PEF at 35 kVcm^{-1} for a total treatment time of 59 μs was conducted on orange juice by Yeom et al. [30]. Microbial population was then compared for different storage temperatures over a period of 120 days, as shown in fig. 1.10 and 1.11. PEF is therefore reported to have a similar ability to inhibit

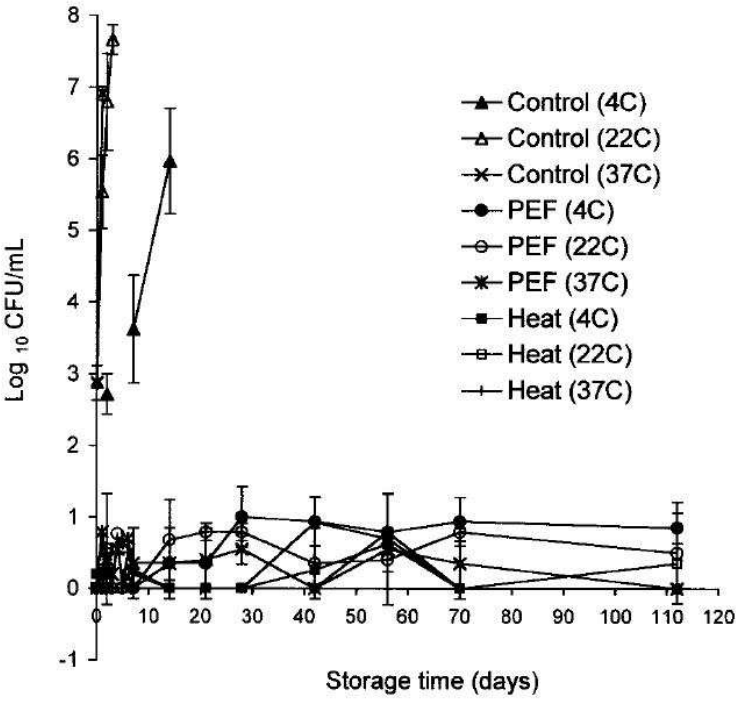

Figure 1.10: Effects of PEF and heat on total aerobic population of orange juice at different temperatures [30].

bacterial growth compared to heat pasteurization over long periods. At 4 °C PEF-treated orange juice showed significantly higher content of ascorbic acid, higher content of flavor compounds, lower browning index, higher whiteness, higher hue angle and smaller particle size (notably, with no difference compared to the untreated sample) compared to the heat-treated juice. Combined effect of mild heat (55 °C) and PEF treatment at 34 kVcm^{-1} on the bacterial population of apple and red grape juice was investigated by Heinz et al. [31]. This hurdle approach was found to optimize the energy efficiency of PEF and greatly increase its effectiveness. Data are reported in table 1.8

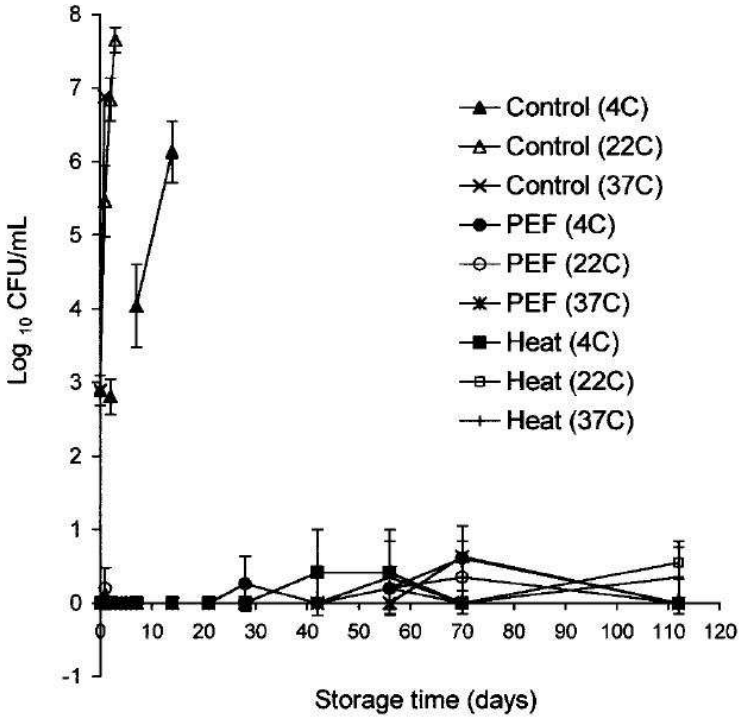

Figure 1.11: Effects of PEF and heat on yeast and mould population of orange juice at different temperatures [30].

Shelf-life of cranberries juice and chocolate milk as a function of PEF and the interaction of PEF with heat treatments was investigated by Everendilek et al. [24]. PEF treatment for cranberries juice consisted in 34 bipolar pulses, 32 kVcm^{-1} for 1.4 μs, at a frequency of 500 Hz. Treatment temperature was 25 °C or 60 °C, then the liquid was stored aseptically at three different temperatures, 4 °C, 22 °C and 37 °C, for 197 days and microbial population was compared to control samples. At both 22 °C and 37 °C the control cranberries juices spoiled after 14 days of shelf-life, while bacterial population was still under control in PEF treated and PEF+heat treated juices after 197 days, with no significant difference between PEF only and PEF+heat treatment. No difference in bacterial population were reported among untreated, PEF and PEF+heat treated juices ad 4 °C. This result suggest the possibility to use PEF to increase shelf-life of juices without forcing low temperature storage.

A paper by Simpson et al. [32] investigated the extension of shelf life of both fresh and concentrated apple juices. The authors report that 10

	Microorganism	Initial population	Log red.
Apple Juice	*E. coli*	$1.58 \cdot 10^7$	6.3
pH 3.4	*Rh. rubra*	$3.63 \cdot 10^6$	6.5
	A. niger	$4.28 \cdot 10^4$	4.3
	L. rhamnosus	$4.17 \cdot 10^7$	4.9
	L. innocua	$5.20 \cdot 10^5$	4.3
Red Grape Juice	*E. coli*	$1.10 \cdot 10^7$	6.4
pH 3.3	*Rh. rubra*	$1.05 \cdot 10^6$	5.4
	A. niger	$4.00 \cdot 10^4$	4.6
	L. rhamnosus	$2.45 \cdot 10^6$	4.6

Table 1.8: Inactivation of different microorganisms in apple juice and red grape juice by PEF and mild heat [31].

pulses at 50 $\mathrm{kVcm^{-1}}$, with pulse width of 2 μs and maximum processing temperature of 45 °C were able to extend shelf life until 28 days, compared to the normal 21 days.

Tables 1.9 and 1.10 provide a summary of other important publications and their results on the application of PEF to fruit juices.

PEF treatments of juices.				
Microorganisms	Process condition	Log or % reduction (max)	Treatment Vessel	Source
E. coli	30°C, 30 kVcm^{-1}, 100 L/h, 2 ms	5.0	Continuous, coaxial d= 5 mm	[33]
E. coli	30°C, 25-40 kVcm^{-1}, t=40-300μs, 10^{-3} L/s, 2.5 μs pulse	2.6	4 to 6 Co-field chamber, continuous	[34]
E. coli	40°C, 25-40 kVcm^{-1}, t= 40-340 μs, square wave bipolar pulses, 2.5 μs pulse	2.8	6 co-field treatment chamber, D = 0.23 cm, 0.293 cm gap	[35]
E. coli	35° − 70°C, 8-40 kVcm^{-1}, 2-95 Hz, 3 Kg/h, 1.5-6 μs width, exponential decaying pulses, t = 6-230 μ	> 6.0	continuous parallel treatment chamber, 2.5 mm gap, A = 2 cm	[31]
E. coli	20°C, 20 and 40 kVcm^{-1}, 0-100 pulses	5.0	hollow container with 8.15 mm gap	[36]
E. coli	42°C, 80 kVcm^{-1}, 2 μs, 30 pulses	5.35	Static, parallel plates, 50 ml, d = 0.3 cm	[37]

Table 1.9: Summary of PEF treatments of juices in literature, taken from [20].

PEF treatments of juices.				
Microorganisms	Process condition	Log or % reduction (max)	Treatment Vessel	Source
E. coli	$< 35°$C,85 L/min, 18-30 kVcm^{-1}, 1 kHz, bipolar pulses (3-6 μs), t= 86-172 μs	5.0	Continuous, 4 parallel plate chambers	[38]
Lactobacillus plantarum	30°C, 25-40 kVcm^{-1},t=40-300 μs, 10^{-3} L/s, 2.5 μs	1.3	4 to 6 Co-field chamber continuous	[39]
Aerobic bacteria, molds and yeasts	$< 60°$C,35kVcm^{-1}, 59μs, mono square pulses,600Hz,98L/h,1.4μs	7.0	6 Tubular chambers, d = 1 cm	[30]
S. cerevisea	$> 30°$C, 1.2 V/μm, 20 pulses, square wave	4.2	Bench, parallel plates	[29]
S. cerevisea	$20° - 30°$C, 10-28 kVcm^{-1} 8.3 pulses or 4.2-10.4 kVcm^{-1} qt 20 kVcm^{-1}, bipolar square wave pulse of 2 μs duration, 84 ml/min	4.0	6 co-field treatment chambers, 0.29 cm gap	[40]
Zygosaccharomyces Bailii	$19° - 22°$C, 32.2-36.5 kVcm^{-1}	~ 4.8	PEF + High hydrostatic pressure	[41]

Table 1.10: Summary of PEF treatments of juices in literature (Continued), taken from [20].

1.2.3 PEF applications to liquid eggs

Liquid egg is another interesting substrate to test PEF treatment. Contamination with *Salmonella* is an important public health problem in the United States and in many European countries, and it is mainly associated with eggs food products containing raw or inadequately cooked eggs, like for example homemade ice creams, egg nod and mayonnaise [42].

A work by Hermawan et al. [43] investigated the inactivation of *Salmonella enteritidis* inoculated into liquid whole eggs. Exponential decaying pulses were used, with time constant $\tau = 2.12\mu s$ for a maximum total treatment of 250 μs. PEF inactivation at 38 °C was tested for three different electric field intensity, 20, 22.5 and 25 kVcm^{-1}, and results are shown in table 1.11. Maximum reduction was 1 Log(CFU/ml), reached at 25 kVcm^{-1}, although

Treatment Time	**20 kVcm^{-1}**	**22.5 kVcm^{-1}**	**25 kVcm^{-1}**
0 μs	5.40 ± 0.31	5.50 ± 0.25	5.73 ± 0.15
50 μs	5.27 ± 0.30	5.30 ± 0.18	5.13 ± 0.31
100 μs	5.18 ± 0.38	5.15 ± 0.28	5.10 ± 0.35
150 μs	5.18 ± 0.41	5.08 ± 0.30	4.92 ± 0.29
200 μs	5.15 ± 0.36	4.97 ± 0.54	4.85 ± 0.30
250 μs	5.09 ± 0.43	4.98 ± 0.30	4.74 ± 0.48

Table 1.11: PEF treatment of liquid eggs at 38 °C. Bacterial concentrations are given in Log(CFU/ml) [43].

the difference among the three electric field conditions was not significant (P>0.05). Synergistic effect of PEF combined with mild heat was also tested, and compared to effect of 3.5 min heat alone at both 55 °C and 60 °C. Fig. 1.12 shows the different levels of inactivation reached, compared to the control samples. It is evident that PEF treatment followed by 3.5 min 55 °C could reach a level of inactivation compatible with the levels of 60 °C treatment alone, and that the effect of PEF + 55 °C was greater than the sum of inactivations by PEF and 55 °C separately. The shelf life of this substrate was also tested and compared to the control samples, and PEF + 55 °C treated sample were found to have a shelf life of over 60 days, 46 days more than the control samples.

Martin-Belloso et al. [44] studied the inactivation of *Escherichia coli* at 26 kVcm^{-1}, inoculated in liquid egg, comparing pulse durations of 2 and 4 μs and repetition frequencies of 1.25 and 2.50 Hz. Processing temperature was kept at 37 °C. Figure 1.13 shows a comparison between the effects of 2 and 4 μs pulses. As expected, 4 μs pulses were significantly more effective than

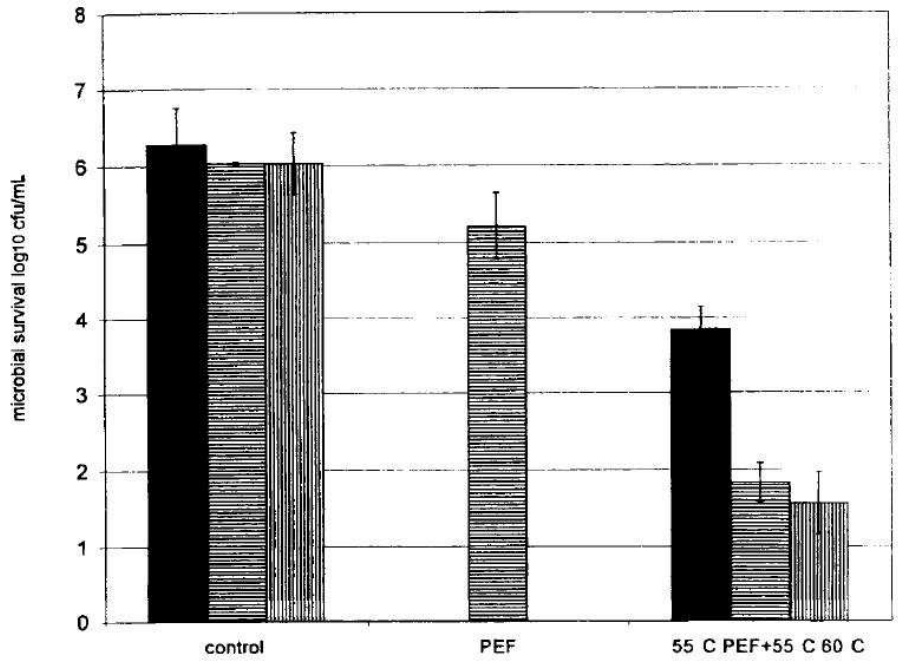

Figure 1.12: Inactivation of *Salmonella Enteritidis* under different conditions, compared to the control samples [43].

the 2 μs ones, while no difference was reported between 1.25 and 2.50 Hz. The maximum levels of inactivation could reach 6 Logs for 100 4 μs pulses.

Calderon-Miranda et al. [45] studied the interaction between PEF and nisin in the treatment of *Listeria innocua* suspended in liquid whole egg. Figure 1.14 shows this synergistic effect for a field intensity of 50 kVcm^{-1} and 21 applied pulses. The highest level of inactivation was 3.5 Logs, for 32 pulses at 50 kVcm^{-1}.

Dunn and Pearlman [2] also studied the application of PEF on liquid eggs, heat-pasteurized liquid egg products, and egg products with potassium sorbate and citric acid added as preservatives, using a static parallel electrode treatment chamber with 2 cm gap and 25 exponentially decaying pulses with peak voltages of around 36 KV. They were able to reach a low final bacterial concentration which remained stable for 4 and 10 days, when stored at a temperature of 10°C and 4°C respectively. Eggs treated with heat-pasteurization, instead, developed an high bacterial population in a few hours.

A recent work by Amiali et al. [20] studied the inactivation of *Salmonella Enteritidis* in liquid eggs products using 20 or 30 KV/cm in a condition of

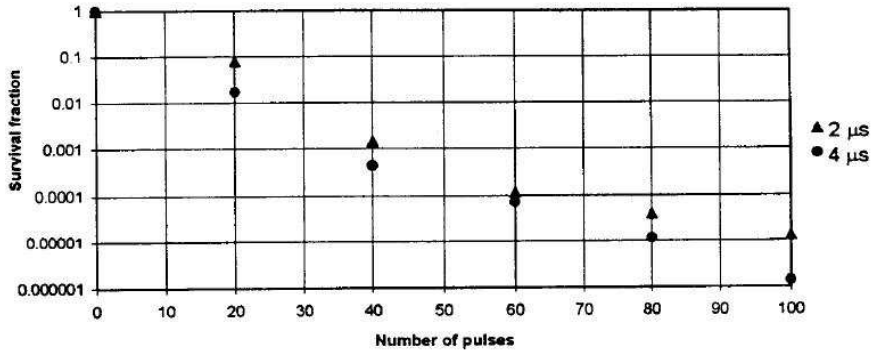

Figure 1.13: Inactivation of *E. coli* in liquid eggs at 26 kVcm^{-1} [44].

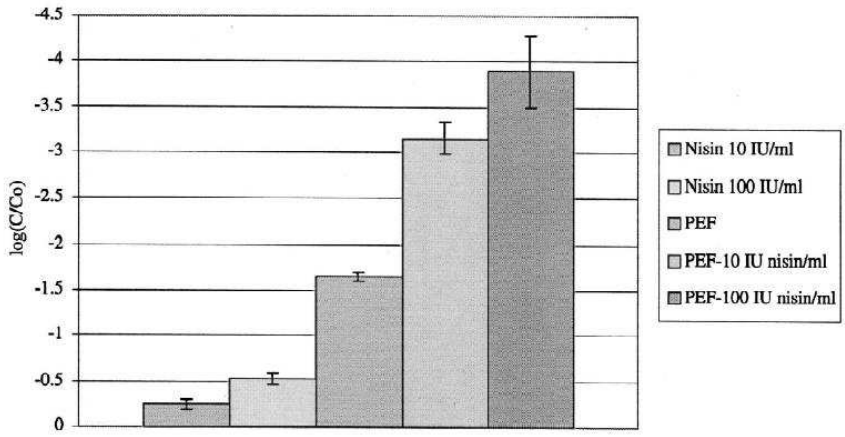

Figure 1.14: Comparison of the effect of PEF and nisin on *Listeria Innocua* suspended in liquid whole eggs. PEF field intensity is 50 kVcm^{-1} for 21 pulses [45].

10°, 20° and 30° C. The results showed the higher efficiency of the 30 KV/cm pulses, particularly when combined with the higher temperature of 30°C.

Salmonella Enteritidis in eggs was also treated by Jeantet et al. [46], who used monopolar exponential decay pulses with an electric field of 30 - 35 KV/cm: this study is particularly interesting for the high frequency of pulses, 900 Hz. The authors were able to reach an inactivation of 3.5 Logs.

Table 1.12 provides a summary of other important publications and their results on the application of PEF to liquid eggs.

PEF treatments of liquid eggs.				
Microorganisms	Process condition	Log or % reduction (max)	Treatment Vessel	Source
E. coli	$< 37°$C, 26 kVcm^{-1}, 4 μs 2.5 Hz, 0.5 ml/min, 100 pulses	6.0	Continuous chamber coaxial electrode, 11.87 ml	[47]
E. coli	$50° - 60°$C, 15 kVcm^{-1}, t=138 μs, 2 μs, 1 Hz, instant-reversal charge square wave	4.0	Batch chamber, parallel plates, V= 2ml, 1 cm gap	[48]
S. Enteritidis	25 kVcm^{-1}, 1.2 ml/s, 200 Hz, 2.12 μs, t = 250 μs	4.3	4 co-field treatment chambers, D=0.23 cm, 0.19 cm gap	[49]
S. Enteritidis	30 - 35 kVcm^{-1}, 900 Hz monopolar exponential decay pulses	3.5	d = 0.2 cm	[46]
L. Innocua	$6°$ to $36°$C, 0.5 L/min, 2 μs, 3.5 Hz, 32 pulses, 50 kV, exponential decay	3.5	Concentric, 25 ml	[50]

Table 1.12: Summary of PEF treatments of eggs in literature, taken from [20].

1.3 Pulsed Power technology

Pulsed power systems are used to to deliver a high peak power to a load in the form of a pulse. The basic concept is to store the energy taken from a power supply into a storage device, then to deliver this energy, over a short period of time, to the load. Traditional applications of Pulsed Power include high power microwave sources, pulsed gas discharge lasers, ion beam generation and acceleration, lightning and EMP simulation, hazardous waste and flue gas treatment, and medical equipment such as defibrillators, X-ray diagnostic equipment and lithotripters. More novel applications include ion beam surface treatment, weapons applications, rock fragmentation, prevention of biofouling, and microbiological control, as in PEF.

Pulse generators can be divided into two categories, capacitor based and inductor based. In the first case, energy is stored in a capacitor C, charged to a voltage V_0, and delivered to the load upon closure of a switch (see fig.1.15, right). In the second case, the pulse is generated upon breakage of a circuit (fig.1.15, left) where an inductor L carries an initial current I_0. The energies

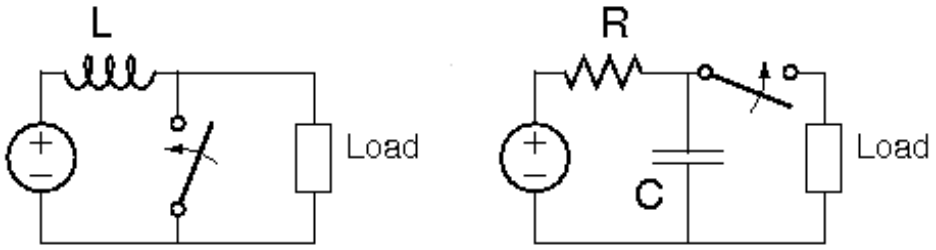

Figure 1.15: Inductive (left) and capacitive (right) Pulse Forming Network.

stored are

$$E = \frac{1}{2} C V_0^2 \tag{1.2}$$

for the capacitor and

$$E = \frac{1}{2} L I_0^2 \tag{1.3}$$

for the inductor. Although it can be shown that energy can be stored at higher density in a magnetic field than in an electric field [51], capacitive storage devices are usually preferred, due to lack of high voltage opening switches [52] and limitations in the rate of energy delivered [53].

Particular applications can require certain pulse shapes, and the use of discrete R, L and C components allows some flexibility in the formation of a pulse profile. Since practically the inductance of a circuit can never be zero, this is also the case in a simple RC circuit. An example of circuit scheme of a capacitor based modulator is found in fig. 1.16. Any modulator is basically composed of a power supply, a pulse forming network, a high voltage switch, controlled by a trigger, and an output. When the switch is open, once the

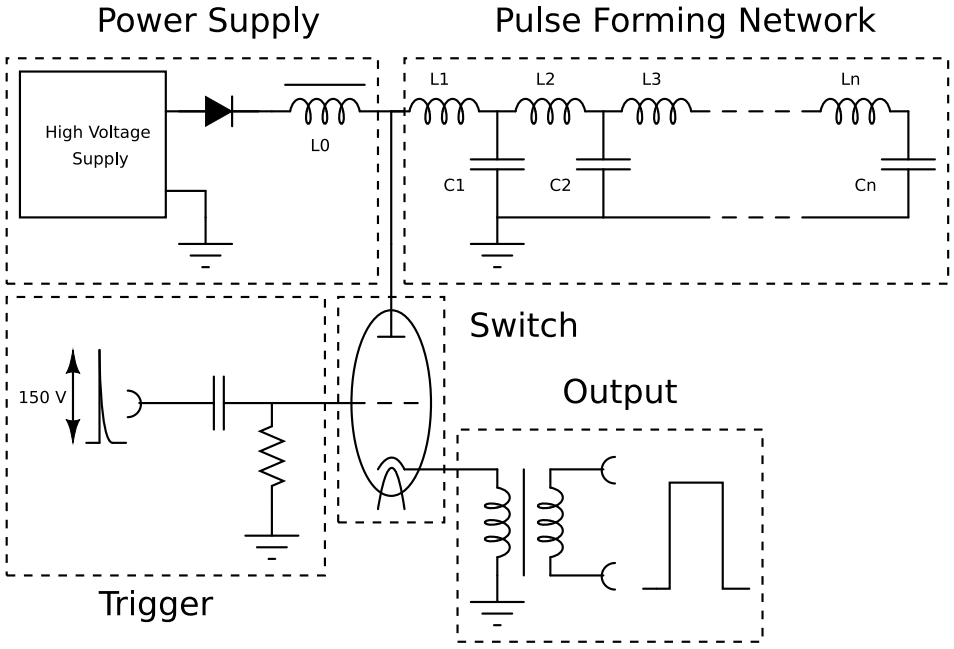

Figure 1.16: General circuit scheme for a capacitor based modulator.

power supply is turned on, the capacitors start to charge (fig. 1.17). The charge would initially follows a normal RC charging curve, but the presence of inductors (particularly the large impedance L_0) builds up a strong inductive resistance and generates a magnetic field. As the voltage approaches the voltage of the power supply U, the current decreases and the magnetic field breaks down, causing an additional induction of a voltage that charges the condensers up to the double voltage of the power supply. At this point the capacitors would discharge through the resistance of the power supply, but the presence of the diode prevents this to happen and thus the energy remains

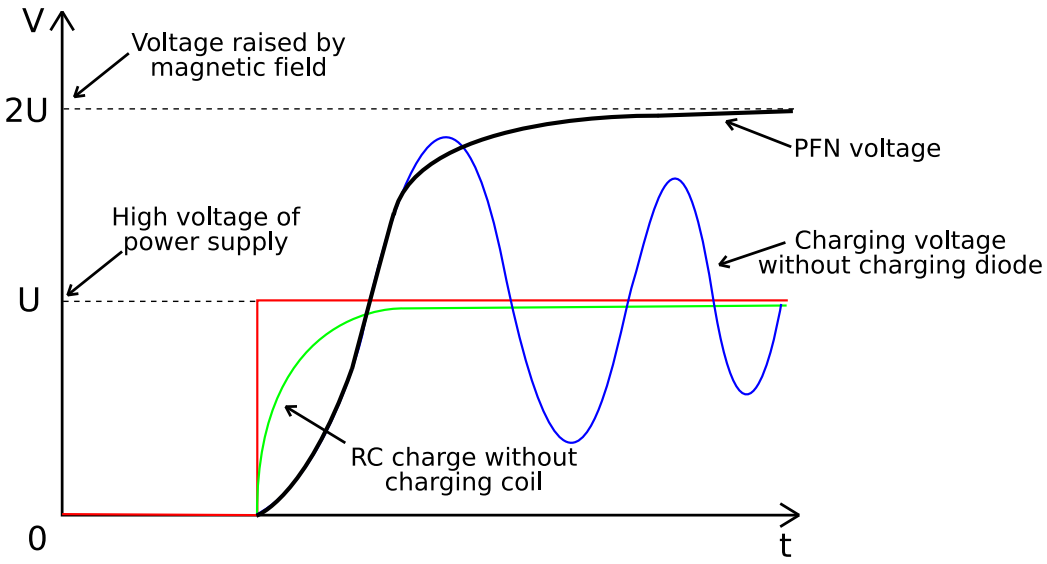

Figure 1.17: Pulse Forming Network voltage in a generic lumped circuit modulator.

stored into the condensers. Instead of using capacitors for the storage of charge, a transmission line cable can be used. When discharged into a load, the distribution of the charge along a physically long storage device causes the energy to be delivered as a pulse over a duration that is defined by the length of the cable. The voltage at the load can be described using the theory of transmission lines. When the resistance of the load perfectly matches the characteristic impedance of the line, a voltage U (half the charging voltage of the PFN) appears across the load, for a time that depends on the length of the line itself, providing the desired squared pulse.

1.4 Research needs

Although PEF has been studied for several years, many area still require further research [54].

- The mechanisms of inactivation has not been understood completely, particularly at cellular and molecular levels;

- The time dependent response of a cell membrane to an external electric field has not been measured in PEF treatments;

- The contribution of the different variables to PEF inactivation has not been studied and quantified properly;
- The effect of PEF on enzymes are the interaction of electric fields with food matrices at molecular level have not been investigated;
- The inactivation kinetics models have not been adequately correlated to the theories explaining the interaction of PEF with cells;
- An explanation of the great variability of inactivation levels found in laboratory tests and the saturation effects shown by inactivation curve has not been given;
- The size of treatment chamber does not meet the requirements of an industrial application on large scale;
- The variation of electric parameters, such as electric field intensity, pulse rate and duration have not been optimized and satisfactory correlated to bacterial inactivation;
- The life of electrodes is still too short to allow an application in continuous operation;
- The effects of combination of PEF with other thermal or non-thermal technologies have not been studied quantitatively;
- The effects of PEF on bacterial endospores have not been investigated.

Among these, the main limiting factors that prevent a scale up of PEF applications from the laboratory to the industrial range are surely the current limitations in treated volumes, the variability of inactivation levels and the saturation effects of inactivation curves.

Chapter 2

Electroporation of lipid membranes

The first observations of an interaction between electric fields and cells were made at the end of the '50 [55], but it wasn't until ten years later that killing of microorganisms by pulsed electric fields was reported [56]. The site of interaction was recognized to the the plasma membrane, whose rupture was reported for transmembrane voltages higher than ~ 0.3 V. A very rough approximation of the transmembrane voltage reached across a cell membrane due to an external electric field was first described by Schwan [57]

$$U = \frac{3}{2} r_c E \tag{2.1}$$

Given an average cell dimension of 1 μm, the range of electric fields needed for PEF inactivation is around 10 kVcm^{-1}.

2.1 The role of Phospholipidic Membrane

Across a cell membrane a resting potential is maintained in normal conditions. In most cells the this potential has a negative value, usually -70 mV, which means that there is excess negative charge inside compared to outside, mostly determined by the concentrations of the ions in the fluids on both sides of the cell membrane and the ion transport proteins that are in the cell membrane (see fig. 2.1). Among the many important functions of a cell membrane, ability to shield cytoplasm from ions and charged molecules is fundamental. This can be explained as a result of the difference in Born energy associated with moving a charge from high dielectric medium, water,

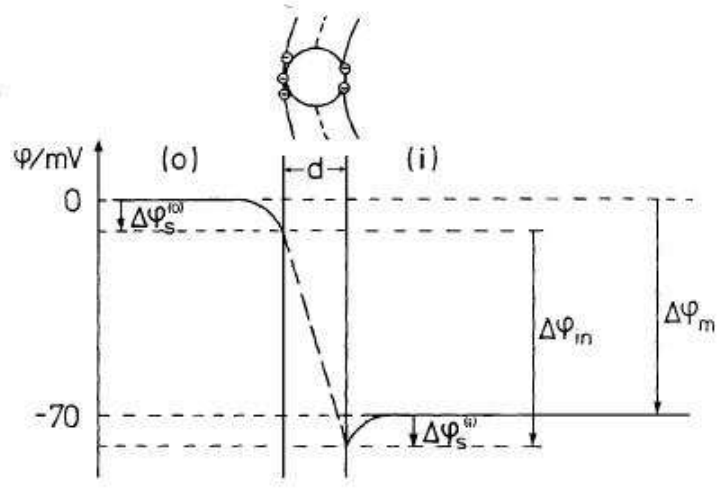

Figure 2.1: Potential across a cell membrane.

to a low dielectric region, the membrane [58].

$$W_{Born} = \int_{\sigma} \frac{1}{2} \epsilon E^2 dV \tag{2.2}$$

where σ is all the space excluding the ion itself. If we consider single, small and isolated ions, the largest contribution to W_{Born} arises from the region close to the ion. Since the ion diameter is significantly smaller than membrane thickness (0.4 nm compared to 6 nm), $W_{Born,i}$, the Born energy in water, is

$$W_{Born,i} = \int_{\sigma} \frac{1}{2} \epsilon E^2 dV = \int_{r_i}^{\infty} \frac{1}{2} \epsilon \frac{e^2}{(4\pi)^2 \epsilon^2 r^4} 4\pi r^2 dr = \frac{e^2}{8\pi \epsilon_w \epsilon_0 r_i} \tag{2.3}$$

where r_1 is the ion radius. The same approach can be followed for an ion in a cell membrane, leading to

$$W_{Born,f} = \frac{e^2}{8\pi \epsilon_m \epsilon_0 r_i} \tag{2.4}$$

thus the energy difference is

$$W_{Born,f} - W_{Born,i} = \frac{e^2}{8\pi \epsilon_0 r_i} \left(\frac{1}{\epsilon_m} - \frac{1}{\epsilon_w} \right) \sim 65 \ kT \tag{2.5}$$

with T=37°C. Spontaneous barrier crossing seems thus negligible. Calculations were carried out also on non-intact lipid membranes, particularly in the

case of mobile aqueous cavities and cylindrical pores. Both configurations were found to lower ΔW, and the greater reduction was achieved by the pore. Early calculation by Parsegian [58, 59], approximating the pore to an infinite cylinder, estimated $\Delta W_p \sim 16$ kT for a pore of 0.3 nm in radius, still too high to explain, for example, the relatively high conductances observed for pores produced by gramicidin A [60]. Levitt [61] improved this calculations taking into account a finite length for the pore, and solving an equivalent problem in which an appropriate surface charge is placed on the boundary between the lipid and aqueous regions. The value of ΔW_p was found to be ~ 6.7 kT.

2.2 Bilayer lipid membranes in electric fields

As mentioned before, early observations suggested that some kind of electrical breakdown occurs in electrically stimulated membranes. Since then, the behavior of both natural and artificial lipid membrane has been studied in depth. Particularly important are the results of experimental measures of the transmembrane current in artificial bilayer lipid membranes (BLM) [62]. The typical currents measured are shown in fig. 2.2. Upon application of a

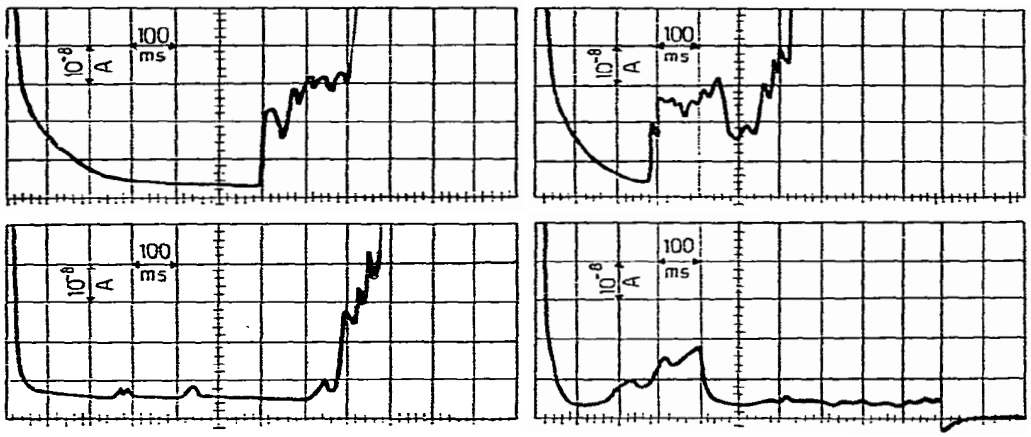

Figure 2.2: Electric current through bilayer lipid membranes at U=400 mV. Sometimes reversible electroporation occurs, like in bottom right figure [62].

stepwise voltage U (400 mV in this example), the membrane charges with a time constant $t_c = C_m(R_L + R_e)$, where C_m is the membrane capacitance and R_e the electrolyte resistance, then a steady current sets in for a while. After a short period, the intensity of current increases and fluctuations begin to

appear. Shortly after the begin of these fluctuations, the membrane breaks down, a fact that is registered by a sharp increase in current. The general current behavior scheme is shown in fig. 2.3, in which the main characteristic times are indicated: the membrane charging time t_c, the duration of constant current before the appearance of fluctuations t_f, the membrane lifetime t and the time of rupture of the membrane as a whole t_m. There is also the possi-

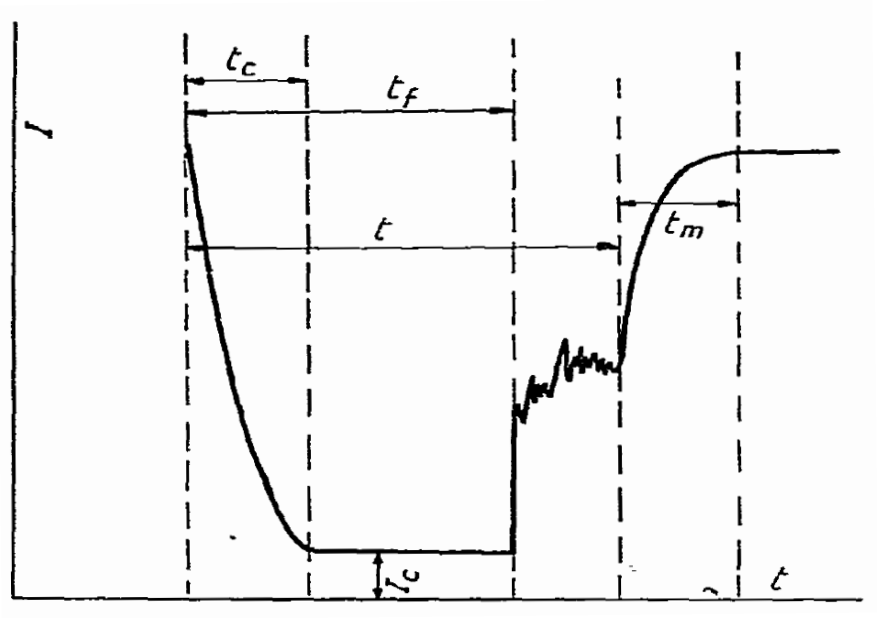

Figure 2.3: Generalized scheme for breakdown of bilayer lipid membranes after a stepwise change in U [62].

bility of appearance of long lived current fluctuations, with amplitutes in the order of $10^{-11}A$. This *stress state* can last for several minutes. In fig. 2.4 the logarithm of membrane mean lifetime is shown for different kinds of lipids. In a potential range between 0.3 V and 0.6 V, the dependence of log t on U is close to linear. Repeating the tests over a large number of membranes it was noted that for each potential, lifetimes are distributed over a wide range. The distribution density curves are asymmetric, with the maximum shifting towards lower t for higher U. Another interesting aspect reported was the influence of the initial value of membrane voltage on the mean lifetime, making membrane breakdowns more likely the higher this initial value of U. This indicates that the mechanism leading to membrane breakdown is already acting during the pre-fluctuations period.

Another important aspect to understand electroporation is the measure-

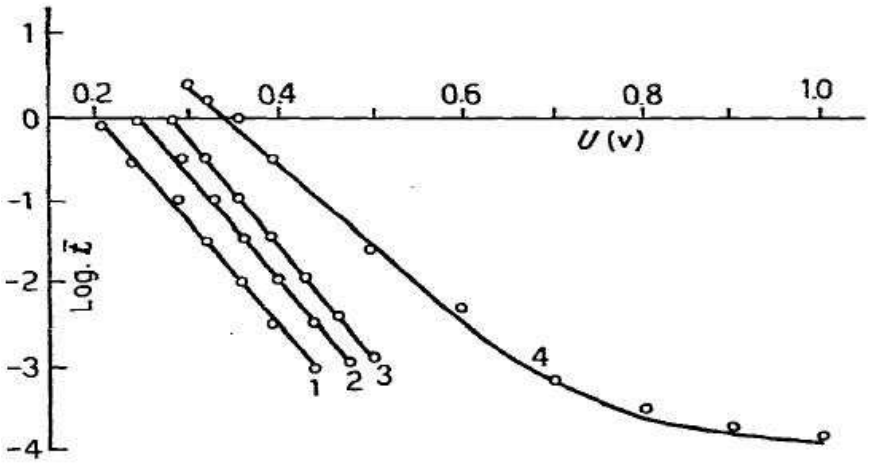

Figure 2.4: Logarithm of membrane mean lifetime as a function U for different kinds of lipids [62].

ment of membrane capacitance. If there is a large scale process that dominates the process of electroporation, such as changes in membrane thickness h, this would be revealed by a change in membrane capacitance C_m in the pre-breakdown phase. Several studies have investigated the influence of U on BLM capacitance [63, 64, 65], showing that C_m can be modified at elevated U. The amount of change reported in this works was $\sim 10\%$ of the original capacitance at 100 mV. The possible sources of this increase are:

- formation of new membrane from the surrounding torus
- exclusion of solvent from the membrane into the torus or microlenses
- membrane thinning

Among these mechanisms only the third one can have a physiological relevance since the biological membranes neither have solvent nor are in equilibrium with a torus. Experiments that could simulate more accurately the biological membranes were carried out by other groups [66], using membranes formed by the apposition of two lipid monolayers [67]. For modest transmembrane voltages ($\sim 0.3 - 0.8$V) experiments have shown a rapid but small change in C_m, described by the equation

$$C_m = C_{m,0}(1 + \alpha U^2) \tag{2.6}$$

with $\alpha \sim 0.02$ V^{-2}. The authors were therefore able to verify that the increase in capacitance was linear with the square of the membrane potential, as it was earlier demonstrated for BLMs, but the change was much faster and three order of magnitude smaller (in the order of 2% of the initial capacitance). As confirmed by several other experiments, the change in capacitance due to a transmembrane potential is rapidly attained and then remains constant until the moment of breakdown. This result demonstrates that pre-breakdown current fluctuations are not associated with significant changes in membrane thickness h, and therefore that a large scale membrane electrocompression can be ruled out as the cause of breakdown.

2.3 Non-pore theories of electroporation

Many different theoretical models have been developed to explain the behavior of BLMs exposed to elevated U. The early models did not take into account the possibility of pore formation and did not considered the membrane as a metastable system. As we will see, all these models failed to provide explanation for the stochastic nature of rupture and for the strong (non-linear) dependence of membrane lifetimes on transmembrane voltage.

2.3.1 Electromechanical collapse

The first attempt to explain membrane rupture was made by Crowley [68], suggesting that it could be caused by electromechanical collapse due to compression of the entire membrane. The membrane is treated as an elastic capacitor filled with a dielectric with permittivity ϵ_m. When a small pressure dp is applied to the ends of the elastic material, a compression will take place, according to Hooke's Law

$$Y_m \frac{dh}{h} = -dp \tag{2.7}$$

where Y_m is the Young modulus and h the length of the material. Total compression from a finite pressure p will be

$$-p_m = Y_m \int_{h_0}^{h} \frac{dh}{h} \tag{2.8}$$

The electrical pressure exerted on this dielectric when a voltage drop U is experienced between the two faces is

$$p_{el} = \epsilon_m \frac{U^2}{2h^2} \tag{2.9}$$

The condition for mechanical equilibrium is clearly

$$p_{el} = p_m \tag{2.10}$$

from which we can derive an equation for h

$$Y_m log\Big(\frac{h_0}{h}\Big) = \frac{\epsilon_m U^2}{2h^2} \tag{2.11}$$

It is easy to see that this equation as no roots for

$$\frac{\epsilon_m U^2}{2Y_m h_0^2} = 0.184 \tag{2.12}$$

and we can therefore define a critical voltage

$$U_c^2 = 0.368 \frac{Y_m h_0^2}{\epsilon_m} \tag{2.13}$$

A first estimation of U_c was made by Crowley for phosphotidylcholine and cholesterol, using the values of Y_m, respectively, of $2.9 \cdot 10^4$ Nm^{-2} and $2.7 \cdot 10^5$ Nm^{-2}, and led to a value of U_c around 0.120 V in the first case and 0.230 V in the second. Comparison between predicted and measured values is shown in fig. 2.5, from which it is clear that the agreement of this theory with experiments is not very accurate. Even if we do consider this, many other arguments are against this explanation of PEF inactivation:

- from eq. 2.1 and eq. 2.13 it follows that breakdown takes place when

  $$\frac{h}{h_0} = e^{-0.5} \sim 0.61 \tag{2.14}$$

  thus for a compression of the 39% of the membrane. Under this condition the assumption that Y_m is constant is not realistic anymore

- if more realistic values of compressibility for solvent-free membranes are used, the predicted U_c can be calculated to be around 5 V, about one order of magnitude too large

- the absence of a relevant change in capacitance C_m for a membrane under external electric field, as reported before, is in contradiction with a 39% decrease of h

- rupture of membrane for this theory depends only on U, while experiments have shown a dependence also on the pulse duration t_p

- this model predicts that sub critical voltages do not cause membrane rupture, while experiments have shown that rupture is a stochastic process and that the dependence of membrane lifetime τ_m on the transmembrane voltage is highly non-linear

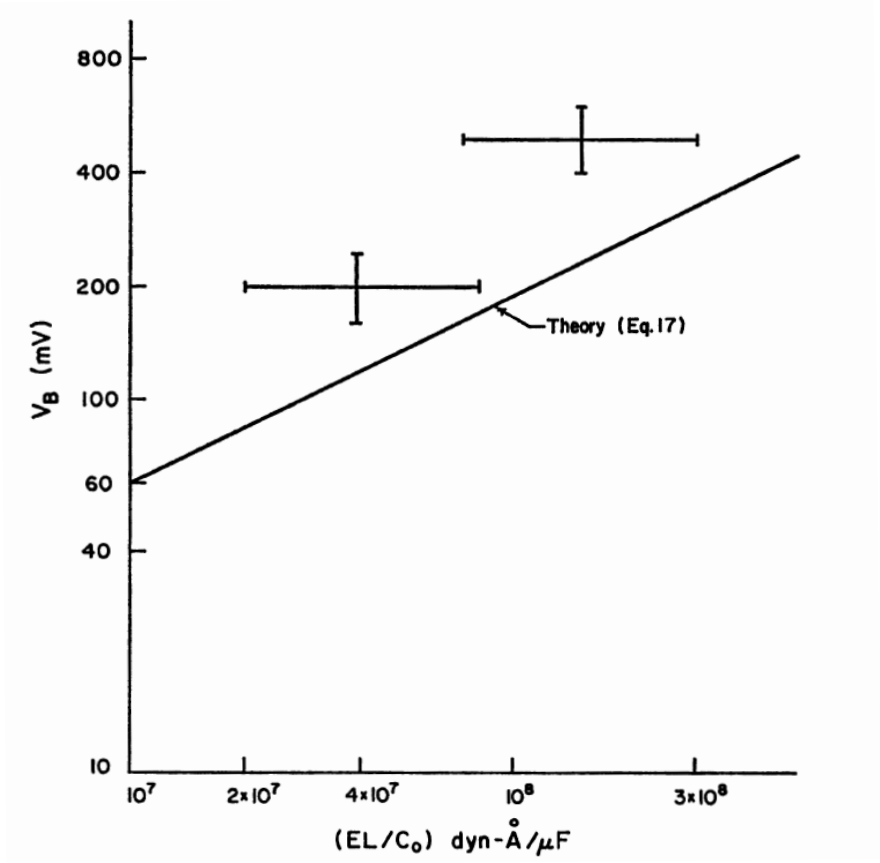

Figure 2.5: Comparison between predicted and measured critical voltages for two Bilayer Lipid Membranes [68].

2.3.2 Electrohydrodynamic effect

The system formed by two layers of conducting liquid separated by a layer of non-conducting liquid is similar to a membrane (if we neglect the fact that motion within the membrane cannot be described by the usual hydrodynamic equations), and has been used to describe its rupture [5, 69]. Stability with respect to two kinds of perturbations of plane surfaces are analyzed, symmetric and antisymmetric to the mid-plane of the dielectric. BLMs are known to have a moderate flexural rigidity, thus it could be expected that the membrane will develop symmetric wave, while the development of antisymmetric waves is impeded by the large elasticity of membrane compression.

According to this model, a membrane would be unstable if

$$U^2\epsilon_m > \frac{1}{2}\Gamma h \tag{2.15}$$

where $\Gamma/2$ is the surface tension at the interface between the liquids. The breakdown voltage is therefore

$$U_c = \left(\frac{\Gamma h}{2\epsilon_m}\right)^{\frac{1}{2}} \tag{2.16}$$

Using the average values of $\Gamma = 10^{-3}$ Jm^{-2} and h = 5 nm, the breakdown voltage is 0.375 V, in reasonable agreement with experimental results. This model, however, fails completely to account for both the stochastic nature of rupture and the strong dependence of membrane lifetime on U.

2.3.3 Wave instability

Viscoelastic properties of membranes have been used to analyze the rupture as a wave instability. In particular, membranes were described within the framework of models of Kelvin and Maxwell. The first one yields stability of the membrane, while the second, which also takes into account the compression owing to van der Waals attraction forces, yields instability. In this latter case, the membrane is analyzed in terms of the time evolution of symmetric waves, leading to a characteristic time of the process, τ_{el}, which depends on the wave number k

$$\tau_{el} = \left(-\frac{Y_m}{3\mu_m} + \frac{\epsilon_m U^2 k^2}{12\mu_m} - \frac{\Gamma h^2 k^4}{24\mu_m}\right)^{-1} \tag{2.17}$$

where μ_m is the effective membrane viscosity and Γ the tension. The membrane lifetime is then calculated as the minimal time for the increase of the surface disturbance

$$\tau_{el} \sim \frac{\mu_m}{\frac{\epsilon_m^2 U^4}{24\Gamma h^3} - \frac{Y_m}{3}} \tag{2.18}$$

Finally, a threshold voltage can be calculated

$$U_c = (24 Y_m \Gamma h^3)^{\frac{1}{4}} \tag{2.19}$$

However, this model, as the previous ones, does not explain the stochastic behavior of rupture and the strong dependence of membrane lifetime on U.

2.4 Transient aqueous pore model

The most adequate approach to describe membrane stability relates to the kinetic studies of first order phase transitions. Planar bilayers are a metastable system, as can be easily understood noting that work has to be done to form a bilayer from a lipid solution. The surface tension Γ is for this reason positive, and therefore a broken membrane state has lower free energy than an intact membrane state. Breakdown is considered as a phase transition to a more stable state. The basic approach was developed by Gibbs, who introduced the concept of formation of a nucleus of a new phase. The lifetime of the metastable phase depends exponentially on the work done to form a critical nucleus, W_c

$$\tau = \tau_0 \exp\left(\frac{W_c}{kT}\right) \tag{2.20}$$

where τ_0 is the lifetime pre-factor.

Many authors contributed to the development of the theory of phase transition [70, 71, 72, 73] applying this framework to many different fields. The possibility of pore formation in cell membranes was introduced before the discover of membrane electroporation, as a theory to explain the breakdown of free soap films [74]. The application of this model to lipid membranes was then suggested by two groups to investigate the spontaneous rupture of red blood cell membranes [75] and the molecule transport across the lipid bilayer [76]. The basic idea is to use a *cookie cutter* model for pore formation energy $\Delta W_p(r)$, where a gain in energy, due to the formation of a pore edge, and a reduction in energy, due to the loss of a circular region of membrane are taken into account.

$$\Delta W_p(r) = 2\pi\gamma r - \pi\Gamma r^2 \tag{2.21}$$

This equation describes a large parabolic barrier for pore formation, with maximum

$$\Delta W_p^{max} = \frac{\pi\gamma^2}{\Gamma} \tag{2.22}$$

Using the typical values of $\Gamma = 10^{-3}$ Jm^{-2} and $\gamma = 10^{-11}$ Jm^{-1} [77], formation energy barrier ΔW_q^{max} is $\sim$ 76 kT (T=298°K). Once a pore reaches an energy over this threshold it indefinitely expands causing membrane rupture. The frequency of appearance of a pore with energy higher than ΔW_q^{max} can be calculated, according to [76], as

$$K_p = \nu V_B exp\left(-\frac{\Delta W_q^{max}}{kT}\right) \sim 7.9 \cdot 10^{-16} s^{-1} \tag{2.23}$$

where $V_B = 4 \cdot 10^{-15} m^3$ is the membrane volume and $\nu \sim 10^{32}\ s^{-1} cm^{-3}$ the attempt rate density of lateral fluctuations scaled for 25°C and for the

molecular weight of a typical phospholipid liquid [78, 79]. The conclusion of these early works was therefore that spontaneous pore formation was very unlikely.

Other groups [62, 80] improved the transient aqueous pore theory taking into account the effect of an external electric field and various other corrections, among which the most important is the distinction between hydrophobic and hydrophilic pores. As described before, cell membranes are made of lipid molecules, more specifically phospholipids. The presence of a hydrophilic and a hydrophobic end in these molecules naturally leads to the formation of lipid bilayers. Lateral thermal fluctuations of the lipids, however, can occur, and lead to the formation of hydrophobic pores in the lipid matrix (fig. 2.6, left). A formation energy is associated to this pore, depending on the pore radius, that will determine the rate of pore formation as in eq. 2.23. The first attempt to compute ΔW_p for this pores was

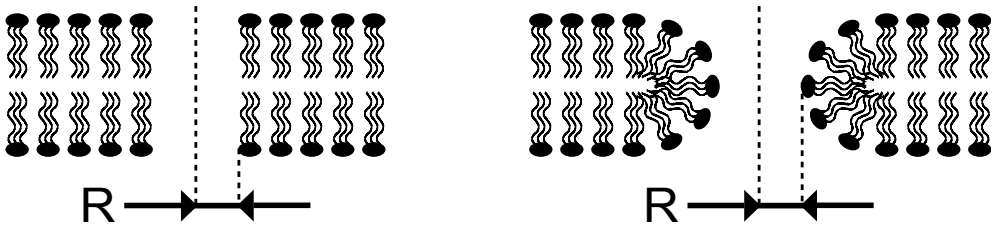

Figure 2.6: Hydrophobic (left) and hydrophilic (right) pores.

$$\Delta W_p(r) = 2\pi r h \sigma_0(\infty) \tag{2.24}$$

where h is the thickness of the membrane and $\sigma_0(\infty)$ the interface tension between lipid tails and water [81]. This equation does not take into account the interaction between the walls of the pore, that laboratory measures demonstrated to significantly reduce the interface tension σ_0 [82]. In presence of a membrane, water structure is modified, and from the interface to the bulk phase its properties undergo a gradual transition with a characteristic length of 1 nm. The origin of interface tension is in the excess energy of this thin layer of disturbed water structure. When two hydrophobic surfaces come to a distance in the order of nanometers, the overlapping of these layers reduces the effective surface tension and causes hydrophobic attraction between the surfaces. Based on this model [83] the effective value of $\sigma_0(r)$ was calculated [80]

$$\sigma_0 = \sigma_0(\infty) I_1(R/\rho)/I_0(R/\rho) \tag{2.25}$$

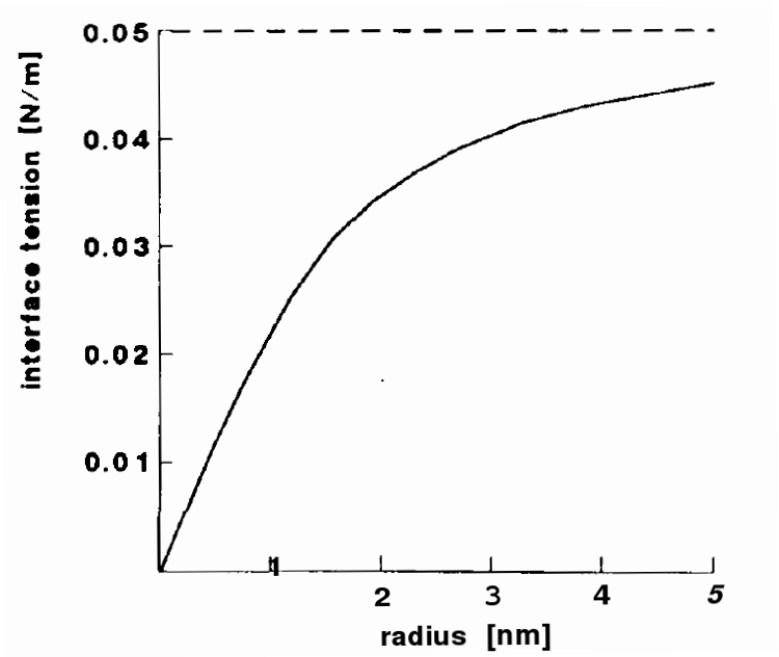

Figure 2.7: Effective interface tension between hydrophobic pore wall and water as a function of pore radius. Dashed line shows interface tension without hydrophobic interaction [80].

where $I_n(x)$ are the modified Bessel functions of n-th order and σ_0 the effective interface tension (see fig. 2.7). ΔW_p was calculated accordingly (fig. 2.8).

$$\Delta W_p(r) = 2\pi r h \sigma_0(r) \tag{2.26}$$

The energy of a hydrophilic pore was first calculated in eq. 2.21, where r is the radius of the narrowest part of the channel in the membrane (see fig. 2.6, right). The approximation of constant γ, however, is inapplicable for pores with small radius [81]. The packing of liquids along the wall side of a narrow pore leads to substantial deformation of the molecular order, which increases the pore energy particularly when r is comparable with the size of lipid heads. In addition repulsive forces between the hydrophilic compounds of the pore wall are caused by hydration interaction, the strong repulsive force observed between lipid bilayers approaching each other [84]. For these reasons ΔW_p for hydrophilic pores increases for very small radii, although an expression to describe this rise of ΔW_p has not been derived. Anyway, a qualitative description is possible and it is shown in fig. 2.9. The formation of hydrophobic pores is energetically more favorable at small radii. These pores

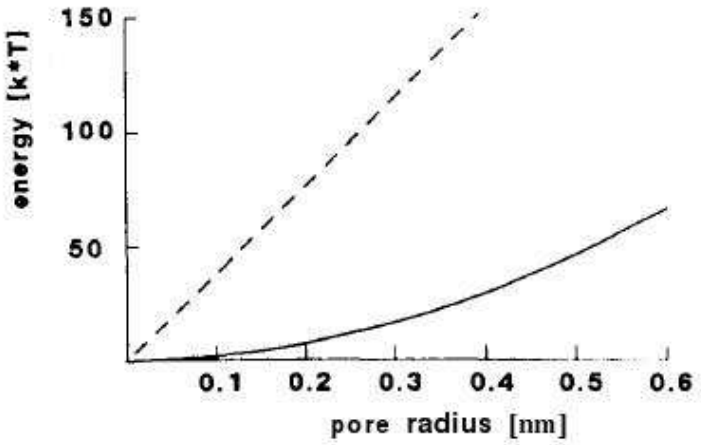

Figure 2.8: Energy of hydrophobic pores as a function of pore radius: dashed line without considering hydrophobic interaction between pore walls, solid line considering it [80].

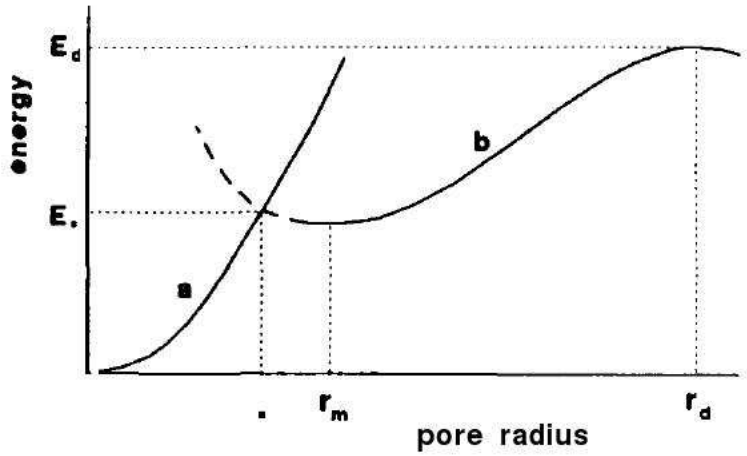

Figure 2.9: Comparison between hydrophobic (a) and hydrophilic (b) pore energy formation at different radii [80].

are formed spontaneously by lateral thermal fluctuations, of lipid molecules. If their radius exceeds the critical value r_*, hydrophilic pores become energetically favorable and thus a reorientation of the lipids occurs. This process is often referred to as inversion of the pore. In this picture, hydrophobic pores are just intermediate stages in the process of formation of hydrophilic pores. These pores are considered metastable, because of the presence of a

local minimum around r_m, suggesting an explanation for the phenomenon of reversible electroporation.

This model is valid as well when the voltage across the membrane differs from zero. When a hydrophilic pore is experiencing an electric field, an energy can be associated with the change of its specific capacitance, C_{LW}, as lipid is replaced by water [62].

$$\Delta W_p(r,U) = 2\pi\gamma r - \Gamma\pi r^2 - \frac{1}{2}C_{LW}U^2\pi r^2 \tag{2.27}$$

is the expression for the pore formation energy in presence of a transmembrane potential U, where the chance in pore specific capacitance is

$$C_{LW} = \left(\frac{\epsilon_w}{\epsilon_m} - 1\right)C_0 \tag{2.28}$$

with $C_0 = \epsilon_0\epsilon_m/h$. It is clear that eq. 2.27 also describes an energy barrier, but this barrier decreases at the increase of the transmembrane potential U. This is evident from the computation of $\Delta W_{p,c}$ and r_c, the critical energy barrier and the critical radius

$$\Delta W_{p,c} = \frac{\pi\gamma^2}{\Gamma + 0.5C_{LW}U^2} \tag{2.29}$$

$$r_c = \frac{\gamma}{\Gamma + 0.5C_{LW}U^2} \tag{2.30}$$

The critical pore radius becomes smaller as U is increased, as does the corresponding pore energy. A single supra-critical pore is enough to cause membrane rupture, therefore we can relate the rate of formation of these pores to the membrane lifetime, and compute this lifetime as we have done before

$$K_p = \nu V_B exp\left(-\frac{\Delta W_{p,c}}{kT}\right) \tag{2.31}$$

$$\tau = K_p^{-1} = \frac{1}{\nu V_B}e^{\frac{\Delta W_{p,c}}{kT}} \tag{2.32}$$

The population survived to exposure to a transmembrane potential U for a time dt therefore will be

$$S(U,\Delta t) = S_0 exp\left(-\frac{\Delta t}{\tau}\right) = S_0 exp\left(-\frac{\nu V_B}{exp\left(\frac{\Delta W_{p,c}}{kT}\right)}dt\right) \tag{2.33}$$

Recalling eq. 2.29, we can write

$$exp\left(\frac{\Delta W_{p,c}}{kT}\right) = exp\left(\frac{\Delta F}{1+\beta U^2}\right) \tag{2.34}$$

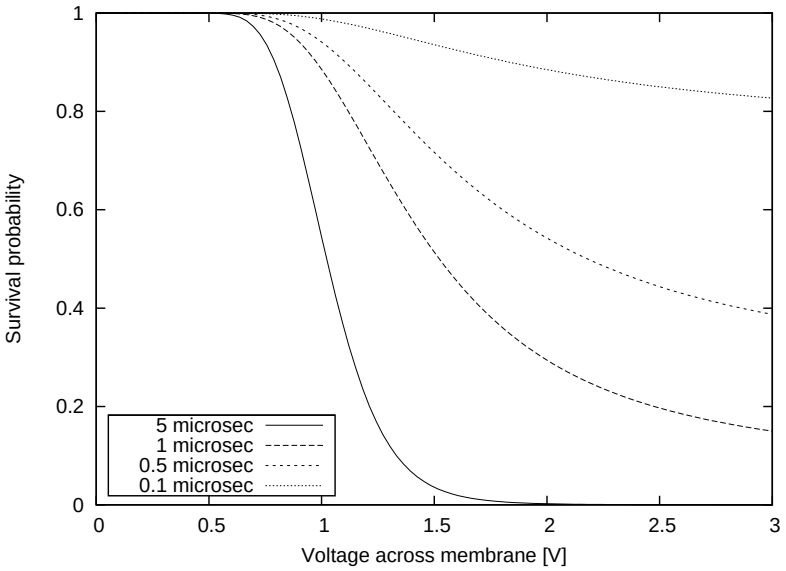

Figure 2.10: Variation of survival probability with transmembrane potential for different pulse durations.

where we introduced

$$\Delta F = \frac{\pi\gamma^2}{kT\Gamma} \tag{2.35}$$

and

$$\beta = \frac{C_{LW}}{2\Gamma} \tag{2.36}$$

If we also define

$$\tau_\infty = \frac{1}{\nu V_B} \tag{2.37}$$

we arrive to the usual definition of $S(U, \Delta t)$

$$S(U, \Delta t) = S_0 exp\Bigg(- \frac{\Delta t}{\tau_\infty exp\Big(\frac{\Delta F}{1+\beta U^2}\Big)}\Bigg) \tag{2.38}$$

From fig. 2.10 and 2.11 it is clear that survival probability becomes significantly different from 1 for voltages higher than 1 V and exposure times longer than 1 μs. The behavior of $S(U, \Delta t)$ is highly non-linear, and for high voltages or long exposure times S approaches a step-like shape. This is the reason that first led to the idea of a threshold voltage for PEF inactivation, usually identified at 1 V, although this revealed to be an oversimplification.

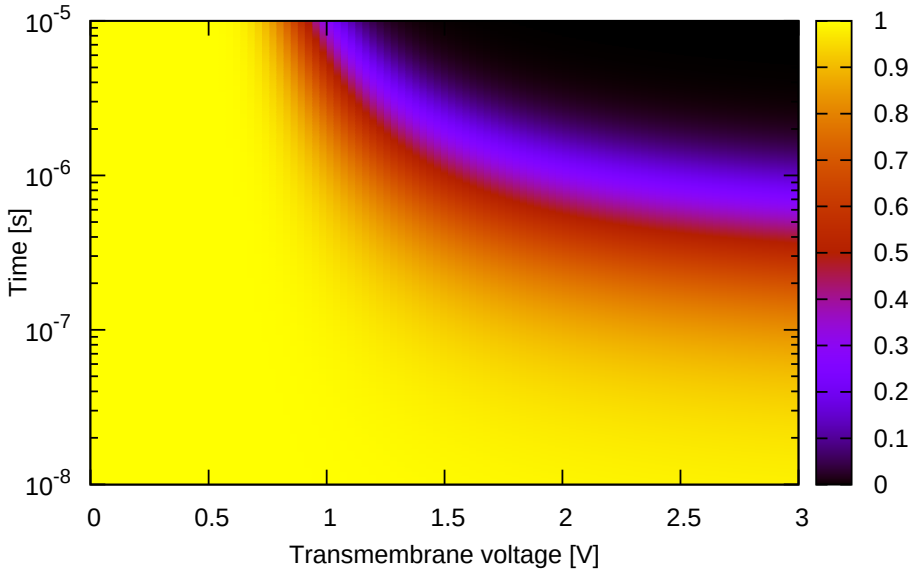

Figure 2.11: Plot of survival probability for a membrane experiencing a transmembrane voltage U for a time Δt, from eq. 2.38.

2.5 Corrections to the transient aqueous pore model

As previously mentioned, formation energy for hydrophilic pores in presence of a transmembrane potential U is generally described as

$$\Delta W_p(r) = 2\pi\gamma r - \pi\Gamma r^2 - \pi\frac{(\epsilon_w - \epsilon_m)}{2h}U^2 r^2 \tag{2.39}$$

This equation represents a parabolic barrier to the formation of hydrophilic pores. A more general expression for this is

$$\Delta W_p(r) = 2\pi\gamma r - \left[\int_0^r 2\pi\Gamma(r^*)r^* dr^*\right] + \left(\frac{C}{r}\right)^4 - \\ - \pi\frac{(\epsilon_w - \epsilon_m)}{2h}U^2 \int_0^r \alpha^2(r^*)r^* dr^* \tag{2.40}$$

Here the first term expresses the formation energy of the edge of a pore, the second term accounts for variations of surface tension Γ, the third term

describes the sterical repulsion between the lipid heads lining the pore and the fourth includes voltage-dependent Born energy corrections arising from the presence of ions in water near pores.

2.5.1 Surface tension

The assumption that surface tension Γ remains constant over the entire membrane and is not modified by the formation of pores becomes questionable when the results of molecular dynamics simulations on lipid membranes are considered [85]:

- In order to maintain a given cellular shape and size, a finite tension is required;
- The tension must change with the system area, and indirect experimental evidence of this variation is available for example in the activation of the 3-ns MscL channel cloned from *E. coli* [86] as well as in the influence of tension of vesicles under stress on lytic peptides [87] and in the catalytic activity of a β isoform of phospholipase C [88]. All these experiments suggest that tension must naturally be variable in order to allow certain biological activities;
- Since tension is, at least to the first order, proportional to the membrane area, formation of pores leads to variations in Γ proportional to the square of pore radius. A simple heuristic model has been proposed to describe this variation [89]

$$\Gamma(r) = \Gamma_0 \left[1 - \frac{r^2}{r_0^2} \right] \tag{2.41}$$

  with r_0 being a parameter whose value depends on time and voltage, to include dynamic effects. Thus pore formation and growth leads to reduction of Γ and to the creation of an additional local minimum in the pore formation energy $\Delta W_p(r)$ which could induce some pore to stabilize at some large radius rather than expand indefinitely;

A pore-density-dependent correction to the surface tension Γ has been proposed by [90]. Here the surface tension Γ_{eff} is defined as

$$\Gamma_{eff}(A) = \partial W / \partial A \tag{2.42}$$

where $W(A)$ is the total interface energy of a lipid bilayer of total area A, consisting of $2M$ lipid molecules, given by [91]

$$W(A) = 2M\eta = 2M[\sigma^{'} a + K/a] \cong 2[A\sigma^{'} + KM^2/A] \tag{2.43}$$

with $\sigma^{'}$ representing the interfacial energy per area of the hydrocarbon-water interface ($\sim 2 \times 10^{-2}$ Jm^{-2}), a the area per lipid head and K a constant. When pores of total area A_p are formed in the membrane, the total area A remains the same, but the effective membrane area sections reduces to $A_M = A - A_p$, leading to

$$W(A_M) = 2\sigma^{'}\left[A - A_p + \frac{A_0^2}{A - A_p}\right] \tag{2.44}$$

The constant A_0 is the equilibrium area for $\partial W/\partial A = 0$

$$A_0^2 = \frac{KM^2}{\sigma^{'}} \tag{2.45}$$

thus

$$\Gamma_{eff}(A_M) = 2\sigma^{'}\left[1 - \left(\frac{A_0}{A - A_p}\right)^2\right] \tag{2.46}$$

and we can express the effective tension in presence of pores in terms of the value without pores

$$\Gamma_{eff}(A_p) = \Gamma_{eff}(A_p = 0)\left[\frac{1 - \left(\frac{A_0}{A - A_p}\right)^2}{1 - \left(\frac{A_0}{A}\right)^2}\right] \tag{2.47}$$

Effective tension can be positive, zero or negative. The zero level is reached when $A_p = A - A_0$, while for larger pore areas the value of Γ_{eff} can be negative. Thus, while the second term in eq. 2.40 decreases the barrier for pore formation when Γ_{eff} is positive, i.e. when the membrane is not porated, the presence of pore can change the value of Γ_{eff} and force the surface energy term to act against the formation of pores.

2.5.2 Steric repulsion

Sterical repulsion between the lipid heads lining the pore can be taken into account, as suggested by [92], leading to to the third term in eq. 2.40, proportional to r^{-4}, where a typical value of C has been reported to be $9.67 \times 10^{-15} J^{0.25} m$.

2.5.3 Voltage-dependent Born energy corrections

The presence of ions in water near the pores can be taken into account to compute corrections to the Born energy associated to the presence of a transmembrane voltage across the pore [93, 94]. The electrostatic contribution to

formation energy in eq. 2.40 is expressed as a function of

$$\alpha(r) = \left[1 + \pi r \frac{\sigma_p(r)}{2h\sigma_b}\right]^{-1} \tag{2.48}$$

Here $\sigma_p(r)$ is the conductivity in a pore of radius r, while σ_b is the bulk electrolyte conductivity

$$\sigma_b = \Sigma_i (qZ_i)^2 \mu_i c_i \tag{2.49}$$

where q is the electron charge, Z_i, μ_i and c_i the charge state, mobility and concentration of the ith ion. The conductivity inside the pore is given as

$$\sigma_p(r) \sim \Sigma_i (qZ_i)^2 \mu_i c_i H_i(r) \times exp\left[\frac{P(\epsilon_w \epsilon_m)(qZ_i)^2}{4kT\pi r \epsilon_m}\right] \tag{2.50}$$

where $H_i(r)$ is a factor accounting for the sterically hindered motion of ions and molecules within the small volume of a pore, given by Renkin [95] in terms of the radius of the ith ion (r_i)

$$H_i(r) = \left[1 - \left(\frac{r_i}{r}\right)^2\right]\left[1 - 2.1\left(\frac{r_i}{r}\right) + 2.09\left(\frac{r_i}{r}\right)^3 - 0.95\left(\frac{r_i}{r}\right)^5\right] \tag{2.51}$$

and $P(\epsilon_w \epsilon_m)$ is the function described by Parsegian [58]. From these equations it is clear that $\alpha \to 0$ when $r \to \infty$, while $\alpha \to 1$ when $r \to 0$. Electrostatic energy factor in eq. 2.40 then tends to the factor in eq 2.27 in the limit of small pores, while it disappears for large pores.

2.5.4 Pore population

A single membrane can experience the presence of a large number of pores. The evolution of this pore population is described in the transient aqueous pore model as a combination of eq. 2.40 with a diffusion governed by continuum Smoluchowski theory

$$\frac{\partial n(r,t)}{\partial t} - \frac{D}{kT}\left[\frac{\partial}{\partial r}\left(n(r,t)\frac{\partial \Delta W_p(r)}{\partial r}\right)\right] - D\left[\frac{\partial^2 n(r,t)}{\partial^2 r}\right] = S(r) \tag{2.52}$$

where $n(r,t)$ is the pore density distribution function, D a pore diffusion constant and $S(r)$ the source term. The value of D as been estimated in two different experiments [96, 97], and can be taken in the range of $5 \cdot 10^{-14} ms^{-1}$. In this approach, the diffusion process is represented as a *random walk* of the pore radius in r space, brought by fluctuation in radius arising from the constant entry and egress of water molecules and other species. Here, again,

the stochastic nature of electroporation is revealed, which leads to a highly non-linear behavior very similar to a threshold behavior. The source term $S(r)$ represents the rate of pore formation. It is assumed that a collisional kinetic theory remains valid even for non gaseous phases, and the rate is estimated to be

$$S(r) = \frac{v_c h}{kT} \frac{\partial \Delta W_p(r)}{\partial r} exp\left(\frac{-\Delta W_p(r)}{kT}\right) dr dt \tag{2.53}$$

where v_c is an attempt rate density [78]. Pores are assumed to form initially as hydrophobic and to transform into hydrophilic if their radius exceeds a value r_* (see fig. 2.9). Thus $\Delta W_p(r)$ here is assumed to be

$$\Delta W_p(r) = 2\pi r h \sigma_0(\infty) I_1(R/\rho)/I_0(R/\rho) - \pi \frac{(\epsilon_w - \epsilon_m)}{2h} U^2 r^2 \tag{2.54}$$

Due to the exponential term in eq. 2.53 most of the pores will be created with very small radii. However, a non-zero probability for the formation of pores of any radius exists even in absence of a transmembrane voltage. Upon application of an external electric field, this probability greatly increases and formation of many pores of different sizes is predicted, leading to the phenomenon of electroporation. The information in $n(r,t)$ can be used in relation to eq. 2.47, since the total pore area of a membrane can be estimate as

$$A_p(r,t) \sim A_0 \left[\int_0^r 2\pi r^* n(r^*,t) dr^* \right] \tag{2.55}$$

provided mutual pore coupling and pore-pore interaction are negligible. Once we put everything together, the pore formation energy for hydrophilic pores in eq. 2.40 becomes

$$\Delta W_p(r) = 2\pi\gamma r - \left[\int_0^r 2\pi \Gamma_{eff}(A_p(r^*,t)) r^* dr^* \right] + \left(\frac{C}{r}\right)^4 - \\ - \pi \frac{(\epsilon_w - \epsilon_m)}{2h} U^2 \int_0^r \alpha^2(r^*) r^* dr^* \tag{2.56}$$

The stability of porated cells is therefore controlled by a combination of different parameters, including the surface tension, the ion conductance and the pore population. Analysis of eq. 2.56 in simple cases of fixed A_p can help visualize the effects of the variation of these parameters. In fig. 2.12 $\Delta W_p(r)$ is shown as a function of r with and without the electrostatic correction term, i.e. for $\alpha < 1$ and for $\alpha = 1$. In both the cases a situation of non-porated membrane ($A_p/A_0 = 0$) and of a specific pore area ($A_p/A_0 = 0.05$) is considered. The transmembrane voltage is taken to be 0.4 V.

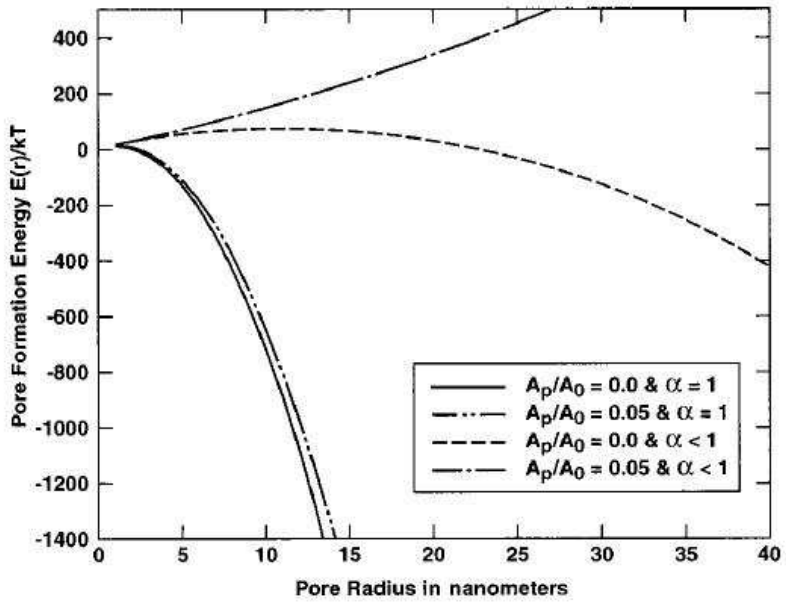

Figure 2.12: Pore formation energy for a 0.4 transmembrane voltage under various conditions of surface tension and pore population [90].

- $[\alpha = 1,\ A_p/A_0 = 0]$ The contribution to pore formation energy arising from the applied voltage is dominant, thus there is no energy barrier to pore formation. Pore can expand indefinitely and thus cause rupture of membrane;

- $[\alpha = 1,\ A_p/A_0 = 0.05]$ Formation energy is slightly higher than in the $A_p/A_0 = 0$ case, but still there is no barrier to pore formation;

- $[\alpha < 1,\ A_p/A_0 = 0]$ Pore formation energy dramatically increases, leading to the creation of a local minimum around 13 nm. The existence of a barrier for pore formation introduces a certain probability for membrane rupture, if we use the approach summarized in eq. 2.38;

- $[\alpha < 1,\ A_p/A_0 = 0.05]$ Inclusion of surface tension (and thus pore population) correction completely changes the energy function, which becomes a positive concave curve. Pores are thus naturally driven towards closure, and in fact under this conditions a pore population of such large radii able lead to $A_p/A_0 = 0.05$ could not be created in the first place;

As we see from the great difference between the first case, where no correction was considered, and the last case, the inclusion of surface tension and voltage corrections is of pivotal importance in order to describe the fate of an electroporated membrane. It is also clear that the effect of the membrane tension correction is stronger when the voltage correction term is considered. Analysis of pore formation energy in different conditions of applied voltage

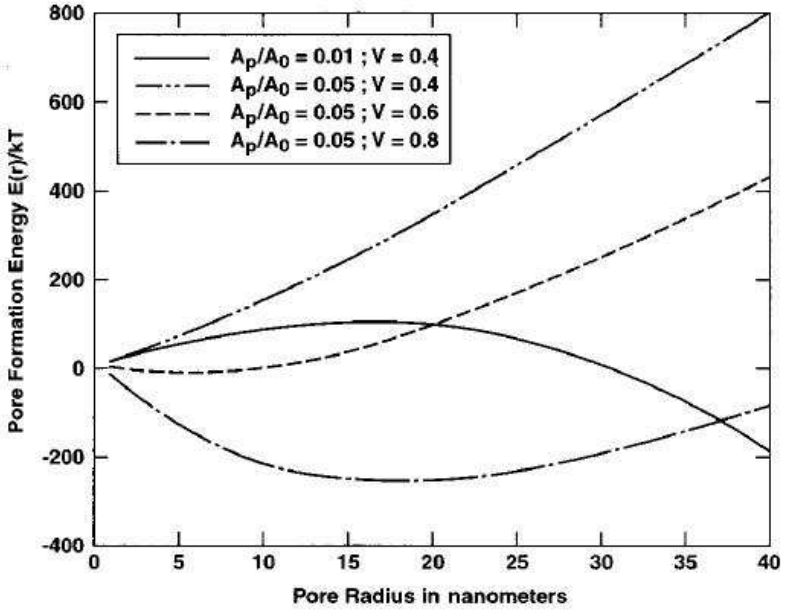

Figure 2.13: Pore formation energy for different transmembrane voltages and different values of pore population [90].

is considered in fig. 2.13. With a transmembrane voltage of 0.4 Volt, the difference between a relative porated area $A_p/A_0 = 0.01$ and $A_p/A_0 = 0.05$ is dramatical, showing a local maximum in the first case, around 16.5 nm, and a monotonic increase with radius in the second. The system could therefore evolve form an unstable condition when the pore population is lower, towards a stable condition with a greater porated area. When the transmembrane voltage is higher, but the porated area is kept at $A_p/A_0 = 0.05$, the effects of voltage contribution to energy formation start to be more important, and the creation of a local minimum around 7 nm is expected for 0.6 V. When the voltage is raised to 0.8 V, the trend remains unaltered, but the position of the minimum moves towards higher values. It is therefore expected that transmembrane voltages even higher could lead to membrane rupture. It is important to note here that this model predicts that changes in slope and

magnitude of $\Delta W_p(r)$ can easily occur and impact profoundly the evolution of pores and therefore the fate of the membrane.

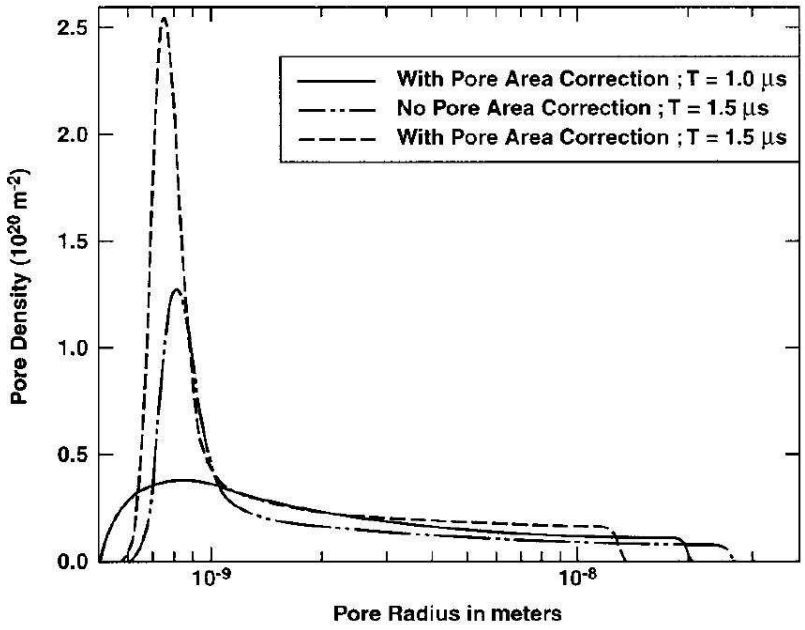

Figure 2.14: Pore distribution function at 1.0 μs and 1.5 μs in response to a 1.0 V, 1 μs pulse [90].

When eq. 2.56 is coupled with Smoluchowski eq. 2.52 dynamic effects are taken into account. In fig. 2.14 the pore distribution function is shown at 1.0 μs and 1.5 μs upon application of a 1.0 V, 1 μs electric pulse. In order to draw a comparison, a curve for 1.5 μs without the pore-area correction is also plotted. The 1.0 μs curve shows the situation at the point when the pulse is about to be turned off. In this moment the pore distribution is largely out of equilibrium, leading to the presence of pores with large radii. After 0.5 μs, however, the profile of $n(r)$ is shifted towards equilibrium, with the presence of a strong peak for the most probable pore radius, around 0.77 nm. For a comparison, the pore population predicted by the model without the pore area correction would lead to a lower peak shifted towards an higher radius, and, noticeably, largest maximum pore radii.

The forces arising from eq. 2.56 that drive the pores towards expansions are clearly the second and fourth term. It is anyway clear from what discussed in this section that the action of these forces decreases as the pore radius itself increases, and while the α factor and therefore the contribution of external

electric field goes to zero as the pore radius goes to infinity, the Γ_{eff} becomes negative for large radii, starting to act like a force driving the pore population towards smaller radii. The presence of pores in the membrane inhibits the pore growth itself. This mechanism of self-adjustment in $\Delta W_p(r)$ can limit uncontrolled pore expansion even for high voltages applied, and could give an hint to understand the deviations from first order kinetics of the microbial inactivation curves.

2.6 Transmembrane potential induced by an external electric field

The analysis of transmembrane potential in electroporation is carried out searching solutions to Laplace equation $\nabla^2 U = 0$ with appropriate boundary conditions (Ohmic model), i.e. the spacial distribution of charges ρ is not taken into account. The reason for this is found in the impossibility to solve analytically the equations when including a space charge distribution. Computer simulations carried out to investigate the validity of this approximation [98], anyway, revealed that, although the Ohmic model predicts a different electric field distribution in the suspension liquid and in the cytoplasm near the cell membrane, the prediction for the electric field inside the membrane and therefore the transmembrane potential is the same in both the Ohmic and the charge space model.

Transmembrane potential in cell electroporation has first been analyzed by Schwan [57] in the approximation of non-conductive membrane and spherical shape.

$$U = \frac{3}{2} r_c E \cos(\theta) \tag{2.57}$$

where r_c is the membrane radius, E the applied electric field and θ the polar angle with respect to the electric field. Although this result is correct, it describes only the steady state situation without giving any information about the time development of this potential. Since PEF involves application of short pulses, in the order of microsecond, the charging process needs to be analyzed in depth. The correct solution to this problem has been given by Kotnik [99]

$$\begin{aligned}\frac{\Delta\Phi_m(t)}{R\cdot\cos\theta} = \frac{a_3}{b_3}\cdot E_0(t) + \left[\frac{a_1}{2b_1} - \frac{a_3}{2b_3} + \frac{\frac{a_1 b_2}{2b_3} - a_2 + \frac{a_3 b_2}{2b_3}}{\sqrt{b_2^2 - 4b_1 b_3}}\right]\cdot\left(1 - e^{-\frac{t}{\tau_1}}\right)\cdot E_0(t) \\ + \left[\frac{a_1}{2b_1} - \frac{a_3}{2b_3} + \frac{\frac{a_1 b_2}{2b_3} - a_2 + \frac{a_3 b_2}{2b_3}}{\sqrt{b_2^2 - 4b_1 b_3}}\right]\cdot\left(1 - e^{-\frac{t}{\tau_2}}\right)\cdot E_0(t)\end{aligned} \tag{2.58}$$

upon the application of a squared pulse $E_0(t)$ for a cell of radius R, where

$$\tau_1 = \frac{2b_3}{b_2 - \sqrt{b_2^2 - 4b_1b_3}}$$

$$\tau_2 = \frac{2b_3}{b_2 + \sqrt{b_2^2 - 4b_1b_3}} \tag{2.59}$$

and

$$\begin{aligned}
a_1 &= 3d\lambda_0(\lambda_i(3R^2 - 3dR + d^2) + \lambda_m(3dR - d^2)) \\
a_2 &= 3d((\lambda_i\epsilon_0 + \lambda_0\epsilon_i)(3R^2 - 3dR + d^2) + (\lambda_m\epsilon_m)(3dR - d^2)) \\
a_3 &= 3d\epsilon_0(\epsilon_i(3R^2 - 3dR + d^2) + \epsilon_m(3dR - d^2)) \\
b_1 &= 2R^3(\lambda_m + 2\lambda_0)\Big(\lambda_m + \frac{1}{2}\lambda_i\Big) + 2(R-d)^3(\lambda_m - \lambda_0)(\lambda_i - \lambda_m) \\
b_2 &= 2R^3\Big(\lambda_i(\frac{1}{2}\epsilon_m + \epsilon_0) + \lambda_m(\frac{1}{2}\epsilon_i + 2\epsilon_m + 2\epsilon_0) + \lambda_0(\epsilon_i + 2\epsilon_m)\Big) + 2(R-d)^3 \\
&\quad \times(\lambda_i(\epsilon_m - \epsilon_0) + \lambda_m(\epsilon_i - 2\epsilon_m + \epsilon_0) - \lambda_0(\epsilon_i - \epsilon_m)) \\
b_3 &= 2R^3(\epsilon_m + 2\epsilon_0)\Big(\epsilon_m + \frac{1}{2}\epsilon_i\Big) + 2(R-d)^3(\epsilon_m - \epsilon_0)(\epsilon_i - \epsilon_m)
\end{aligned} \tag{2.60}$$

while λ_i,ϵ_i,λ_m,ϵ_m,λ_0,ϵ_0 are the conductivities and permittivities of cytoplasm, membrane and extracellular medium. In fig. 2.15 the behavior of $\Delta\Phi_m(t)$ is plotted for different cell radii. Although this result is correct and accepted, it describes $\Delta\Phi_m(t)$ only for spherical cells and, most importantly, does not take into account the effects of electroporation itself, since the conductivity of the membrane is considered to remain constant during the pulse. This is clearly a great limitation when we want to use this result to analyze the process of electroporation, since the creation of pores in the membrane, filled with the conductive suspension liquid, will increase the conductivity of the membrane itself and thus reduce the voltage drop. Imaging of transmembrane potential by means of a pulsed-laser fluorescence microscope confirms this observation [100]. Transmembrane potential was visualized in sea urchin eggs with a voltage-sensitive fluorescent dye, and the results can be seen in fig. 2.16. Urchin eggs used in this experiment have a radius of about 50 μm, thus an applied electric field of 100 V/cm as reported in fig. 2.16 should rise a transmembrane voltage of 0.75 V for the position $\theta = 0$. In this situation electroporation is likely to happen, but the formation of pores could still be small enough not to influence $\Delta\Phi_m(t)$ too much. Anyway, when the electric field was increased to reach 400 kVcm^{-1} and compared to a 67 V/cm, the effects of electroporation could be visualized as in fig. 2.17. Dotted lines in figure as used as a control, since for such an intensity of electric field the

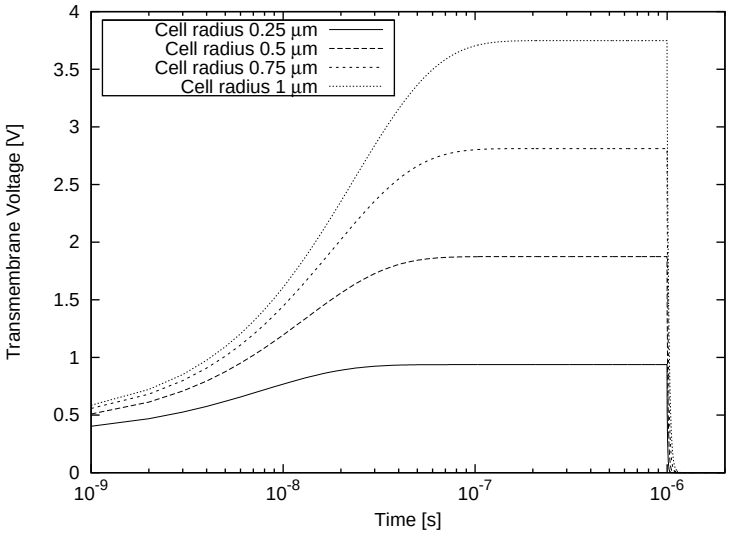

Figure 2.15: Transmembrane potential for different cell radii at $\theta = 0$, $\rho = 5$ Ωm, $E_0 = 25$ kVcm^{-1} and Δt $= 1$ μs.

electroporation is considered very unlikely, and in fact they approximately follow a cosine shape and remain constant, after an initial increase, up to 1 ms, as expected from eq. 2.58. If electroporation had not taken place, or if it had not influenced the transmembrane potential, we would expect the solid lines, obtained for a 400 V/cm pulse, to be just a 6-fold magnification of the dotted profile. As a matter of fact, these lines are instead at the top and the bottom, showing a saturation behavior. This saturation can be explained with the creation of pores. Very interesting to note here, the process of electroporation seems to start first on the side of the cell facing the positive electrode, but the majority of damages seems to occur to the side facing the negative one. An explanation for this phenomenon could be found in the resting potential of the cell membrane itself (around 80 mV), although this is probably just a partial cause, while the major reason for this asymmetry is probably in the structure of the cell membrane.

This results demonstrate that a combined approach between a description of electroporation probability and of transmembrane potential is needed to understand many observed features of PEF.

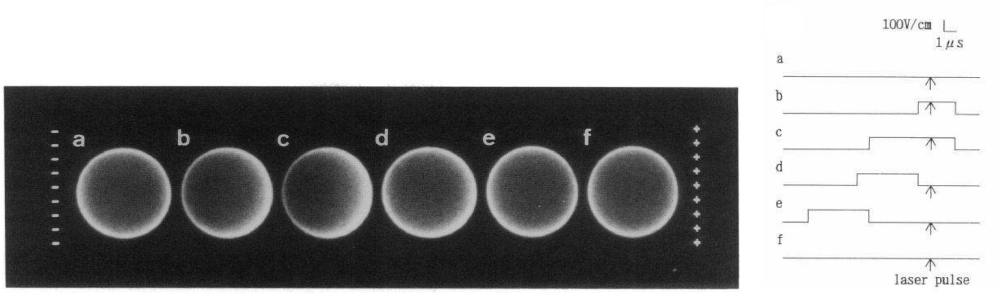

Figure 2.16: Fluorescent images of sea urchin eggs. The timing sequence used to obtain the six images is reported on the right [100].

2.7 Combination of transient aqueous pore model and transmembrane potential analysis

The models described in previous sections either focus on the pore creation and evolution, using a very simple description of transmembrane potential, or solve in details the problem of voltage across the membrane for an intact membrane. Recent works try to combine these approaches [101] by means of numerical simulations. A spherical cell of radius a in a conductive medium is exposed to an electric field E. Based on the Laplace equations for intracellular and extracellular potentials Φ_i and Φ_e, and the inclusion of the external electric field E as a condition on Φ_e

$$\Phi_e(t, \rho, \theta) = -E\rho\cos\theta \tag{2.61}$$

for $\rho \to \infty$, where ρ is the radial spherical coordinate and θ the polar angle measured with respect to the direction of E, the current density across the cell membrane is described as

$$-\hat{n}\cdot(\sigma_i\nabla\Phi_i) = -\hat{n}\cdot(\sigma_e\nabla\Phi_e) = C_m\frac{\partial V_m}{\partial t} + g_s(V_m - V_{rest}) + I_p \tag{2.62}$$

where $\hat{n}$ id the outward unit vector normal ti the membrane, $V_m(t,\theta) \equiv \Phi_i(t,a,0) - \Phi_e(t,a,0)$ is the transmembrane potential, σ_i and σ_e the intracellular and extracellular conductivities, g_s the surface conductance of the membrane and V_m the rest potential of a membrane not exposed to external electric field. The current density is therefore defined as the sum of a capacitive current, a current through protein channels and a current through

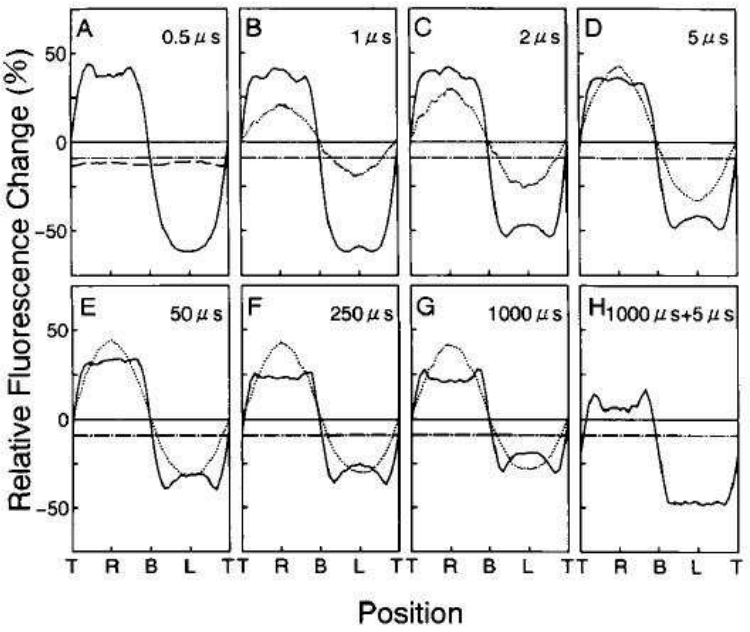

Figure 2.17: Fractional fluorescence change observed at indicated time points in a rectangular electric pulse, for different positions on the cell. Dotted line 67 V/cm, solid line 400 V/cm. Positions are indicated as T, top ($\theta = \pi/2$), R, right ($\theta = 0$), B, bottom ($\theta = -\pi/2$) and L, left ($\theta = \pi$) with respect to fig. 2.16 [100].

electropores, I_p, expressed as

$$I_p(t,\theta) = \sum_{j=1}^{K^\theta} \frac{i_p(r_j^\theta, V_m)}{\Delta A} \tag{2.63}$$

where ΔA is a portion of cell area corresponding to a discrete angle $\Delta\theta$, containing K^θ pores. The current through a single pore i_p is defined as

$$i_p = \frac{V_m}{R_p + R_i} \tag{2.64}$$

This definition takes into account the impossibility for a pore (at least for a large pore) to maintain the same voltage drop V_m that develops across an intact membrane. The drop V_m occurs across two resistances connected in series, with

$$R_p = \frac{h}{\pi\sigma r^2} \tag{2.65}$$

the actual pore resistance, and

$$R_i = \frac{1}{2\sigma r} \tag{2.66}$$

the input resistance. Here h is the membrane thickness and σ the conductivity of the liquid filling the pore. Nucleation of an hydrophilic pore

$$\frac{dN}{dt} = \alpha e^{(V_m/V_{ep})^2}\left(1 - \frac{N}{N_{eq}(V_m)}\right) \tag{2.67}$$

where $N(t,\theta)$ is the pore density and N_{eq} the equilibrium pore density for a given voltage V_m

$$N_{eq}(V_m) = N_0 e^{q(V_m/V_{ep})^2} \tag{2.68}$$

In these equations a voltage threshold for electroporation is considered, V_ep. The parameter q in eq. 2.68 is r_m/r_*, where r_m is the minimum energy radius for $V_m = 0$ and r_* is the minimum radius for hydrophilic pores. Pore evolution is controlled by

$$\frac{dr_j}{dt} = U(r_j, V_m, \Gamma_{eff}) \tag{2.69}$$

where U is the advection velocity

$$U(r_j, V_m, \Gamma_{eff}) = \frac{D}{kT}\left[\frac{V_m^2 F_{max}}{1 + \frac{r_h}{r+r_t}} + 4\beta\left(\frac{r_*}{r}\right)^4 \frac{1}{r} - 2\pi\gamma + 2\pi\Gamma_{eff} r\right] \tag{2.70}$$

for $r \geq r_*$. The first term accounts for the electric force induced by the local transmembrane potential V_m, the second for the steric repulsion of lipid heads, while the third and fourth are analogous to the terms of eq. 2.21. F_{max} is defined as the maximum electric force for $V_m = 1V$, while r_h and r_t are constants for the advection velocity. Finally, Γ_{eff} is expressed as

$$\Gamma_{eff}(A_p) = 2\Gamma' - \frac{2\Gamma' - \Gamma_0}{(1 - A_p/A)^2} \tag{2.71}$$

where Γ_0 is the tension of the membrane without pores, Γ' the energy per area of the hydrocarbon-water interface, $A_p = \Sigma_{j=1}^{K} \pi r_j^2$ the total porated area and A the surface of the cell. The results of numerical simulations, carried out for a 50μm cell exposed to a 40 kVcm^{-1} external electric field for 1 ms are shown in fig. 2.18 and 2.19. In fig. 2.19 (A) dotted lines separate

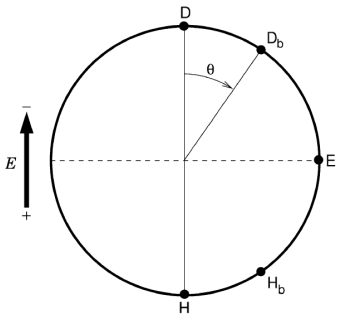

Figure 2.18: Definition of relevant positions on cell membrane [101].

the three fundamental stages of electroporation: charging, pore nucleation, and pore evolution. Charging can be seen to last about 0.51 μs, followed by the formation of the first pore on the hyper-polarized pole (H) of the cell. Locations on the membrane where V_m exceeds $\sim$ 1 V have a great probability to develop pores, and since the presence of such pores will increase the conductance of the membrane, the shape of V_m itself will not follow the charging transient that would be observed in a cell with intact membrane. The result of this can be seen in fig. 2.20. As we can see, the predicted behavior of V_m seems, at least qualitatively, to resemble the measured $V_m(t, \theta)$ in fig. 2.17.

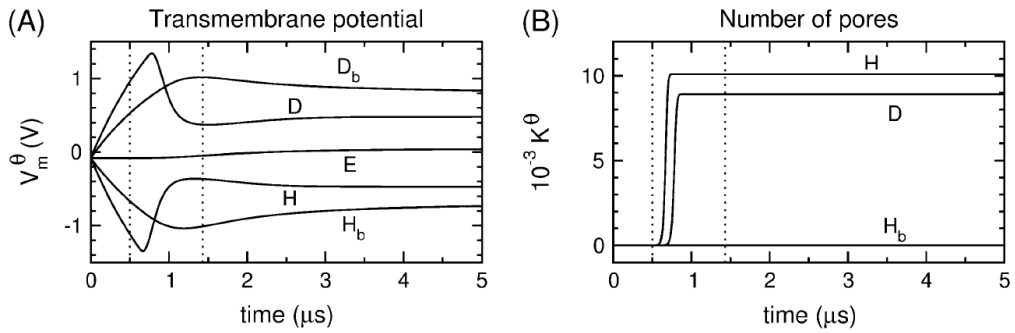

Figure 2.19: Evolution of electroporation in a cell. (A) Transmembrane potential. (B) Number of pores K^θ. K^θ of 10^4 corresponds to a pore density of 10^{13} pores/m^2 [101].

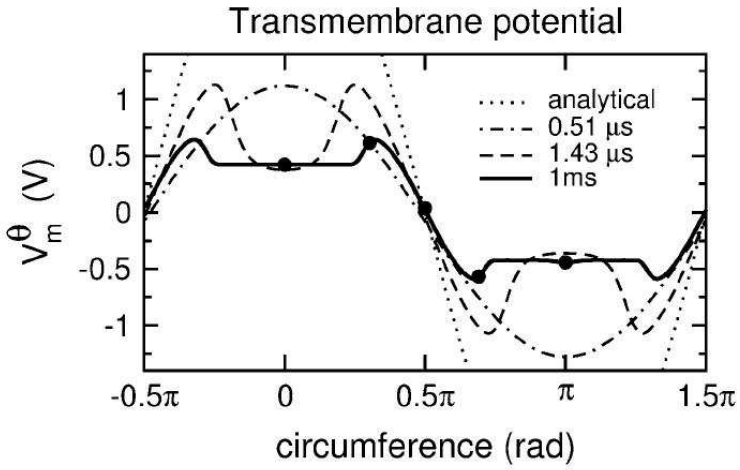

Figure 2.20: Transmembrane potential spatial distribution at times indicated in the legend [101].

2.8 Alternative description of membrane electroporation

A different approach to electroporation has been developed that takes into account Maxwell stresses on the lipid membrane [102]. In previous theories electroporation was explained as related to the appearance of a condenser energy for a pore in a membrane immersed in an external electric field. How-

ever, since the pore becomes conductive, at least for hydrophilic pores over a certain radius, while the lipid membrane remains extremely more resistive (6-7 orders of magnitude), the voltage across the pore will collapse. Instead of using dielectric energies to treat the interaction with the electric field, the forces can be calculated from the Maxwell stresses

$$T_{l,m} = \epsilon_r \epsilon_0 [E_l E_m - \frac{1}{2} \delta_{l,m} E^2] \tag{2.72}$$

Neglecting the the finite thickness of the membrane, the potential ϕ can be expressed as

$$\phi(r,z) = \pm \frac{\phi_0}{\pi} \cot^{-1} \left(\frac{2a^2}{r^2 + z^2 - a^2 + [(r^2 + z^2 - a^2)^2 + 4a^2 z^2]^{\frac{1}{2}}} \right)^{-\frac{1}{2}} \tag{2.73}$$

where ϕ_0 is the potential difference across the membrane far away from the pore, $r^2 = x^2 + y^2$ and a is the radius of the pore. The different signs hold for the upper ($z > 0$) side of the membrane, where the sign is takes positive, and the lower ($z < 0$), where it is taken negative. From this expression it is possible to calculate

$$E_r = -\frac{\phi_0}{\pi} \frac{a}{r(r^2 - a^2)^{\frac{1}{2}}} \tag{2.74}$$

$$E_z = -\frac{2\phi_0}{d\pi} \tan^{-1} \left(\frac{r^2}{a^2} - 1 \right)^{\frac{1}{2}} \tag{2.75}$$

where d is the membrane thickness. The forces acting on the membrane can be divided into those acting at the lipid-water interfaces which are parallel to the xy plane, and those felt by the membrane edge. The normal forces exerted on the upper and lower interface cancel each other, while the radial force density is

$$f_{rz} = -\epsilon_l \epsilon_0 E_r E_z < 0 \tag{2.76}$$

on either interface. The sum of the two forces is related to a Maxwell lateral tension Γ_M

$$2 f_{rz} = \frac{\partial \Gamma_M}{\partial r} \tag{2.77}$$

Integration leads to

$$\Gamma_M = -2\epsilon_l \epsilon_0 \int_a^r dr E_r E_z = -\frac{1}{2} \epsilon_l \epsilon_0 \frac{[2\phi(r, z = +\epsilon)]^2}{d} \tag{2.78}$$

the same result that can be obtained with the usual condenser approach. The force density f_{rz} has to be balanced by a mechanical force, in an immobile

membrane. Thus there is an electrical induced mechanical lateral tension Γ_{el} for which $\Gamma_M + \Gamma_{el}$ =const. This Γ_{el} can be expected to be 0 far away from the pore and

$$\Gamma_{el} = -\frac{1}{2}\epsilon_l \epsilon_0 \frac{\phi_0^2}{d} \tag{2.79}$$

at the pore boundary, where ϕ is practically 0. Being Γ_{el} negative, it will resist the opening of a pore. The force acting of the edge of the pore is obtained by integrating the Maxwell stresses over a cylinder of infinitesimal radius, if the the edge is considered, in a first approximation, a straight line. Starting from

$$\phi = \frac{\phi_0}{\pi}\left(\frac{2\rho}{a}\right)^{\frac{1}{2}} \sin\frac{\theta}{2} \tag{2.80}$$

for the potential in water near the membrane edge, carrying out the integration

$$F_r = \frac{\epsilon_w \epsilon_0 \phi_0^2}{2\pi a} \tag{2.81}$$

and since $F_r = -\gamma_{el}/a$

$$\gamma_{el} = -\frac{\epsilon_w \epsilon_0 \phi_0^2}{2\pi} \tag{2.82}$$

Given equations 2.79 and 2.82, the basic equation of transient aqueous pore model, eq. 2.21, can be modified replacing

$$\gamma \rightarrow \gamma_{eff} = \gamma + \gamma_{el} \tag{2.83}$$

$$\Gamma \rightarrow \Gamma_{eff} = \Gamma + \Gamma_{el} \tag{2.84}$$

as the effective values of the edge energy and of lateral tension acting on pore boundary. The equilibrium radius can be calculated as usual

$$a^* = \frac{\gamma_{eff}}{\Gamma_{eff}} = \frac{\gamma - \epsilon_w \epsilon_0 \frac{\phi_0^2}{2\pi}}{\Gamma - \epsilon_l \epsilon_0 \frac{\phi_0^2}{2d}} \tag{2.85}$$

while the height of the energy barrier is

$$E(a^*) = \frac{\pi \gamma_{eff}^2}{\Gamma_{eff}} = \frac{\pi\left(\gamma - \epsilon_w \epsilon_0 \frac{\phi_0^2}{2\pi}\right)^2}{\Gamma - \epsilon_l \epsilon_0 \frac{\phi_0^2}{2d}} \tag{2.86}$$

Depending on ϕ_0 and the value of the constants γ and Γ, γ_{eff} and Γ_{eff} can be positive or negative. As their initial values, i.e. for $\phi_0 = 0$, are the positive quantities γ and Γ, if we consider ϕ_0 as a parameter and we

increase it continuously, either first γ_{eff} or Γ_{eff} becomes zero. In the first case, an enhancement of the field reduces the critical radius and promotes rupture, while in the second an increase of ϕ_0 stabilizes the membrane and causes stable pores at higher voltages (see fig. 2.21). Experiments seems to

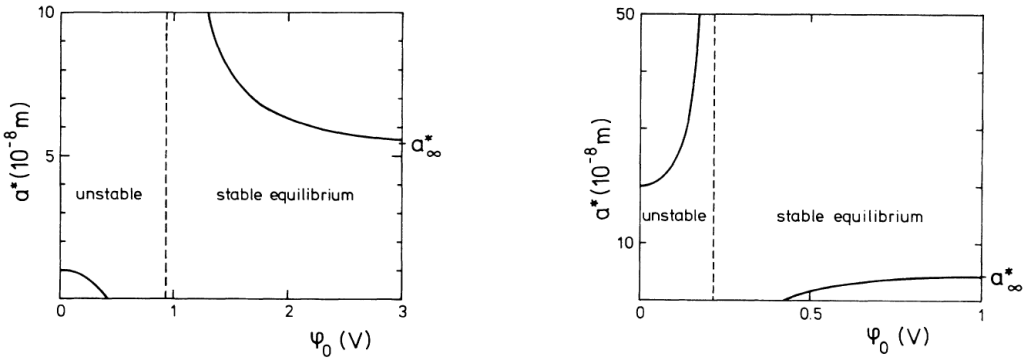

Figure 2.21: Equilibrium pore radius a^* as a function of transmembrane voltage for $\gamma = 2 \cdot 10^{-11}$ Jm^{-1}, $\Gamma = 2 \cdot 10^{-3}$ Nm^{-1} (left) and $\gamma = 2 \cdot 10^{-11}$ Jm^{-1}, $\Gamma = 0.1 \cdot 10^{-3}$ Nm^{-1} (right) [102].

favor the first case, since high voltages are reported to enhance membrane rupture, and thus only this situation is analyzed in details. The evolution of pore radius under electric field is predicted to be

$$a(t) = a_0 + \sqrt{\frac{\Phi\Gamma}{\rho d}} = a_0 + \alpha t \tag{2.87}$$

where ρ is the density of the membrane and Φ a parameter taking irreversible contribution into account [103]. This model can be verified experimentally through the analysis of the time course of conductivity in a flat bilayer lipid membrane, where this conductivity can be related to the equation above with

$$G(t) = 2k(a_0 + \alpha t) \tag{2.88}$$

Fig. 2.22 shows the results for a diphytanoyl phosphatidylcholine membrane bathed in 100 mM LiCl, for a pulse of 1 μs. It is interesting to note that the initial slope of the curve, 0.3 S/s, changed after about 10 μs to 0.6 S/s. This seems to indicate the opening of a second pore. Although this approach seems therefore to be confirmed by experiments, it does not involve any explanation of the stochastic nature of electroporation and it can not be considered as completely satisfying. The energy corrections taken into

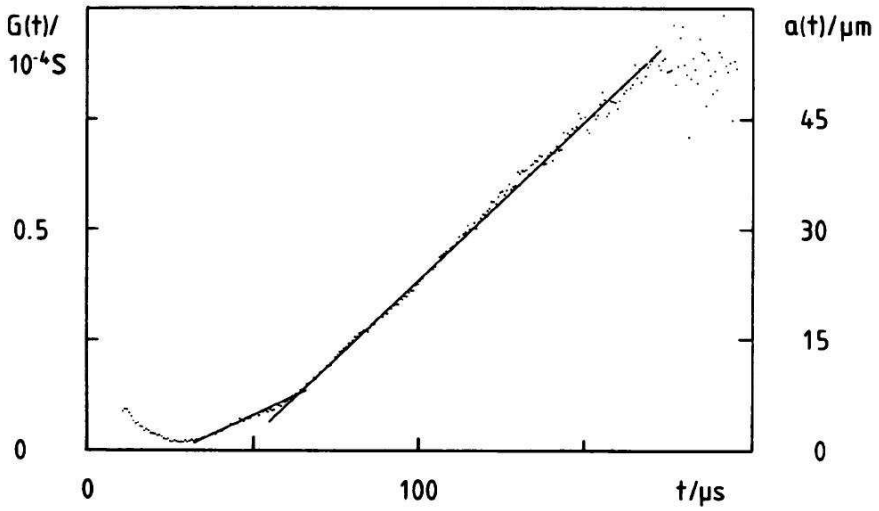

Figure 2.22: Conductance versus time during irreversible breakdown. The radius of the pore is indicated on the right [102].

account in developing the transient aqueous pore model should be included in this approach in order to reach a better description of electroporation. Furthermore, the good agreement between theory and experiments is verified in flat membranes, while remains to be investigated the effects of curvature on this kind of approach.

2.9 Conclusions

The ability of cell membranes to shield cytoplasm from ions and charged molecules is of key importance for the survival of a cell. Probability of spontaneous crossing of an intact membrane is highly improbable but can be shown to increase for porated membranes. Observations of planar lipid bilayers under the effect of electric fields show a general pattern of capacitor charge followed by fluctuations of current and membrane rupture. Current fluctuations are related to the creation of pores across the membrane, and therefore this phenomenon is referred to as electroporation. Among the theories that tries to explain membrane rupture, the transient aqueous pore model is the only one accounting for the stochastic behavior of electroporation revealed by experiments. Membrane rupture is regarded as a phase transition to a more stable state triggered by thermal lateral fluctuations of phospholipids. In normal conditions, the probability of spontaneous break-

down is negligible, but on application of an external electric field the energy barrier for rupture decreases rapidly until indefinite expansion of a pore, and therefore cell death, becomes probable. Further improvements to this model of variations of membrane surface tension, the inclusion of steric repulsion between the lipid heads, voltage-dependent corrections to Born energy and the effect of pore population. The time course of transmembrane potential affects the development of pores and can be included in the theory as well. Alternative descriptions of electroporation have been proposed, particularly analyzing the Maxwell stresses on the lipid bilayer, but they all fail to account for the stochastic nature of membrane rupture.

Although the transient aqueous pore model represents the best explanation of electroporation developed so far, the exact mechanism of this phenomenon has not been understood completely, particularly at molecular level. Experimental tests, furthermore, are mainly carried out on flat artificial membranes, and the validity of these theories has yet to be demonstrated on real cells. Finally, the predictions of transient aqueous pore model on inactivation levels of real cells are not in quantitative agreement with laboratory measures, as will be discussed in Chapter 3 and 4. Although this disagreement can partly be explained by fluctuations in physiological conditions of cells, it also suggests the incompleteness of the present theories of electroporation.

Chapter 3

Theoretical analysis

The survival probability for a cell in an external electric field is predicted to be a constant value for a given choice of field intensity and cell dimensions. Consider, for example, a PEF experiment on *E. coli* at 25 kVcm^{-1}, carried out at 300°K. If we want to use eq. 2.38 to compute the survival probability, as a first approximation, we need to derive the maximum transmembrane potential U from eq. 2.1, in the assumption that the process of membrane charging is instantaneous with respect to the pulse duration. Usually, being *E. coli* not spherical, R is taken to be half of the cell major axis L, whose average value can be estimated in 2.72 μm. Thus probability to survive after each pulse in these conditions is

$$S = 7.1\% \tag{3.1}$$

Cell populations are in the order of 10^8-10^9 CFU/ml and we can therefore safely assume that the frequency of inactivation is well approximated by the probability p=(1−S). The expected inactivation curve, plotted in logarithmic scale, should therefore approximate to a straight line, at least until the number of bacteria involved is large enough. This is in general not found in actual experiments, as can be seen in fig. 3.1. The inactivation curves seem to reach a plateau at 4-5 Logs of relative inactivation. Error bars here are intentionally not drawn, since the evaluation of uncertainties in biological experiments is rather complicated and needs to be discussed. Given the long times involved in growing, plating, incubating and counting bacteria, more than triple measures of the same concentration in each experiment are practically impossible. Taking into account all the possible sources of error, the precision of a single measure can be taken around 5%. In principle, this precision should not depend on the number of applied pulses, if the resulting concentration is not too low for the Gaussian statistical regime. Since the lowest final concentrations of these experiments are more than $\sim 10^4$

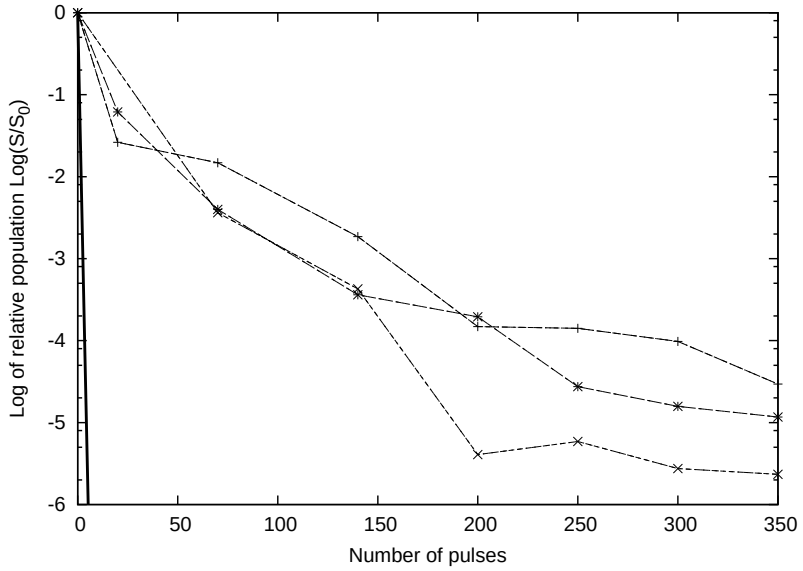

Figure 3.1: Relative survival population in a typical PEF experiment. Solid line gives the expected curve from eq. 3.1, compared to examples of three different real PEF experiments at 25 kVcm^{-1}, 1 μs, 1 Hz, on *E. coli*.

CFU/ml, we should expect the results of different experiments in the same conditions to be distributed following the same relative standard deviation across the entire inactivation curve, whatever this deviation is. This is clearly in contrast with fig. 3.1, and it is a general rule for PEF experiments. This behavior of the standard deviation is therefore not an effect of the biological process of measure, but has to be somehow related to the PEF experiment itself. In order to explain these curves and to be able to reliably predict the inactivation rates, we need to analyze PEF experiments in more depth, carefully evaluating the correctness of each assumption made to derive the expected straight line in Log scale. In particular, we will investigate whether it is correct to consider

- the electric field as constant over the entire treatment region;
- the process of cell charging as instantaneous and influenced by the global dimension of the cell;
- the steady state value of $\Delta\varphi_m$ to be given by eq. 2.1 even for non spherical cells;
- the dimensions of cells in a sample to be identically the same;

- the average cell dimensions of different samples grown in different days of the same species to be constant.

3.1 Simulations of the electric field in a treatment chamber

The treatment cell used in our PEF experiments consists of two cylindrical electrodes made of stainless steel, hold coaxially by a plastic spacer. The size of the spacer defines the gap between the electrodes and the treatment area. Insert of treatment liquid is allowed by a hole in the center of the spacer. A schematic drawing of the apparatus can be seen in fig. 3.2. The gap between

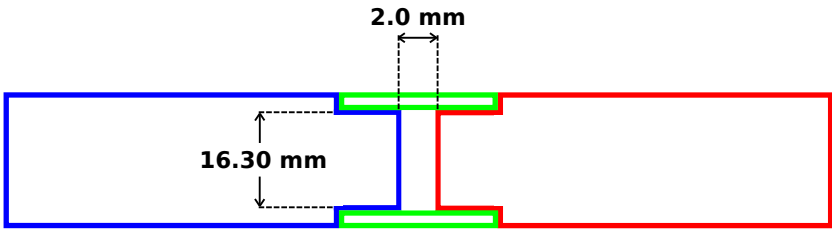

Figure 3.2: Schematic drawing and dimensions of the treatment cell.

the electrodes is 2.0 mm, and the diameter of electrodes 16.30 mm. To match the PFN impedance of 50 Ω, the conductivity of the suspension liquid has to be 0.2 Sm^{-1}. We expect the electric field in the treatment chamber to be 25 $kVcm^{-1}$ for a voltage between the electrodes of 5 kV, but, because of the finite dimensions of the electrodes, it will not be constant over the entire volume of the chamber. Since the survival probability is affected by the intensity of the electric field applied to the cell, the presence of areas where the effectiveness of the treatment is considerably different from the desired one has to be taken into account. The real distribution of the electric field has therefore been simulated, as can be seen in fig. 3.3, where only the area near the edge of an electrode is shown. The distribution of the electric field in the treatment area and the relative volume experiencing at least the electric field in abscissa are shown in fig. 3.4. The electric field near the edges can reach very high intensities, over 100 $kVcm^{-1}$, which could be problematic in terms of possible electric breakdowns. Although the breakdown voltage of a liquid solution in this range of conductivity for a 1 μs pulse has been reported to be in the range of 300 $kVcm^{-1}$ [104], the presence of air bubbles inside the chamber, or the formation of gas due to electrolysis, could highly increase

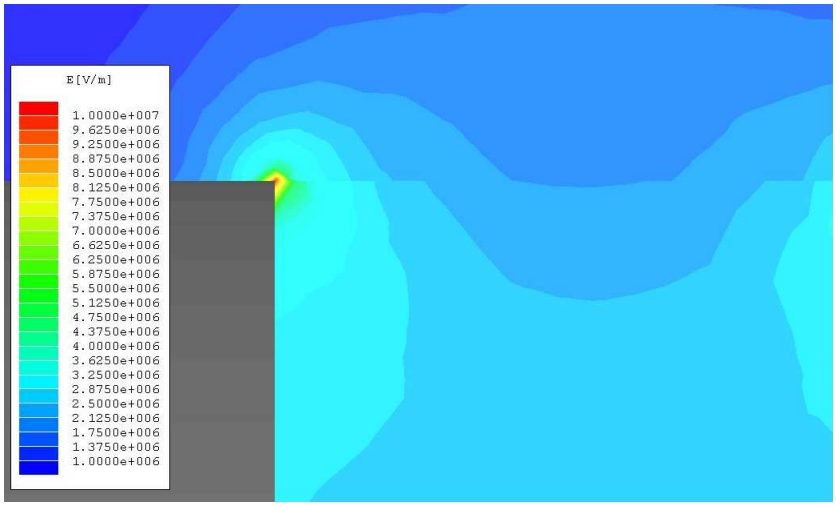

Figure 3.3: Simulation of electric field intensity near the edge of an electrode.

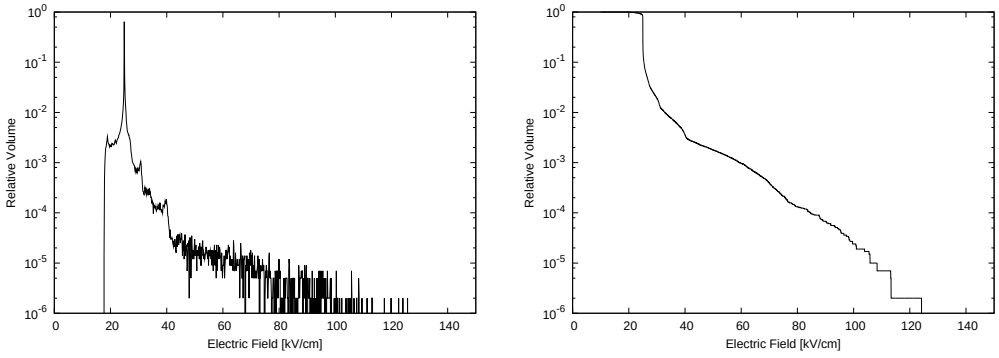

Figure 3.4: Distribution of the electric field in the treatment area (left) and relative volume experiencing at least the electric field in abscissa (right).

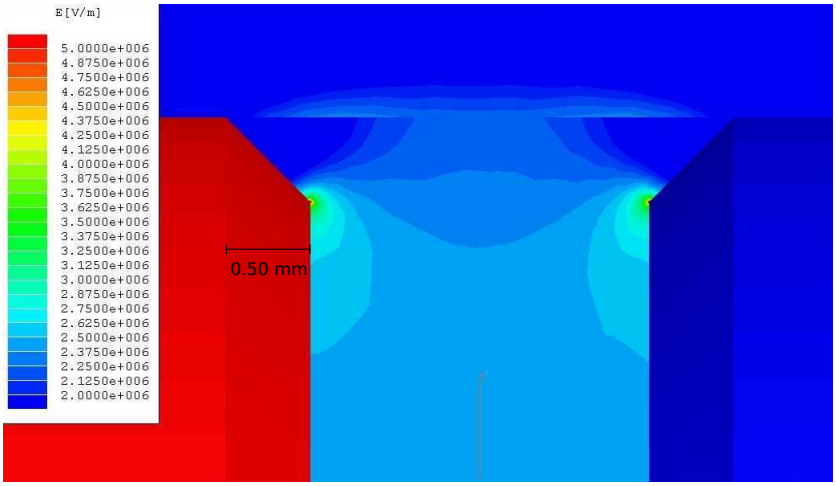

Figure 3.5: Electric field simulation with a bevel edge of 0.50 mm.

the probability of breakdowns for these field intensities. Furthermore, the presence of a sharp edge could make the assembly of the chamber difficult and lead to damages of the plastic spacer. For these reasons, a bevel of 0.50 mm of the edges was decided. In fig. 3.5 the electric field intensity simulated for this configuration is shown. Comparison between fig. 3.4 and 3.5

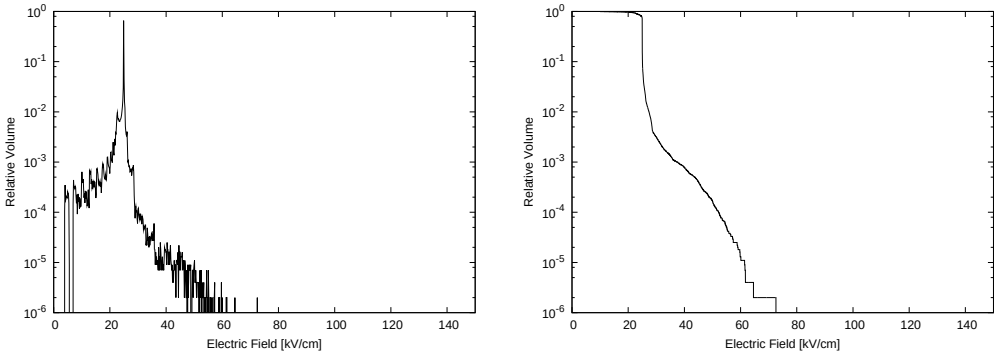

Figure 3.6: Distribution of the electric field in the treatment area (left) and relative volume experiencing at least the electric field in abscissa (right) in the real treatment chamber.

shows how the maximum electric field is consistently decreased by the bevel edge, but on the other side the relative volume where the PEF treatment is less effective than the average is increased. The portion of treatment cell that experiences at least an acceptable electric field of above 24.5 $kVcm^{-1}$

is evaluated in the 82.3% of the total volume. A portion of 13.8% of the total volume experiences an electric field between 20 and 24.5 $kVcm^{-1}$, while for the remaining 3.8% the electric field is below 20 $kVcm^{-1}$. Inactivation probability in the fraction of volume where the electric field is between 20 and 24.5 $kVcm^{-1}$ is still very close to the one expected for the main core of the cell, while for the latter is considerably less. This has to be taken into account when analyzing the inactivation levels that can be reached through our experimental setup.

3.2 Membrane curvature and time course of transmembrane voltage

The steady state value of transmembrane potential can be evaluated from Schwan eq. 2.1 for spherical cells. The process of membrane charging, however, is not instantaneous and, if its time scale is comparable to the length of the electric pulse, the effective value of potential and therefore the inactivation probability could be affected. A solution for spherical cells has already being described by eq. 2.58, but, since the bacteria used in our experiments are not spherical, nor their shape can be approximated to a regular geometrical surface, we need to find a general approach to understand the effect of an external electric field on any membrane. Computer simulations of electric field intensity are not useful in this subject, since they, in general, do not take into account the process of membrane charging due to charge accumulation at the boundaries. The value of electric field given by these simulation is thus very similar to the electric field arising from the disparity between the relative permittivities of the liquids, both cytoplasm and suspension, being around 80, and of the plasma membrane, being around 2. The time course of transmembrane voltage in response to a DC step voltage can be analyzed using the Ohmic conduction approach [105] involving the solution of Laplace equation

$$\nabla^2 \varphi = 0 \tag{3.2}$$

Although a more complete approach would consider also a space charge distribution through solution of the Poisson equation, both the methods can be shown to yield the same results for the computation of electric field and potential inside the membrane, while they differ outside [98].

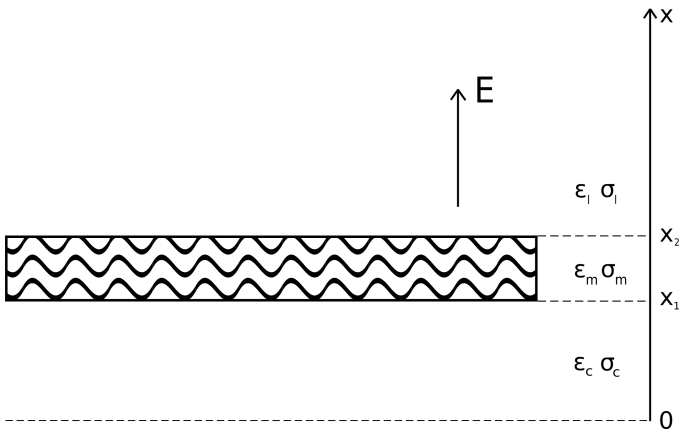

Figure 3.7: Schematic drawing of a planar membrane. Subscripts indicate the three regions of interest, liquid, membrane and cytoplasm.

3.2.1 Planar membranes

We start our analysis with the derivation of time course of transmembrane potential for a planar membrane. Consider a region of space delimited by two membranes. For symmetry reasons we can analyze only half of this hypothetical cell, i.e. a single membrane. A schematic drawing of the model adopted is given in fig. 3.7. The space is divided in three regions, liquid, membrane and cytoplasm, each with a relative electric permittivity ϵ_i and a conductivity σ_i. The electric field is taken as a constant DC step field, oriented normally to the membrane boundary. This is effectively a one dimensional model, and the Laplace equation can be written, in Cartesian coordinates

$$\frac{\partial^2}{\partial x^2}\varphi(x) = 0 \tag{3.3}$$

A solution to this equation is

$$\varphi(x) = -Ax + B \tag{3.4}$$

In the three regions, therefore, the potentials can be written as

$$\begin{aligned} \varphi_l(x,t) &= -A_l(t)x + B_l(t) \\ \varphi_m(x,t) &= -A_m(t)x + B_m(t) \\ \varphi_c(x,t) &= -A_c(t)x + B_c(t) \end{aligned} \tag{3.5}$$

where, in order to derive the variation in time of φ, we let the coefficients A and B be functions of time. These functions can be determined from the application of boundary conditions, namely the continuity of φ

$$\varphi_l(x_2) = \varphi_m(x_2)$$
$$\varphi_m(x_1) = \varphi_c(x_1) \tag{3.6}$$

and the conservation of charge

$$\nabla j + \frac{\partial \rho}{\partial t} = 0 \tag{3.7}$$

at both the interfaces. Furthermore, we need to ensure that the electric field far from the cell is the external electric field E, and since φ is determined up to an additive constant, we can also set the φ to be zero at $x = 0$ in the cytoplasm. Finally, we consider $\sigma_m = 0$ for the membrane, given that its conductivity is reported to be about six order of magnitude less then the liquids involved [99]. Applying these conditions and solving the system using the Laplace transform, the transmembrane potential results

$$\Delta\varphi_m(t) = -E \cdot d \cdot \left(\frac{\sigma_l}{\epsilon_0 \epsilon_m} t + \frac{\epsilon_l}{\epsilon_m} \right) \tag{3.8}$$

where

$$d = x_2 - x_1 \tag{3.9}$$

is the membrane thickness. Transmembrane potential is therefore a linear function of time, and this is consistent with numerical simulations based on Poisson's equation [98]. At $t = 0$ the potential drop across the membrane is, as expected, simply determined by the disparity factor of the permittivities between membrane and liquid solution.

$$\Delta\varphi_m(0) = E \cdot d \cdot \frac{\epsilon_l}{\epsilon_m} = 40E \cdot d \tag{3.10}$$

The behavior of $\Delta\varphi_m$ clearly diverges for $t \to \infty$ due to the unrealistic flatness of the membrane. In this configuration, a steady state finite transmembrane potential does not exist.

3.2.2 Generic membrane

The method developed in section 3.2.1 can be generalized to describe the time course of transmembrane potential in any geometry, provided that the cell shape can be modeled as a coordinate surface in some coordinate system,

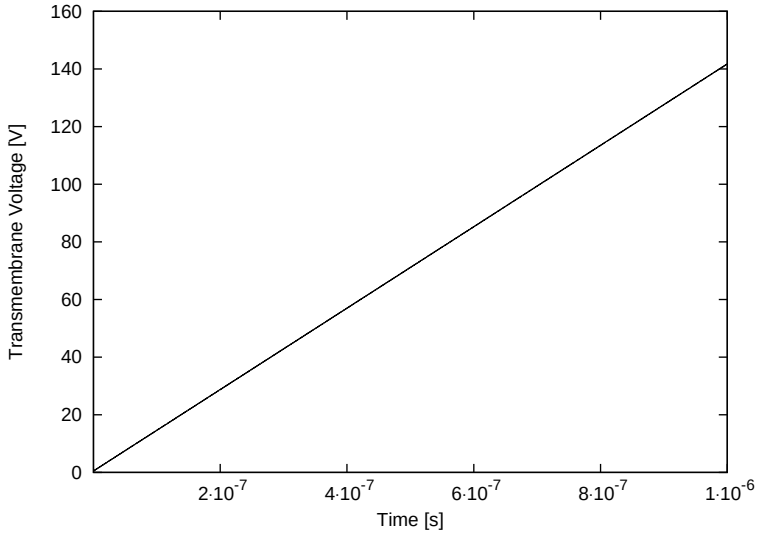

Figure 3.8: Transmembrane voltage across a planar membrane as a function of time. Membrane thickness was taken to be $d = 5$ nm, $\sigma_l = 0.2$ Sm^{-1}.

where the Laplace equation is separable. Let's consider a general curvilinear coordinate system ξ_1, ξ_2, ξ_3 in $\Re^3$, where the Laplace equation is separable. There are 14 different such systems [106], among which particularly important in biology are the spherical, cylindrical and spheroidal prolate coordinates. In each of these, the physically realistic solution to Laplace equation can be written as

$$\varphi(\xi_1, \xi_2, \xi_3, t) = A(t) f_1(\xi_1) f_2(\xi_2) f_3(\xi_3) - B(t) g_1(\xi_1) g_2(\xi_2) g_3(\xi_3) \qquad (3.11)$$

where, as before, we let A and B to be functions of time in order to derive the time course of φ. Space functions f_1,f_2,f_3,g_1,g_2,g_3 are continuous and finite everywhere, except perhaps at the origin and at infinity, where their finiteness as to be imposed as a condition. The space, in presence of a cell, can be divided in three areas (see fig. 3.9), the internal part of the cell, also called cytoplasm, the membrane, and the liquid surrounding the cell. Each of these area is assigned a relative electric permeability ϵ_i and a conductivity σ_i, with $i = c, m, l$ as before. In these areas, once the conditions of finiteness of the electric field and homogeneity far from the cell are applied, the potentials can be written as [107]

$$\varphi_c(\xi_1, \xi_2, \xi_3, t) = A_c(t) f_1(\xi_1) f_2(\xi_2) f_3(\xi_3)$$

$$\varphi_m(\xi_1, \xi_2, \xi_3, t) = A_m(t) f_1(\xi_1) f_2(\xi_2) f_3(\xi_3) + B_m(t) g_1(\xi_1) g_2(\xi_2) g_3(\xi_3)$$

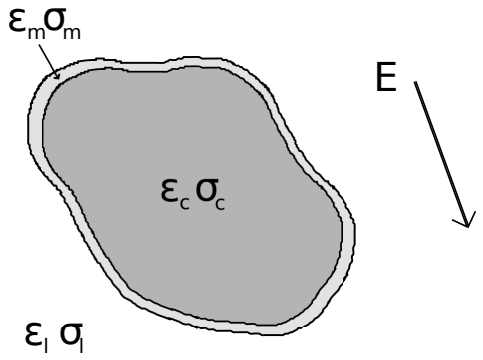

Figure 3.9: Generic model of a cell exposed to an external electric field E. Subscripts $c, m.l$ stand for cytoplasm, membrane, and liquid respectively.

$$\varphi_l(\xi_1,\xi_2,\xi_3,t) = -E(t)f_1(\xi_1)f_2(\xi_2)f_3(\xi_3) + B_l(t)g_1(\xi_1)g_2(\xi_2)g_3(\xi_3) \quad (3.12)$$

Solution to this system can be derived applying the boundary conditions. First of all the continuity of potential

$$\begin{aligned} \varphi_c|_{s_c} &= \varphi_m|_{s_c} \\ \varphi_m|_{s_l} &= \varphi_l|_{s_l} \end{aligned} \quad (3.13)$$

where we denoted S_c and S_l as the boundaries cytoplasm - membrane and liquid - membrane, respectively. We can express the charge conservation at the two interfaces as

$$\begin{aligned} j_m - j_c + \frac{\partial}{\partial t}\Big(\gamma_m - \gamma_c\Big) &= 0 \\ j_l - j_m + \frac{\partial}{\partial t}\Big(\gamma_l - \gamma_m\Big) &= 0 \end{aligned} \quad (3.14)$$

where

$$\begin{aligned} j_i = \sigma_i E_i &= \mathbf{n}\cdot\sigma_i\nabla\varphi_i|_s \\ \gamma_i &= \mathbf{n}\cdot\epsilon_0\epsilon_i\nabla\varphi_i|_s \\ i &= c,m,l \end{aligned} \quad (3.15)$$

are the current and surface charge densities at the interface S and $\mathbf{n}$ is the unit vector normal to S. We introduce now the notation

$$\begin{aligned} f_1(\xi_1)f_2(\xi_2)f_3(\xi_3)|_i &\equiv F^i \\ g_1(\xi_1)g_2(\xi_2)g_3(\xi_3)|_i &\equiv G^i \end{aligned}$$

$$i = C, L \tag{3.16}$$

to indicate that the spatial functions f and g are evaluated at the interface cytoplasm - membrane (C) and liquid - membrane (L). Furthermore, since the gradient operator is applied only to these spatial functions, it is convenient to denote

$$\begin{aligned} \mathbf{n} \cdot \nabla x^y &\equiv \Lambda_x^y \\ x &= F, G \\ y &= C, L \end{aligned} \tag{3.17}$$

Given these definitions, the equations 3.13 and 3.14 can be solved using Laplace transform. The general solution for the transmembrane potential is given by

$$\Delta\varphi_m(t) = A_m(t)(F^L - F^C) + B_m(t)(G^L - G^C) \tag{3.18}$$

The time-dependent functions $A_m(t)$ and $B_m(t)$ are given by

$$\begin{aligned} A_m(t) &= A_m^{(1)}(t) + A_m^{(2)}(t) + A_m^{(3)}(t) \\ B_m(t) &= B_m^{(1)}(t) + B_m^{(2)}(t) + B_m^{(3)}(t) \end{aligned} \tag{3.19}$$

where

$$\begin{aligned} A_m^{(1)}(t) &= -\frac{D_1 G^C}{aF^C}(N_1 + \alpha N_2)\frac{1}{z_2 - z_1}\left(e^{-z_1 t} - e^{-z_2 t}\right) \\ A_m^{(2)}(t) &= -\frac{D_1 G^C}{aF^C} N_2 \frac{1}{z_1 - z_2}\left(z_1 e^{-z_1 t} - z_2 e^{-z_2 t}\right) \\ A_m^{(3)}(t) &= -\frac{D_1 G^C}{aF^C} N_1 \alpha \left(\frac{1}{z_1 z_2} + \frac{e^{-z_1 t}}{z_1(z_1 - z_2)} + \frac{e^{-z_2 t}}{z_2(z_2 - z_1)}\right) \\ B_m^{(1)}(t) &= \frac{D_3}{a}(N_1 + \gamma N_2)\frac{1}{z_2 - z_1}\left(e^{-z_1 t} - e^{-z_2 t}\right) \\ B_m^{(2)}(t) &= \frac{D_3}{a} N_2 \frac{1}{z_1 - z_2}\left(z_1 e^{-z_1 t} - z_2 e^{-z_2 t}\right) \\ B_m^{(3)}(t) &= \frac{D_3}{a} N_1 \gamma \left(\frac{1}{z_1 z_2} + \frac{e^{-z_1 t}}{z_1(z_1 - z_2)} + \frac{e^{-z_2 t}}{z_2(z_2 - z_1)}\right) \end{aligned} \tag{3.20}$$

with

$$z_1 = -s_1, \quad z_2 = -s_2, \quad s_1 = \frac{-b - \sqrt{b^2 - 4ac}}{2a}, \quad s_2 = \frac{-b + \sqrt{b^2 - 4ac}}{2a}$$

$$a = K_1 + K_2, \quad b = K_1(\alpha + \beta) + K_2(\gamma + \delta), \quad c = K_1\alpha\beta + K_2\gamma\delta$$

$$K_1 = \frac{F^L G^C}{F^C G^L} D_1 D_2, \quad K_2 = -D_3 D_4$$

$$D_1 = \epsilon_0 \Big(\epsilon_c - \epsilon_m \frac{\Lambda_G^C F^C}{\Lambda_F^C G^C} \Big), \quad D_2 = \epsilon_0 \Big(\epsilon_l - \epsilon_m \frac{\Lambda_F^L G^L}{\Lambda_G^L F^L} \Big)$$

$$D_3 = \epsilon_0 (\epsilon_c - \epsilon_m), \quad D_4 = \epsilon_0 (\epsilon_l - \epsilon_m)$$

$$\alpha = \frac{\sigma_c}{D_1}, \quad \beta = \frac{\sigma_l}{D_2}, \quad \gamma = \frac{\sigma_c}{D_3}, \quad \delta = \frac{\sigma_l}{D_4} \tag{3.21}$$

$$N_1 = E\sigma_l \Big(\frac{F^L}{G^L} - \frac{\Lambda_F^L}{\Lambda_G^L} \Big), \quad N_2 = E\epsilon_0\epsilon_l \Big(\frac{F^L}{G^L} - \frac{\Lambda_F^L}{\Lambda_G^L} \Big) \tag{3.22}$$

The generic transmembrane potential in eq. 3.18 can also be written, rearranging the equation, as

$$\varphi_m(t) = C_\infty + C_1 e^{-\frac{t}{\tau_1}} + C_2 e^{-\frac{t}{\tau_2}} \tag{3.23}$$

where

$$\tau_1 = \frac{1}{z_1}, \quad \tau_2 = \frac{1}{z_2} \tag{3.24}$$

The solution for a generic geometry can be obtained from equations above, provided that we are able to find a way to express, in the chosen geometry, the spatial functions 3.16 and the electric fields 3.17. For this to be possible, we need to choose a coordinate system in which Laplace equation is separable, as stated before, and we also need to choose it in such a way that the analytic expression of space boundaries between the three areas is simple, in order to make a solution possible.

3.2.3 Spherical membranes

In spherical coordinates $\{r, \theta, \phi\}$, a solution to the Laplace equation is given by

$$\varphi(r, \theta) = \left(Ar + \frac{B}{r^2} \right) \cos\theta \tag{3.25}$$

with r the radial coordinate, measured from the center of the cell, and θ the angle between the electric field and the radial vector defining the position on the cell. The potential φ does not depend on ϕ is we define the direction of the electric field E as the rotational axis of ϕ. The spatial functions F and G are therefore

$$F = r\cos\theta \tag{3.26}$$

$$G = \frac{1}{r^2}\cos\theta \tag{3.27}$$

The boundaries can simply be expressed as $r = R_1$ and $r = R_2$, and the calculation of electric fields involves derivation only in the radial coordinate r (see fig. 3.10). The relevant functions that have to be calculated in order to solve eq. 3.18 - 3.22 are

$$F^C = R_1 \cos\theta, \quad G^C = \frac{1}{R_1^2}\cos\theta, \quad F^L = R_2\cos\theta, \quad G^L = \frac{1}{R_2^2}\cos\theta$$

$$\Lambda_F^C = \cos\theta, \quad \Lambda_F^L = \cos\theta, \quad \Lambda_G^C = -\frac{2}{R_1^3}\cos\theta, \quad \Lambda_G^L = -\frac{2}{R_2^3}\cos\theta \tag{3.28}$$

At the beginning of the pulse, $t = 0$, the potential across the membrane is determined only by the disparity in permittivities, as in the case of a planar membrane. This can be seen by calculating

$$\Delta\varphi_m(0) = 40Ed\cos\theta \tag{3.29}$$

where $d = R_2 - R_1$, while the steady state transmembrane potential can be calculated by letting t $\to \infty$

$$C_\infty = \lim_{t\to+\infty}\Delta\varphi_m(t) = \frac{3}{2}RE\cos\theta \tag{3.30}$$

As expected, this equation is just eq. 2.1. Plots of variation of τ_1 and τ_2 as functions of the variables R and σ_l are given in fig. 3.11, 3.12, 3.13 and 3.14, while a plot of τ_2 as a function of both R and σ_l is given in fig. 3.15. The variation of τ_1 over a wide range of physically possible values of R and σ_l is very small, and its order of magnitude never exceeds $10^{-3}\mu s$. The second term of eq. 3.23 therefore goes to zero very fast if compared with the usual pulse durations of $\sim \mu s$, and can effectively be ignored. The charge of the cell membrane up to the value of C_∞ is therefore dominated by the time constant

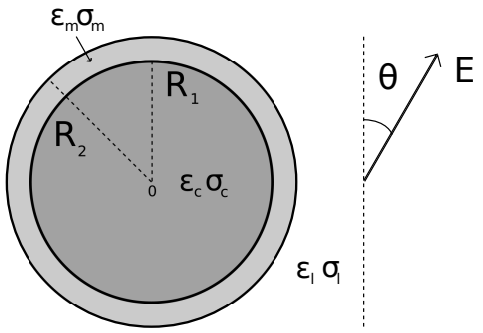

Figure 3.10: Spherical cell exposed to an external electric field E.

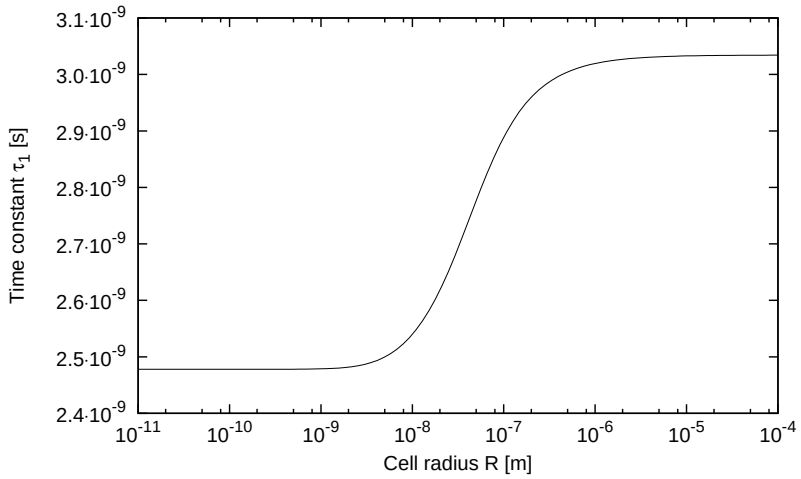

Figure 3.11: Variation of time constant τ_1 for a spherical membrane as a function of radius R, $\sigma_l = 0.2$ Sm^{-1}, $\sigma_c = 0.3$ Sm^{-1}.

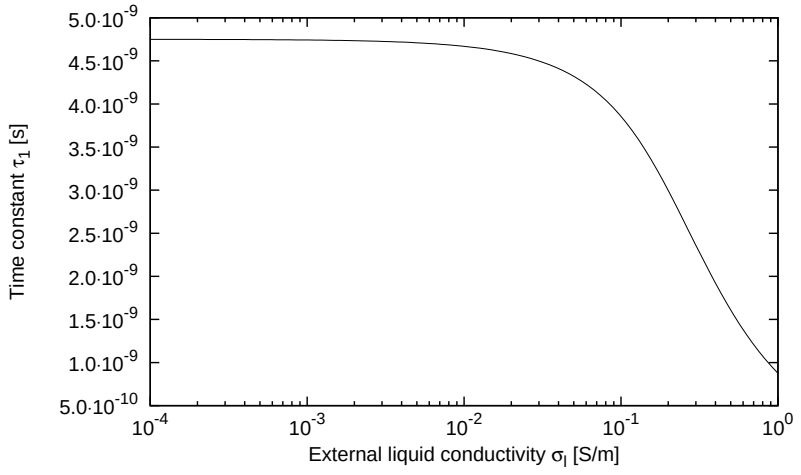

Figure 3.12: Variation of time constant τ_1 for a spherical membrane as a function of suspension liquid conductivity σ_l, $R = 0.4$ μm, $\sigma_c = 0.3$ Sm^{-1}.

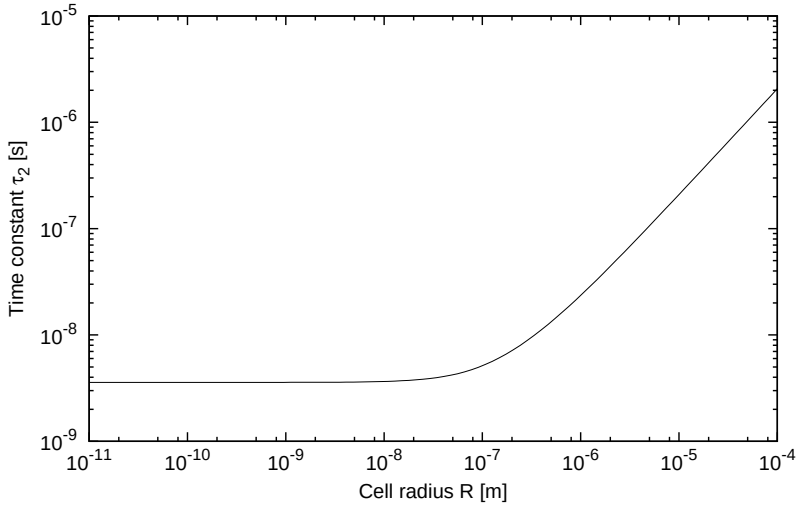

Figure 3.13: Variation of time constant τ_2 for a spherical membrane as a function of cell radius R, $\sigma_l = 0.2$ Sm^{-1}, $\sigma_c = 0.3$ Sm^{-1}.

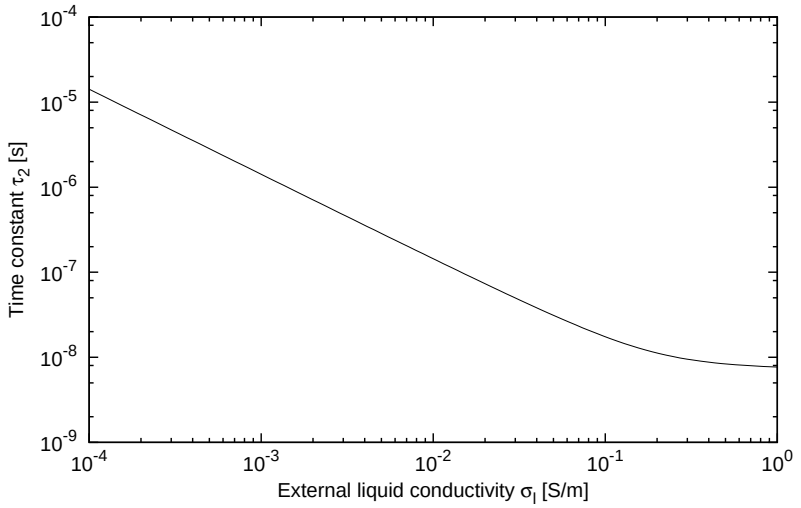

Figure 3.14: Variation of time constant τ_2 for a spherical membrane as a function of suspension liquid conductivity σ_l, $R = 0.4$ μm, $\sigma_c = 0.3$ Sm^{-1}.

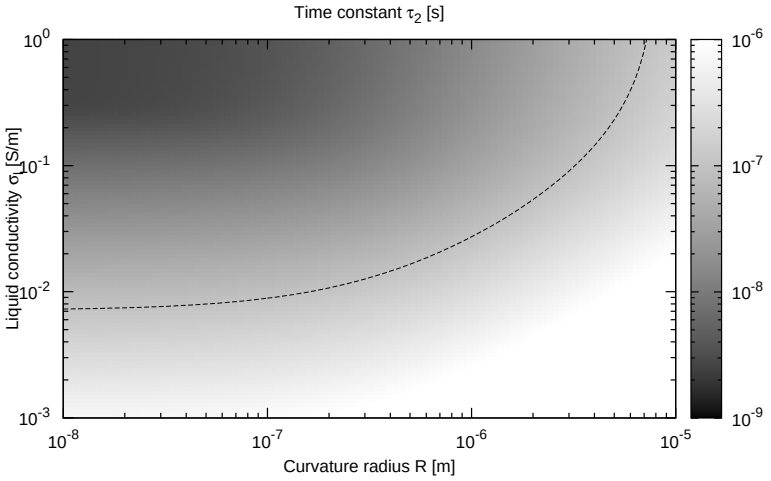

Figure 3.15: Variation of time constant τ_2 for a spherical membrane as a function of cell radius R and suspension liquid conductivity σ_l. Dashed line represents $\tau_2 = 0.1\mu$s.

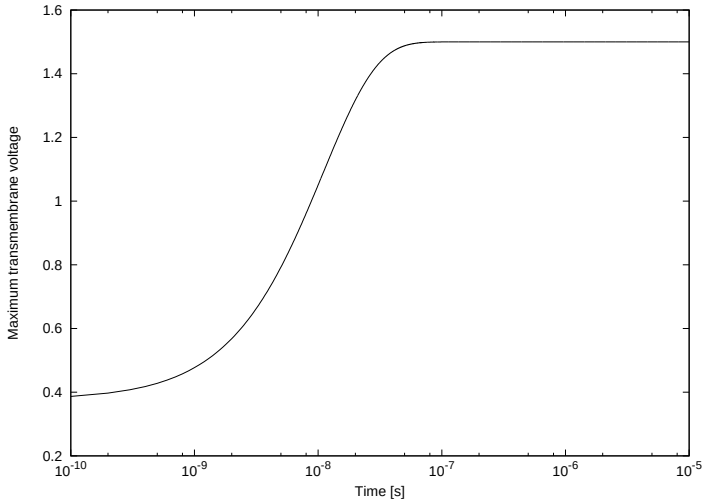

Figure 3.16: Time course of transmembrane potential at 25 kVcm^{-1} for a spherical cell of radius 0.4 μm suspended in a liquid of conductivity 0.2 Sm^{-1}.

τ_2 whose behavior, instead, is more influenced by the variation of the physical parameters R and σ_l, as can be seen also in fig. 3.15. As a general rule, the charge is slower for greater radii R and for smaller liquid conductivities σ_l. For spherical cells, this means that the effectiveness of PEF treatment for large cells (for example yeasts) could be affected by the choice of the treatment liquid, to the point that the charge process could not be completed over the duration of the external pulse, increasing the survival probability of the cell. For our experiments we will consider spherical membranes of radius around 0.4 μm (see section 3.2.6) and conductivities of liquid suspensions around 0.2 Sm^{-1}. For these parameters, the process of membrane charging can be considered instantaneous if compared to the length of a 1 μs pulse. Time course of maximum transmembrane potential is shown in fig. 3.16.

3.2.4 Cylindrical membranes

In cylindrical coordinates $\{r, \theta, z\}$ a solution to the Laplace equation can be written as

$$\varphi(r, \theta) = \left(Ar + \frac{B}{r} \right) \cos\theta \tag{3.31}$$

since the potential φ does not depend on the coordinate z. The functions F and G are therefore

$$F = r \cos\theta \tag{3.32}$$

$$G = \frac{1}{r} \cos\theta \tag{3.33}$$

The boundaries of the cylindrical membrane can simply be expressed by

$$r = R_1, \quad r = R_2 \tag{3.34}$$

thus the relevant functions in this coordinate system are

$$F^C = R_1 \cos\theta, \quad G^C = \frac{1}{R_1} \cos\theta, \quad F^L = R_2 \cos\theta, \quad G^L = \frac{1}{R_2} \cos\theta$$

$$\Lambda_F^C = \cos\theta, \quad \Lambda_F^L = \cos\theta, \quad \Lambda_G^C = -\frac{1}{R_1^2} \cos\theta, \quad \Lambda_G^L = -\frac{1}{R_2^2} \cos\theta \tag{3.35}$$

With $t = 0$ we can derive the transmembrane potential at the beginning of the pulse

$$\Delta\varphi_m(0) \sim 40 E d \cos\theta \tag{3.36}$$

with $d = R_2 - R_1$. By letting $t \to \infty$ we can find the steady state potential

$$\Delta\varphi_m(\infty) = 2 E R \cos\theta \tag{3.37}$$

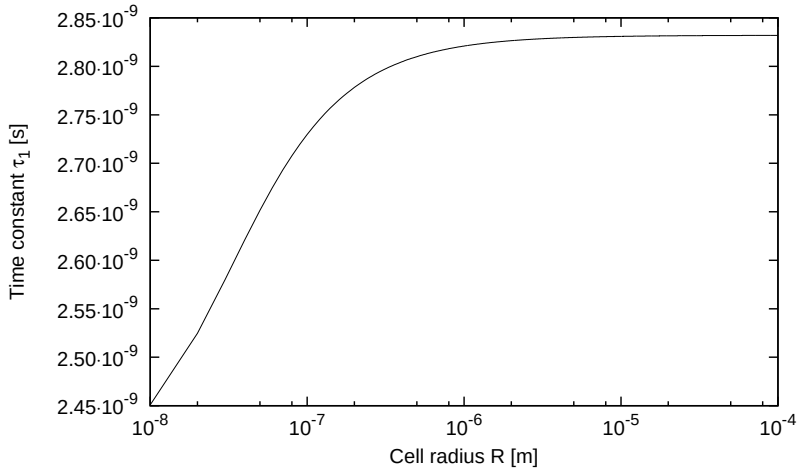

Figure 3.17: Variation of time constant τ_1 for a cylindrical membrane as a function of radius R , $\sigma_l = 0.2$ Sm^{-1}, $\sigma_c = 0.3$ Sm^{-1}.

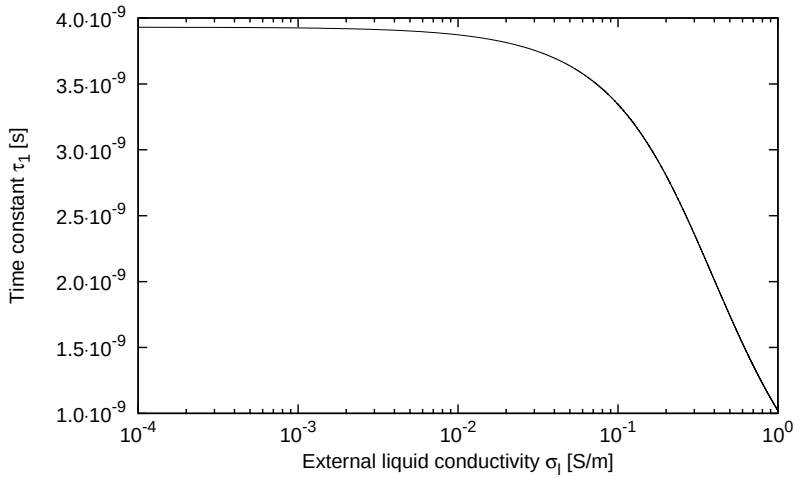

Figure 3.18: Variation of time constant τ_1 for a cylindrical membrane as a function of suspension liquid conductivity σ_l, $R = 0.4$ μm, $\sigma_c = 0.3$ Sm^{-1}.

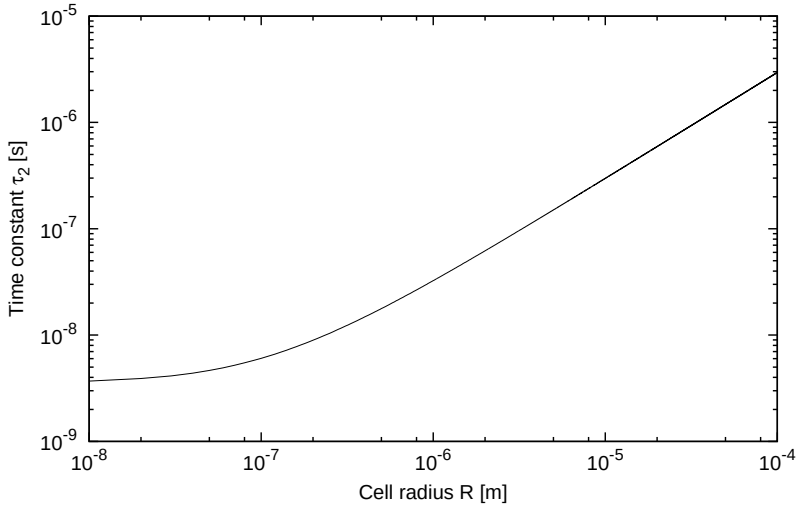

Figure 3.19: Variation of time constant τ_2 for a cylindrical membrane as a function of radius R, $\sigma_l = 0.2$ Sm^{-1}, $\sigma_c = 0.3$ Sm^{-1}.

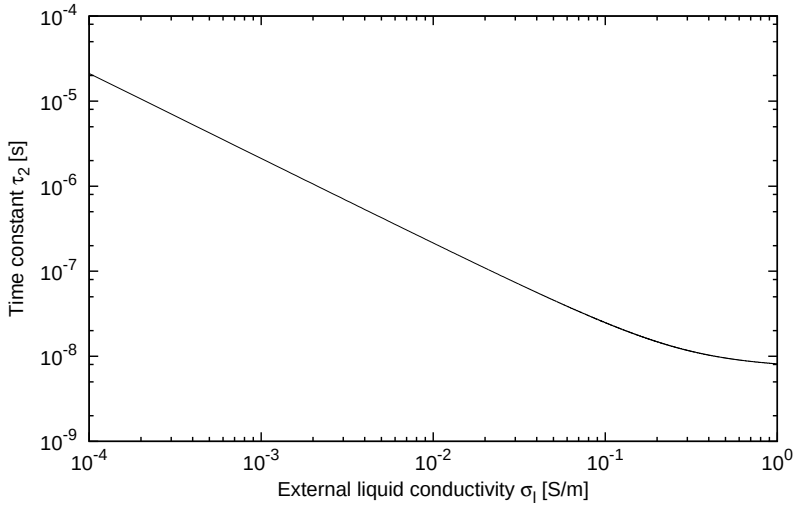

Figure 3.20: Variation of time constant τ_2 for a cylindrical membrane as a function of suspension liquid conductivity σ_l, $R = 0.4$ μm, $\sigma_c = 0.3$ Sm^{-1}.

A membrane with cylindrical shape has therefore a steady state potential higher than a spherical membrane of the same radius. Plots of variation of τ_1 and τ_2 as functions of the variables R and σ_l are given in fig. 3.17, 3.18, 3.19 and 3.20.

By comparison with fig. 3.11-3.14 it is possible to verify how the time constants for spherical and cylindrical shape lies in the same range and vary similarly with R and σ_l, therefore the same limits that allow us to ignore the process of membrane charging and consider only the steady state potential in the case of a spherical membrane are valid for a cylindrical membrane of the same radius.

3.2.5 Spheroidal prolate cells

Spherical cells in external electric fields are known to elongate in the direction parallel to the electric field [108]. A derivation of transmembrane potential for a spheroidal prolate cell, with electric field parallel to the major axis, can therefore give some insight on the mechanisms of PEF. A general solution to Laplace equation in spheroidal prolate coordinates $\{(u, \nu, \theta), u \geq= 0, 0 \leq \nu \leq \pi, 0 \leq \theta < 2\pi\}$

$$x = a \cosh u \cos \nu, \quad y = a \sinh u \sin \nu \cos \theta,$$

$$z = a \sinh u \sin \nu \sin \theta$$

where $2a$ is the distance between the foci, can be written as

$$\varphi(u, \nu, t) = A(t) \cosh u \cos \nu + B(t) \left(1 - \cosh u \log \sqrt{\frac{\cosh u + 1}{\cosh u - 1}} \right) \cos \nu \tag{3.38}$$

since for geometries with $x-$symmetry, the potential is independent on θ. The boundaries of the three regions defining the cell will be expressed simply by $u = U_1$ and $u = U_2$. We can express the length and width of a prolate spheroid, R_1 and R_2, as

$$\begin{aligned} R_1 &= a \cosh U \\ R_2 &= a \sinh U \end{aligned} \tag{3.39}$$

Given a choice of R_1 and R_2, the corresponding parameters a and U can be found from

$$\begin{aligned} a &= \sqrt{R_1^2 - R_2^2} \\ U &= \tanh^{-1} \frac{R_2}{R_1} \end{aligned} \tag{3.40}$$

We weed to ensure that the membrane thickness $d = R_1^{ext} - R_1^{int}$, at least at the poles of the cell, is 5 nm, thus, once the external surface parameters a and U_2 are chosen, the value of U_1 is determined by

$$U_1 = \cosh^{-1}\left(\cosh U_2 - \frac{d}{a}\right) \tag{3.41}$$

The functions F and G are, from eq. 3.38

$$F = \cosh u \cos\nu$$

$$G = \left(1 - \cosh u \log\sqrt{\frac{\cosh u + 1}{\cosh u - 1}}\right)\cos\nu \tag{3.42}$$

To ensure uniformity of the electric field far form the cell, the function $A_l(t)$ must assume the value

$$A_l(t) = -E(t)a \tag{3.43}$$

Given these hypothesis, we can calculate the functions involved in derivation of electric potential

$$\begin{aligned}
F^C &= \cosh U_1 \cos\nu, \quad F^L = \cosh U_2 \cos\nu \\
G^C &= \left(1 - \cosh U_1 \log\sqrt{\frac{\cosh U_1 + 1}{\cosh U_1 - 1}}\right)\cos\nu \\
G^L &= \left(1 - \cosh U_2 \log\sqrt{\frac{\cosh U_2 + 1}{\cosh U_2 - 1}}\right)\cos\nu \\
\Lambda_F^C &= \sinh U_1 \cos\nu, \quad \Lambda_F^L = \sinh U_2 \cos\nu \\
\Lambda_G^C &= \left(\sinh U_1 \log\sqrt{\frac{\cosh U_1 + 1}{\cosh U_1 - 1}} - \frac{\cosh U_1 \sinh U_1}{(\cosh U_1 + 1)(\cosh U_1 - 1)}\right)\cos\nu \\
\Lambda_G^L &= \left(\sinh U_2 \log\sqrt{\frac{\cosh U_2 + 1}{\cosh U_2 - 1}} - \frac{\cosh U_2 \sinh U_2}{(\cosh U_2 + 1)(\cosh U_2 - 1)}\right)\cos\nu
\end{aligned} \tag{3.44}$$

Prolate shape in normal condition is not found in nature, and it also arise problems in the definition of membrane thickness, since it cannot be constant if the shape of a cell has to be defined the way we defined before. Nevertheless, at least for small deformations, the expression derived can be used to study the effect of elongation on transmembrane potential and time constants τ_1 and τ_2. If we consider a spherical cell of initial radius R, the elongation parallel to the electric field can be expressed as

$$R_1 = R + \Delta R \tag{3.45}$$

During the deformation we impose that the volume of the cytoplasm remains constant, being an aqueous solution and therefore non compressible. This allow us to derive the value of R_2 from

$$V_0 = \frac{4}{3}\pi R^3 = \frac{4}{3}\pi R_1 R_2^2 \tag{3.46}$$

and the parameters a and U_2, from which we can calculate U_1 using relations 3.40 by imposing

$$R_1^{int} = R_1^{ext} - d \tag{3.47}$$

where d is the membrane thickness. If the volume remains constant, the membrane has to stretch in order to reach an elongation ΔR, thus its surface, initially

$$S_0 = 4\pi R^2 \tag{3.48}$$

has to enlarge to the surface of a prolate spheroid

$$S_1 = 2\pi R_2 \left(R_2 + \frac{R_1^2}{\sqrt{R_1^2 - R_2^2}} \arcsin \frac{\sqrt{R_1^2 - R_2^2}}{R_1} \right) \tag{3.49}$$

Deformation into highly eccentric shapes have never been observed in biological cells, and the maximum elastic stretching on the plasma membrane is around 2% [109]. From fig. 3.21 we can see that this empirical limitation

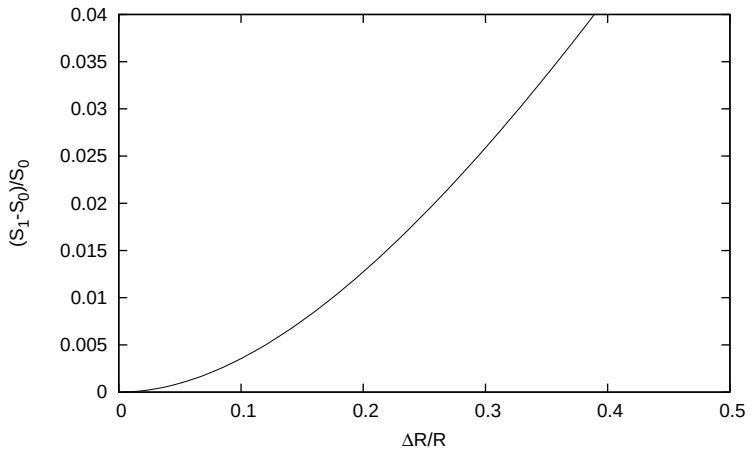

Figure 3.21: Relative variation of cell surface as a function of relative cell elongation.

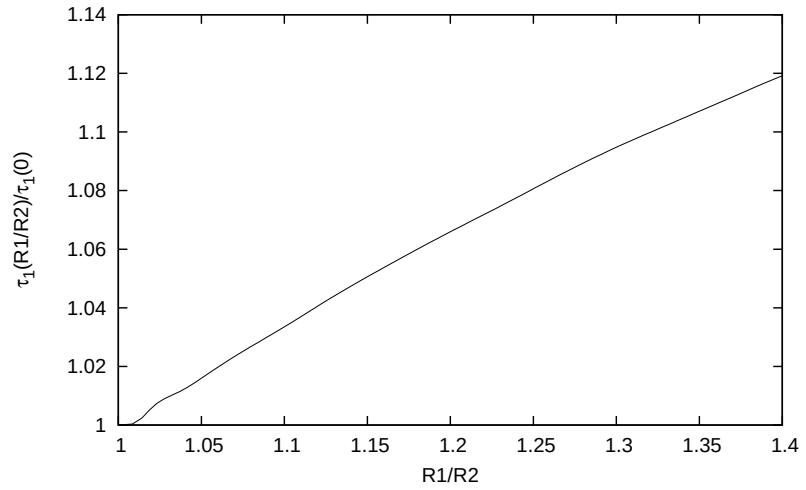

Figure 3.22: Relative increase of time constants τ_1 as a function of the ratio R_1/R_2 in respect to the time constant $\tau_1(0)$ for the spherical case, $\tau_1(0)$.

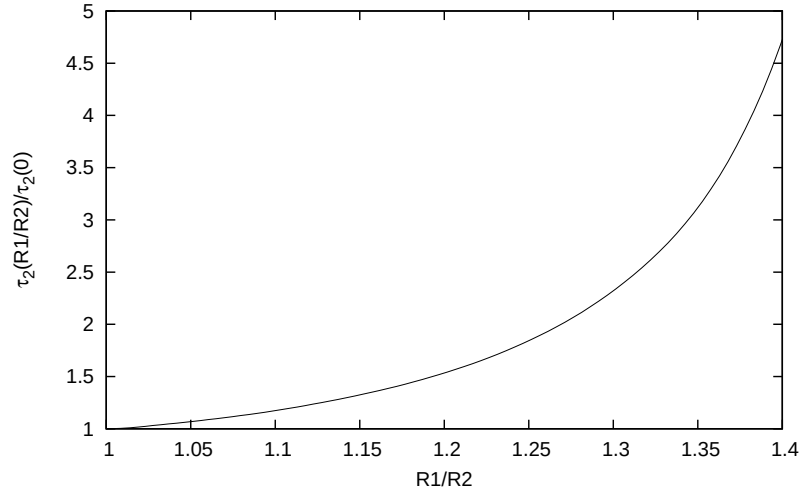

Figure 3.23: Relative increase of time constants τ_2 as a function of the ratio R_1/R_2 in respect to the time constant $\tau_2(0)$ for the spherical case.

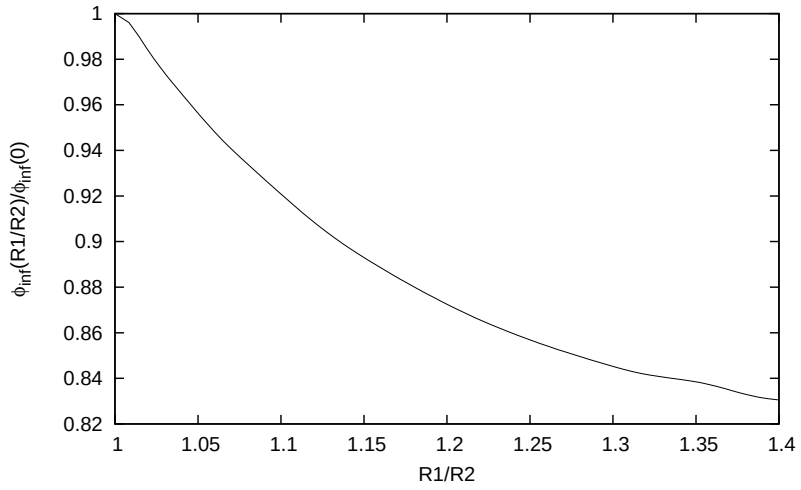

Figure 3.24: Relative value of steady state transmembrane potential as a function of ratio R_1/R_2 in respect to steady state transmembrane potential for a spherical cell $\varphi_{inf}(0)$.

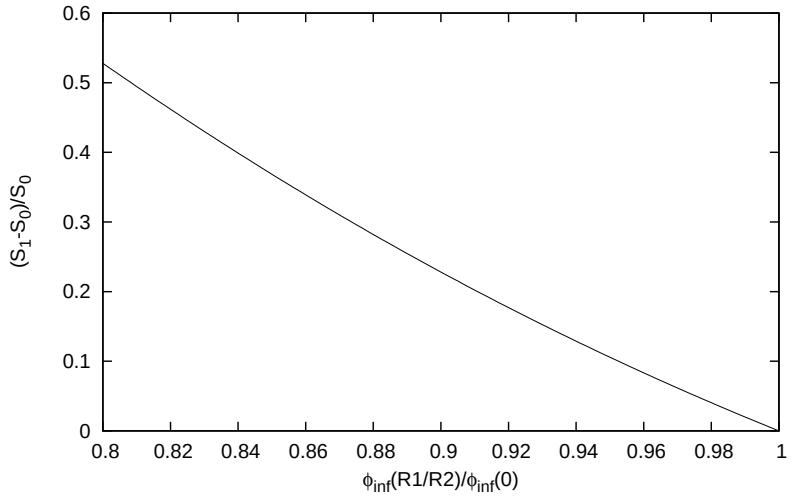

Figure 3.25: Relative increase in survival probability as a function of $\varphi_{inf}(R_1/R_2)/\varphi_{inf}(0)$.

sets a maximum value for the relative deformation $\Delta R/R$ around 0.25. This in turn leads to a limitation for the physically acceptable ratios R_1/R_2

$$\frac{R_1}{R_2} < 1.4 \tag{3.50}$$

Fig. 3.22 and 3.23 show the relative variation of the time constants τ_1 and τ_2 as a function of the ratio R_1/R_2, while a plots of the relative steady state transmembrane potential as a function of the deformation and the relative cell survival probability are given in fig. 3.24 and 3.25. The increase in time constant τ_2 does not reach a consistent value even for high deformations, and therefore the process of membrane charging can be considered as instantaneous in respect to the usual pulse durations in the same limits found for spherical cells. The effect of deformation, anyway, can affect the survival probability of the cell exposed to the external electric field increasing it up to around 50% of the value for a spherical cell. This should be taken into account when analyzing the results of a PEF experiment, but the lack of sufficient experimental data about cell elongations does not allow a quantitative estimation of the influence of this effect on bacterial inactivation. Furthermore, taking in consideration the short duration of the pulses involved in PEF, we can probably ignore the effect of cell elongation, at least as a first approximation.

3.2.6 General response of a membrane to an external electric field

The transmembrane potential $\Delta\varphi_m$ of a real cell is in general derived considering the cell as a whole, but most of the cells treated by PEF cannot be described by a simple geometrical form. To overcome this problem their shape is usually approximated to a sphere and $\Delta\varphi_m$ derived by Schwan eq. 2.1. The idea is to use a sort of effective radius of the cell exposed to the electric field, identified by the maximum length of the cell parallel the field. The development of a transmembrane voltage is therefore regarded as a process influenced by the global shape and dimension of the bacterium. Here we enunciate the hypothesis that, instead, the process of membrane charging is a local phenomenon.

First of all, we can compare the maximum $\Delta\varphi_m(t)$ among spherical, cylindrical and planar membranes in fig. 3.26, where radii of sphere and cylinder are set to the same value, $R = 1$ μm, the electric field is 25 kVcm^{-1} and the liquid conductivity is 0.2 Sm^{-1}. The potential $\Delta\varphi_m(t)$ diverges for a planar membrane, but this is not surprising since planar membrane can not represent a real cell. Anyway, the case of planar membrane is useful to understand

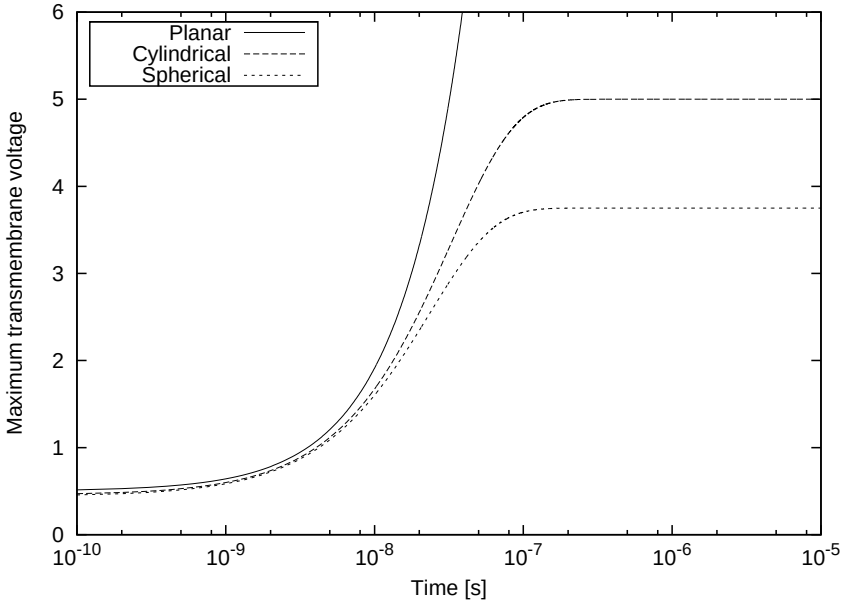

Figure 3.26: Transmembrane voltage as a function of time for spherical, cylindrical and planar membrane.

the variation of the steady state potential $\Delta\varphi_m(\infty)$. The general expression, from eq. 3.30 and 3.37 can be expressed as

$$\Delta\varphi_m(\infty) = f(k) \cdot E \tag{3.51}$$

where $f(k)$ is a shape factor whose value depends on the mean curvature k of the membrane, defined as the average of the principal curvatures. It is easy to see from derivation above how $f(k)$ is proportional to $1/k$, exploding to infinity when k is 0 at R=∞, i.e. for a planar membrane. From this point of view, it is not surprising that a cylinder has greater $\Delta\varphi_m(\infty)$ than a sphere, since its mean curvature is exactly a half of the curvature of a sphere of the same radius. The effect of the membrane shape on $\Delta\varphi_m$, therefore, can be regarded as a function of the k curvature rather than the radius R, with the clear advantage that the curvature can be defined locally on the membrane rather than globally. On the other hand, as seen for all the different shapes in previous sections, the transmembrane potential is initially determined only by the disparity of permittivities between the liquid and the membrane. But a non-conductive membrane immersed in a conductive liquid (or at least a liquid whose conductivity is roughly 6 order of magnitude greater than the membrane conductivity) effectively acts like a capacitor, with charges accumulating on both the surfaces. This process of accumulation locally increases

the intensity of the electric field in the membrane and the value of the voltage drop. Therefore, as t increases, a RC-like behavior of the potential is expected, and in fact shown by eq. 3.23. Being the cytoplasm and the external liquid both aqueous solutions, their permittivity is largely dominated by the permittivity of water and can be considered equal. The conductivity, instead, is in general different, being the conductivity of the cytoplasm a fixed value around 0.3 Sm^{-1} and the conductivity of the external liquid dependent on the particular type of media. The time constant in a RC-like circuit is expected to depend on the resistance of the current path and on the capacitance. We can describe the membrane charging, therefore, as an initial charge due to the disparity of permittivities, followed by accumulation of charges on the internal and external surface of the cell. These two accumulation processes will be dominated by two different time constants. In the cytoplasm, τ_c is expected to depend on σ_c and R, while the time constant τ_l in the liquid will be influenced by σ_l and R. Given these considerations, it is easy to identify $\tau_c{=}\tau_1$, and $\tau_l{=}\tau_2$. Again, the process of membrane charging can be described as a local process, driven by charge accumulation, and whose quantitative effect depends on the local values of σ and k. When analyzing the effects of PEF in our simulations, we will therefore consider the local shape and curvature of the membranes and compute the transmembrane potential. This scheme generally fits the experimental evidence that larger cells are more susceptible to PEF than smaller ones, but this, rather than being an effect of the dimensions themselves, can be related to the lower local mean curvature of the membrane.

3.3 Distribution of cell dimensions

The shape of *Escherichia coli* resembles a rod, and is therefore not possible to approximate it to a single geometrical surface. Using the idea that only local curvature determines the local value of transmembrane potential, we parametrize *E. coli* as a cylinder with two semi-spherical caps, as in fig. 3.27. The average dimensions used in our simulation are L = 2.72 μm and W = 0.8 μm. Dimensions of *E. coli* determines the inactivation probability as described in previous section 3.2. The size of each cell in a single sample of bacteria is distributed around an average value which depends on many factors, among which are the growth medium, temperature and time. Even if all the parameters are kept constant, the average size of two different samples of the same bacterium species is in general not exactly the same, particularly if they are not grown on the same day. Usually it is impossible to collect data to draw more than one single inactivation curve during a day of

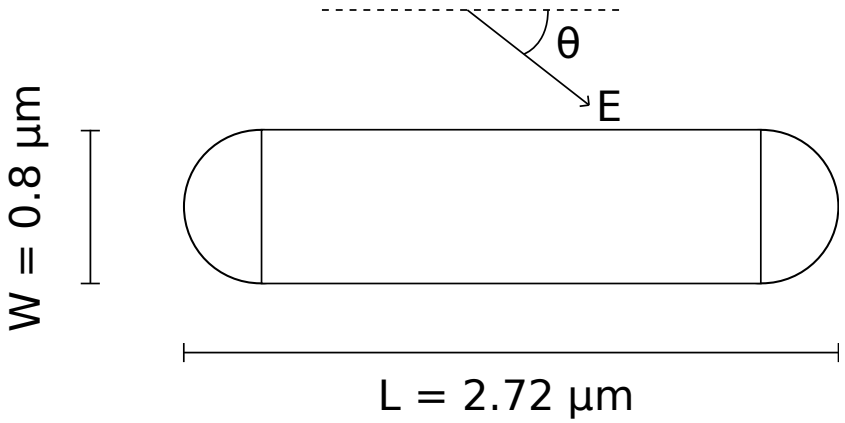

Figure 3.27: The model of *E. coli* and average dimensions. Inclination θ of electric field E is taken with respect to the major axis of the cell.

experiments, so upon repetitions of the same measure in the same conditions, the average dimensions of cells in the samples will in general not be the same, but normally distributed, with a standard deviation ∼10% [110], around an expected mean value characteristic of that particular cell in those particular conditions. This spread in average dimensions clearly affects the effectiveness of PEF treatment, and could be the source of the great variability of results among different experiments and the apparent increase of standard deviation with the number of applied pulses. On the other hand, even the distribution of cell dimensions in a single sample could affect the inactivation curves: in fact, the presence of a tail of cells with smaller dimensions, on which PEF treatment is less effective, could explain the apparent saturation of microbial inactivation around 4-5 Logs.

3.4 Simulations of microbial inactivation

We have now the possibility to investigate the influence of the different approximations usually made in the analysis of PEF inactivation curves. The electrical conditions of the simulation were taken accordingly to the inactivation PEF experiments carried out in our laboratory, and therefore the nominal electric field was set to 25 $\mathrm{kVcm^{-1}}$, the liquid conductivity to 0.2 $\mathrm{Sm^{-1}}$ and the pulse duration to 1 μs. Given the mean dimensions of *E. coli* discussed before, it is easy to see from fig. 3.15 how the process of membrane charging is practically instantaneous compared to the length of the pulse, and therefore we can approximate the transmembrane potential to the

steady state potential $\Delta\varphi_m(\infty)$. As a first step, we try to evaluate the impact of four hypothesis on inactivation kinetics, namely the inclusion of cell rotation, real shape of bacteria, distribution of cell dimensions and real distribution of electric field. Each one of these hypothesis can be included or not in the simulation, and therefore their various combinations can be investigated. Clearly, not all the combinations are worth investigation, as for example the impact of cell rotation on spherical cells. To facilitate the reading of the results, particularly on the plots, the inclusion of a hypothesis in the simulation is denoted by a binary digit, 0 or 1, with 1 corresponding to the inclusion of the relative hypothesis and 0 to its exclusion. The order of appearance of these digits is always given as [Rotation,Shape,Dimensions,Field], thus the notation [0110], for example, corresponds to a simulation in which the cells do not rotate during the time between a pulse and the following, cell shape is rod-like, cell dimensions are normally distributed around a mean value and the electric field is identically 25 kVcm^{-1} in every portion of the treatment chamber. The simulation procedure can be described as follows:

1. A population of 10^7 bacteria is created, with dimensions determined by the choice of the second and third parameter. Precisely, if the shape digit is set to 1, the simulation assigns the mean dimensions of *E. coli* described at the beginning this section to the relative variables, then, if the distribution digit is set to 1, a random dimension, normally distributed around this mean value, is assigned to each cell

2. If the field digit is set to 1, a random position in the treatment chamber is assigned to each cell, with a uniform distribution, and therefore the value of the electric field intensity experienced by the cell is derived by the simulation of the real electric field in the chamber described in section 3.1

3. A random angle with respect to the electric field is assigned, with uniform probability, to each cell. The angle range is taken from 0 to $\pi/2$, given the symmetry of the cell with respect to the electric field

4. For each pulse, from the parameters assigned to each cell, a value of the maximum transmembrane potential is derived, using the steady state equations 3.30 and 3.37. If the shape digit is set to 1 the cell can be considered as formed by a cylinder and a sphere, so there exist in principle two maximum transmembrane potentials, $\Delta\varphi_m^{(sphere)}(\infty)$ and $\Delta\varphi_m^{(cylinder)}(\infty)$. For any orientation of the cell with respect to the external electric field the two semi-spherical caps form a complete sphere and the maximum of $\Delta\varphi_m^{(sphere)}(\infty)$ is always derived from eq.

Parameter	**Value**	**Parameter**	**Value**
Number of cells	10^7	Number of pulses	400
Cell mean length L	$2.72\mu m$	Cell mean width W	$0.8\mu m$
Standard Dev. σ_x/x	10%	Cytoplasm conductivity	0.3 Sm^{-1}
Electric field	25 kVcm^{-1}	Liquid conductivity	0.2 Sm^{-1}

Table 3.1: Parameters used in the simulations of microbial inactivation.

3.30 by setting $\theta = 0$, and is therefore only a function of E and R. For the cylindrical part, if θ is the angle between the major axis of the cell and the direction of the electric field, $\Delta\varphi_m^{(cylinder)}(\infty)$ will be determined also by $\sin\theta$. Given the orientation of the cell, therefore, the maximum between $\Delta\varphi_m^{(sphere)}(\infty)$ and $\Delta\varphi_m^{(cylinder)}(\infty)$ is taken as the cell maximum transmembrane potential

5. The survival probability $0 < S(cell) < 1$ for each cell is calculated from eq. 2.38

6. A random real number between 0 and 1 is generated for each cell, with a uniform probability, and if this number is greater than $S(cell)$, the cell is killed, otherwise it survives and will be processed for the next pulse

7. Finally, if the digit rotation is set to 1, a new random orientation is assigned to each cell survived to the pulse, then the procedure restarts from point 4 until the total number of 400 pulses is reached.

A table summarizing the parameters used in the simulations is given in 3.1 Plots of the relevant microbial inactivations simulated can seen in fig. 3.28. For a simulation were none of the four hypothesis is included, the predicted curve is a straight line, where as much as 7 Logs of inactivation are reached in just 6 pulses. Notably, our simulation also predicts that the impact of the real cell shape and the possible distribution of cell dimensions inside the same colony cannot explain the tail effect of inactivation curves. The inclusion of the real electric field distribution in the treatment chamber, instead, gives a possible explanation to this effect, as can be seen from the last two plots in fig. 3.28. Microbial inactivation seems therefore to saturate around 4 Logs, due to the presence of areas of the chamber where the electric field, and thus the inactivation probability, is considerably lower than expected. It is interesting to note how, on one hand, the saturation effect is only apparent, since higher levels of inactivation can be in principle reached increasing the

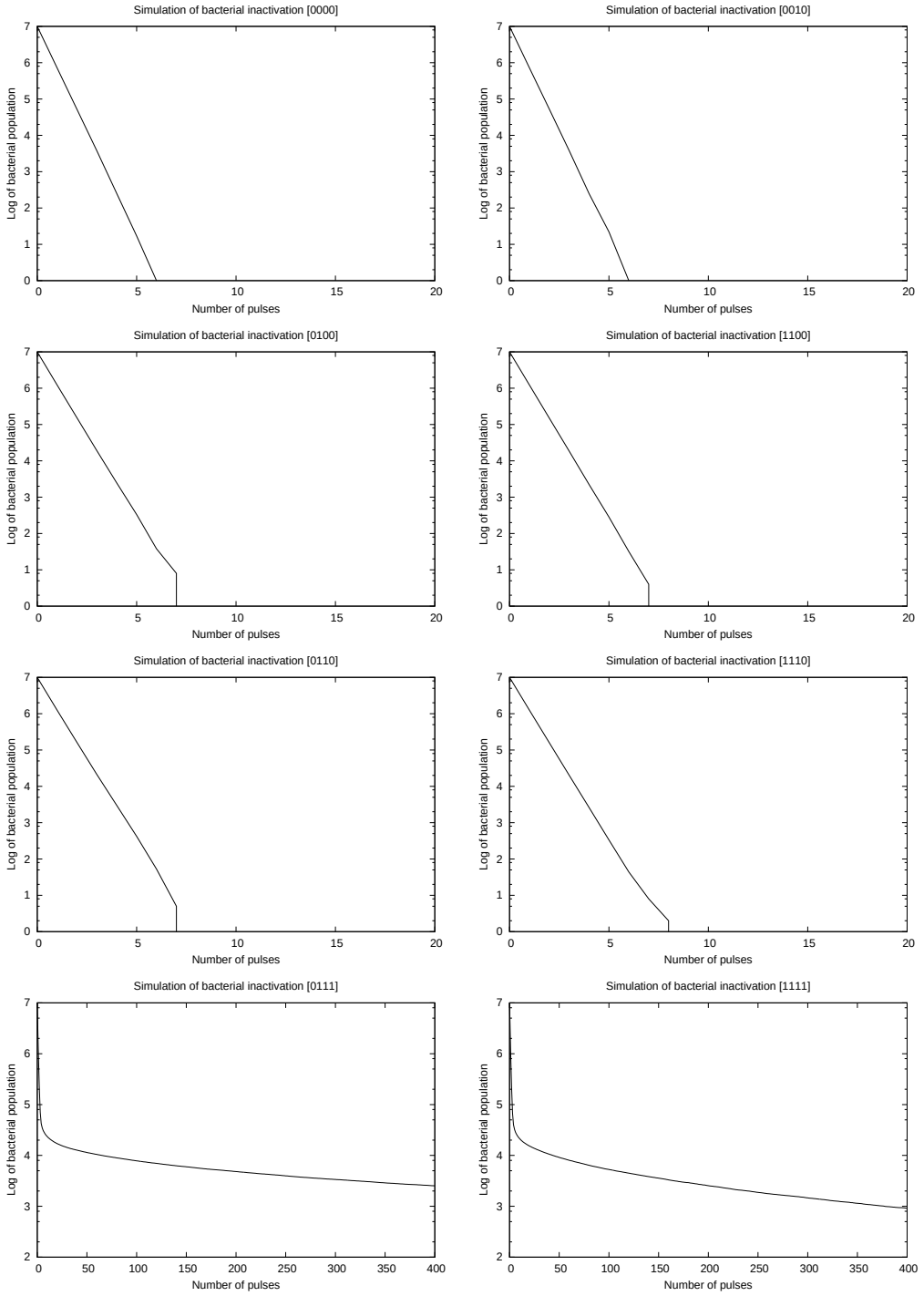

Figure 3.28: Results for the simulation of bacterial inactivation. The notation corresponds to [Rotation,Shape,Dimensions,Field].

number of pulses delivered to the treatment chamber. On the other hand, while about 3 Logs inactivation can be reached with the first 50 pulses, other 350 pulses are necessary to gain the following 1 Log. Better designs of treatment chambers can in principle reduce the tail effect, avoiding areas where the electric field is considerably lower than desired. Another possible solution can be, for static chambers, the mixing of the liquid by, for example, rotation of the chamber around its main axis. Affecting in this way the position of each cell in the interval between two consecutive pulses, the effect of the real distribution of electric field can be averaged during the treatment and its impact reduced.

In order to find an explanation for the variability of PEF results, and particularly the apparent dependence of sigma on the number of applied pulses, we take in consideration the possibility that, among different experiments, the average dimensions L and W of cells in each sample is normally distributed around the average dimensions of *E. coli* grown in our growth medium, as described in section 3.3. We prepare a set of 30 mean lengths L, distributed around the value 2.72 μ m with σ=0.272, and carry out a simulation for each of these dimensions. The mean value of W is derived form L as described before. Given the results of the previous simulation, we take in consideration only the hypothesis [1111]. Figure 3.29 shows the dependence of $\sigma(C_N)/C_N$, where C_N is the average of the predicted bacterial concentration, on the number of applied pulses. The value of $\sigma(C_N)/C_N$ is therefore expected to increase with the number of pulses. The 68% of the concentrations measured in our inactivation experiments are therefore predicted to fall between the highest and the lowest curve in fig. 3.30.

3.5 Conclusions

The predictions of electroporation theory are significantly in disagreement with inactivation levels measured in PEF treatments, and the spread of experimental results can not be explained by the accuracy of biological measures alone. In order to explain this, a careful analysis of experimental conditions has been carried out along with detailed theoretical considerations on the process of membrane charging. The electric field distribution in the PEF chamber used in our experiments has been studied through computer simulations and the impact of the finite dimensions of electrodes evaluated. A model to analytically compute the time course of transmembrane potential for a cell of generic shape has been developed and related to the accumulation of charges at both sides of the membrane. The behavior of $\varphi(t)$ for planar, spherical, cylindrical and prolate spheroidal membranes have been

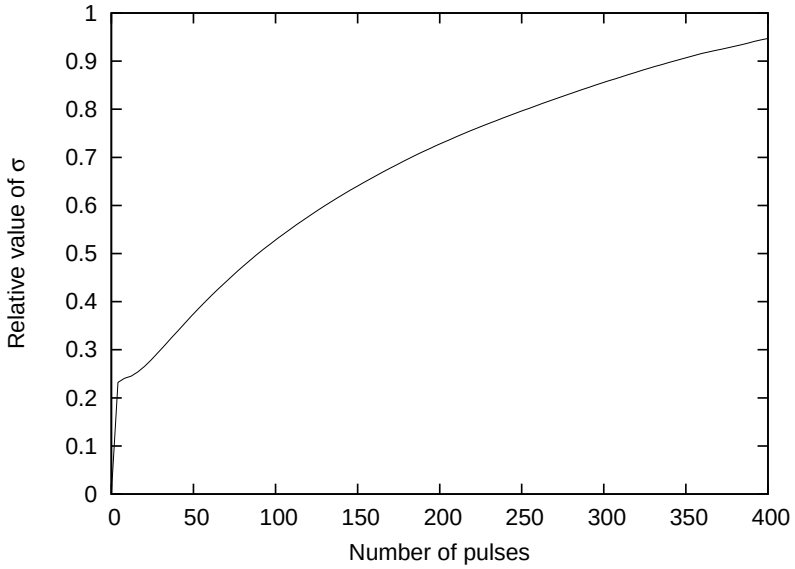

Figure 3.29: Variation of standard deviation σ with the number of applied pulses in a PEF experiment.

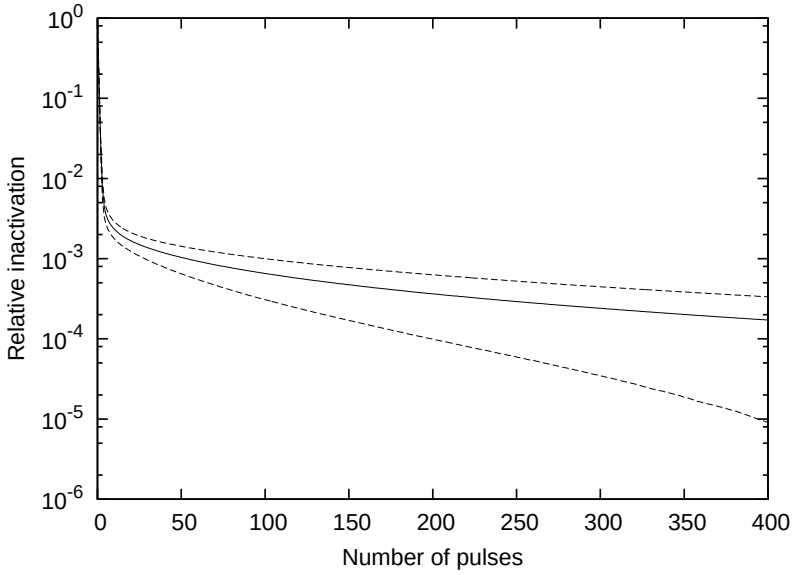

Figure 3.30: Range of relative microbial inactivation expected at 25 kVcm^{-1} for 1 σ.

derived and analyzed. The key parameters influencing both the speed and the intensity of the charging process have been identified in the local mean curvature and the suspension liquid conductivity. The time constants have been found to be small compared to the length of PEF pulses, and therefore the steady state potentials have been used in evaluation of inactivation probability. The impact of a distribution of dimensions of cells in a colony have been evaluated along with the possible variations of physiological conditions of cell populations upon repetitions of the same experiment. Computer simulations accounting for all the physical conditions analyzed have been carried out, resulting in the explanation of inactivation kinetics with the edge effects of the electric field caused by finite dimensions of the treatment chamber. The variability of results, furthermore, has been related to the variation of physiological conditions in cell populations between different experiments.

Chapter 4

PEF inactivation experiments

Measures of the inactivation by PEF of *Escherichia coli* were carried out at the laboratories of the Department of Science and Advanced Technology (DISTA) and of the Department of Environmental and Life Science (DISAV) at the University of Piemonte Orientale in Alessandria, Italy. The aim of the measures is to determine the effectiveness of PEF in controlling microbial populations and investigate possible variations in PEF effectiveness for different bacterial concentrations.

4.1 Experimental apparatus

As described in section 1.3, any pulse modulator is basically composed by a power supply, a pulse forming network (PFN), a high voltage switch, controlled by a trigger, and an output. In our experimental setup, a DC power

Figure 4.1: The DC power supply and the trigger generator.

supply (see fig. 4.1, left), with a voltage range from 0 to 250 Volts, feeds a switching circuit made by an SCR diode, followed by a transformer with a step up ratio of 1:100 (see fig. 4.2, right). The PFN is made of a 100 meters coaxial cable RG213, whose capacitance and inductance per unit length are 100 pF/m and 250 nH/m respectively. The characteristic impedance is

therefore 50 Ω and the pulse duration 1 μs. A custom air spark-gap switch

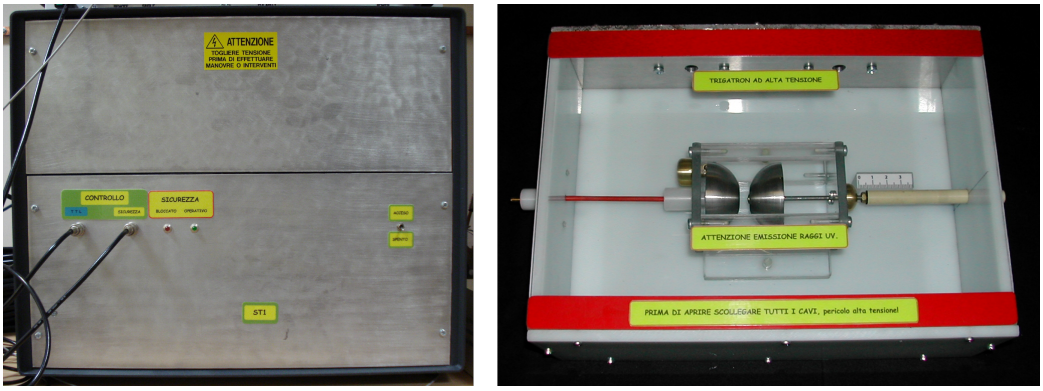

Figure 4.2: The air spark-gap switch, the SCR diode and transformer.

(fig. 4.2, left) connects the PFN to the treatment cell. It is made by two hollow spherical caps, whose distance can be varied according to the different voltage settings used. A metallic electrode, connected to a trigger generator (fig. 4.1, right), is placed in the middle of the hole pierced at the top of one of the spherical caps. A first spark is given by the trigger generator between this electrode and the pierced hollow spherical cap to initiate the operation, then the spark propagates between both caps leading to the full discharge of the cable on the treatment cell. The treatment cells, already described in section 3.1, are connected to the cable through a high voltage case (see fig. 4.3), where a HV probe is permanently connected via an oscilloscope for on-line monitoring of the height, duration and quality of the pulses. A series of HV safety devices are present all along the system to prevent accidental injuries to operators and damages to the apparatus. Before carrying out the PEF experiments on normal treatment cells, the apparatus was tested using a phantom cell made by two copper electrodes connected by a plastic tube containing a solution of copper-sulphate and water, acting like a 50 Ω power resistor. In this way it was possible to check the intensity, duration and shape of the pulse, and reveal possible reflections. A typical pulse measured across a treatment cell is shown in fig. 4.4, while the circuit scheme of the whole apparatus can be found in fig. 4.5. The apparatus was tested in continuous operation with the phantom cell for 2 hours, with a voltage between the electrodes of 5 kV and a repetition frequency of 1 Hz, without reporting any fault. Subsequently, higher voltages, up to 10 kV, were successfully tested for shorter periods of time. The PEF apparatus was funded by the Piedmont Region (Italy) in the frame of the CIPE 2007 program in the section Food

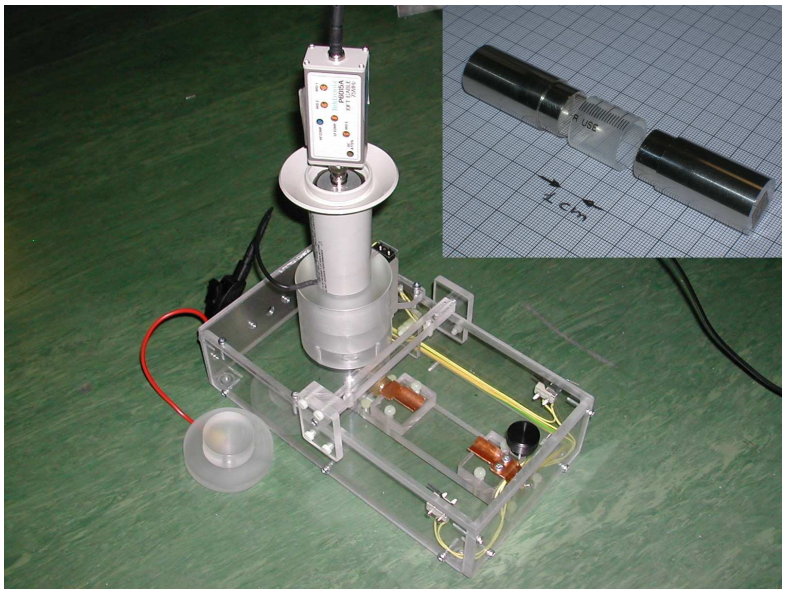

Figure 4.3: The treatment cell and the high voltage case.

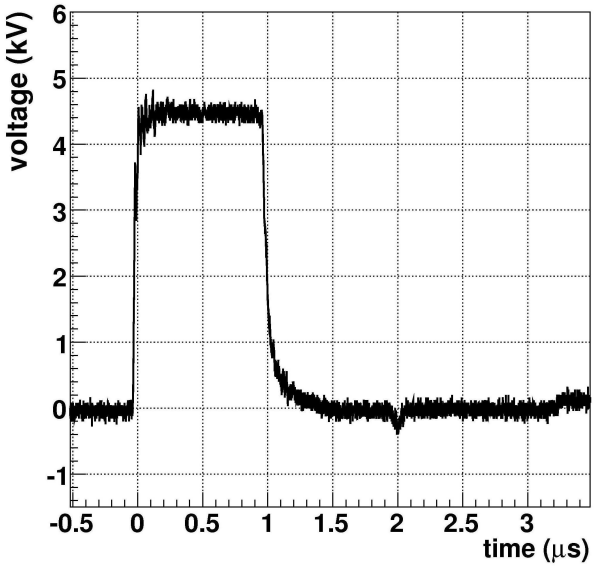

Figure 4.4: A high voltage pulse measured across the treatment cell.

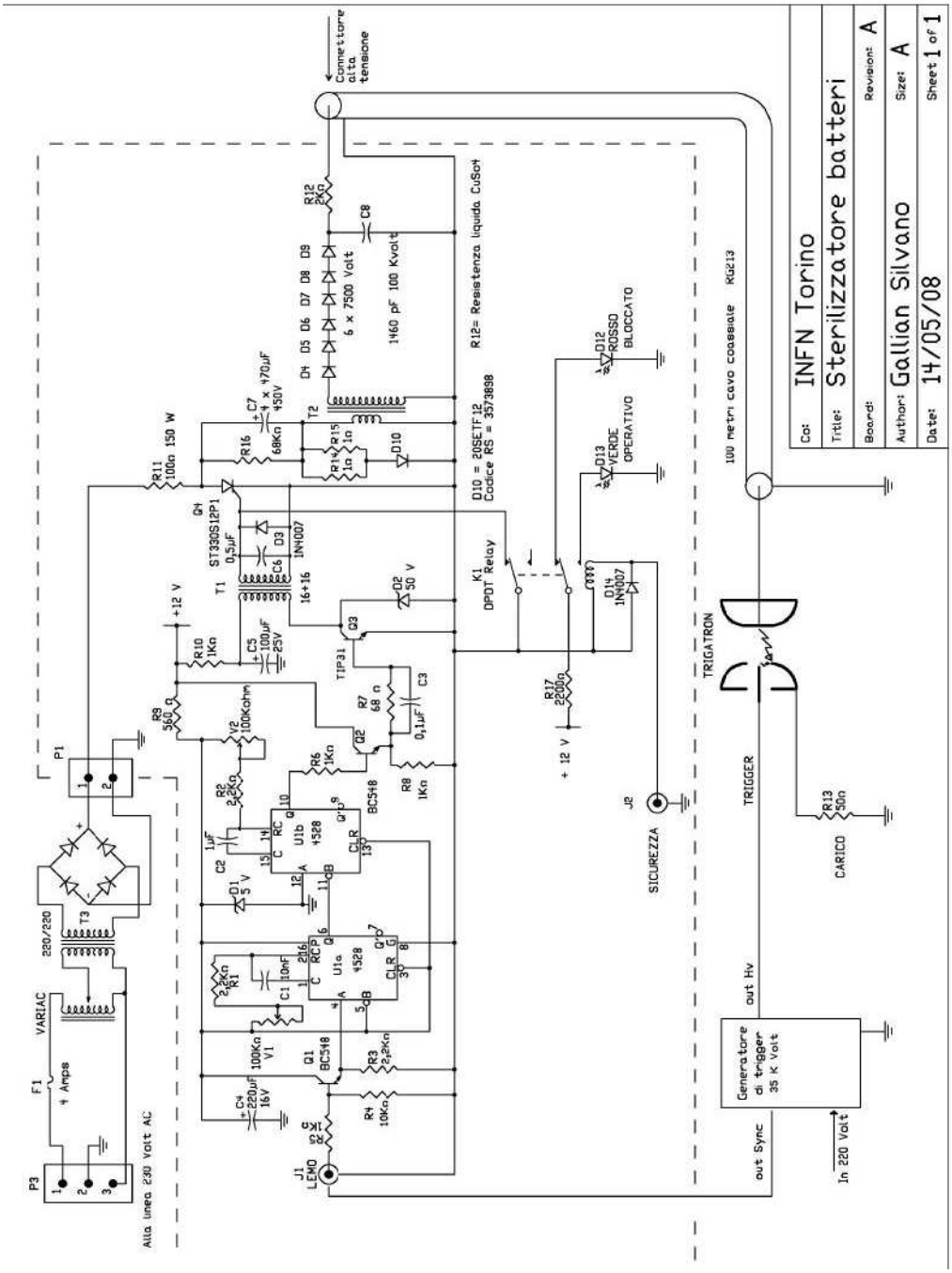

Figure 4.5: Pulse modulator circuit scheme.

Security.

Inactivation tests were then conducted using a standard *Escherichia coli* strain (ATCC 25922). The growth phase of bacteria in all the experiments was stationary (see Section 1.1.3), since higher resistance to PEF treatment has been shown in this condition [111]. A growth curve has been measured in order to determine the time required for this strain of *E. coli* to reach the stationary phase. Broth cultures were prepared by inoculating 30 ml of Tryptic Soy Broth (TSB) (Applichem, Darmstadt, Germany). During the incubation time (24 h at 37°C) *E. coli* growth was checked collecting at specific times 1 ml aliquots of the culture and determining the bacterial concentration pour plating in triplicate 100 μl of serial dilutions in physiological solution (0,9 % w/v) onto Tryptic Soy Agar (TSA) (Applichem, Darmstadt, Germany). Plates were incubated for 24 h at 37°C. The growth curve was repeated three times and the mean time to reach the stationary phase resulted about 12 h. The bacterial mean concentration in this phase was about 10^9 CFU/ml.

4.1.1 Experimental procedure

In order to measure the effects of PEF on bacterial populations we need to evaluate the reduced viability of cells in a sample after exposure to electric fields of given duration and intensity. By comparing, for example, the population in N samples exposed to different number of pulses, in the assumption that the initial concentration is the same in each sample, it is possible to study the variation of effectiveness of PEF as a function of the number of applied pulses in a given electrical condition. The typical experiment procedure consists in:

1. Preparation of a cell culture with the desired concentration;

2. Inoculation of treatment liquid in N identical cells;

3. PEF treatment, delivering different number of pulses to each cell, at the desired electric field and repetition frequency.

4. Serial dilution of PEF treated and control cell suspensions in physiological solution (0,9 % w/v) and double plating of 100 μl onto Tryptic Soy Agar (Applichem, Darmstadt, Germany) to evaluate the number of survived bacteria.

Each of these steps can be a source of errors and therefore has to be analyzed in depth.

Step 1-2: bacterial concentration

Given the complexity of a system made of alive components, like a bacterial culture, the problem of concentrations is not trivial. Bacteria grow in number, at least in favorable environmental conditions (see Section 1.1.3), and therefore both the initial and final concentration in a sample could change in a rather unpredictable way and affect the readability of results. Cells has therefore to be suspended in a batch solution, a medium where bacterial growth is extremely suppressed by lack of nutrients. In our experiments we used a McIlvane buffer, a solution of disodium phosphate and citric acid, which can be prepared to cover a range of pH from 2.2 to 8.0. A neutral pH of 7.2 was chosen to minimize cell stress, while the conductivity was set to 0.2 S/m to obtain the desired 50 Ω impedance matching. On the other hand, obviously, bacteria has to be grown in another medium, the TSB, before suspension in McIlvane. Once the stationary phase is reached, we can be reasonably sure that the bacterial concentration is around 10^9 CFU/ml. Subsequently bacteria has to be transferred from TSB to McIlvane, and in the process the desired concentration at which we would like to carry out the test has to be reached. This is achieved by centrifugation of a given volume of TSB, (10.000 x g, 10 min at 4°C) resulting in the deposition of the entire bacterial population in a solid *pellet*. The remaining liquid can therefore be expelled and the pellet resuspended in the desired quantity of McIlvane. The most common procedure for filling N treatment cells is to take N volumes of 1 ml out the TBS flask, dilute each one to reach the desired concentration (assuming that the initial concentration is 10^9 CFU/ml), than centrifuge and resuspend each pellet in 1 ml of McIlvane. Each dilution process, anyway, is intrinsically a source of errors, and the final concentration of bacteria in the treatment samples can be different. To overcome this problem we decided to take a single sample of N ml from TBS, dilute to reach the desired concentration, centrifuge and finally suspend the remaining single pellet in McIlvane (see fig. 4.6). Subsequently we can use this solution to fill each treatment cell, and we are therefore sure the the bacterial population is the same, even if the uncertainty on the initial population in TBS and the one introduced by the dilution do not allow us to derive exactly this concentration. For this reason a control sample, usually marked as C_0, left untreated, is used to measure the real initial concentration. Even in a batch solution like McIlvane a minimum degree of bacterial growth can be experienced. To reduce this possible source of errors the treatment cells, once inoculated, are kept refrigerated in ice until and immediately after the PEF treatment. The low temperatures also reduce the risk of electrical breakdown in the treatment cell.

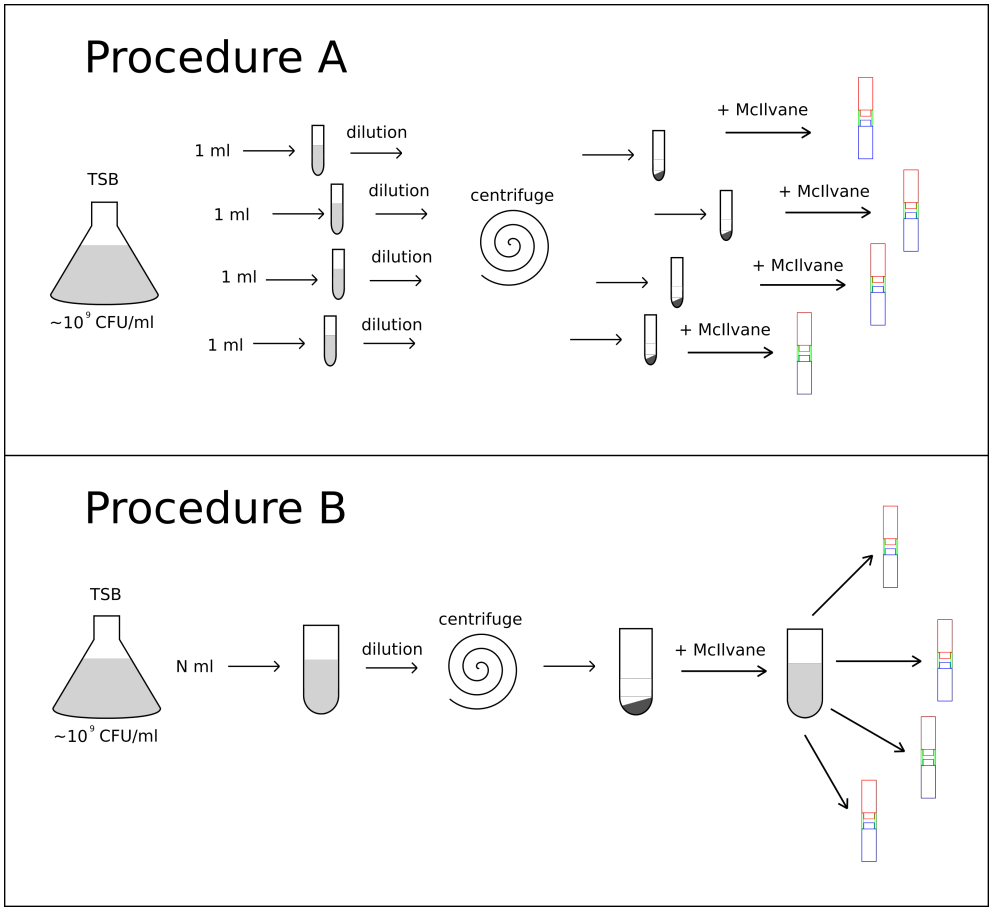

Figure 4.6: The two possible inoculation procedures of *E. coli* in treatment cells.

Step 3: PEF treatment

The McIlvane solution conductivity was originally chosen to 0.2 S/m to reach perfect matching of impedance at room temperature. The choice to run the experiments using refrigerated samples changes the real impedance of the cell, and also the presence of a great concentration of bacteria can affect the resistivity of the liquid. The voltage between the electrodes, therefore, will be higher than in perfect matching, forcing the use of another treatment cell to calibrate the output of the modulator before the actual test, in order to reach the desired electric field in the chamber. During long treatments, furthermore, the temperature of the liquid rises, hence the voltage across the electrodes decreases, but this can easily be compensated by manually adjust the output of the modulator. This modification of the voltage across

the electrodes is anyway quite small even for long treatments ($\sim$ 5 minutes). The reliability of the modulator has been tested (with the phantom cell) for very long treatments reporting a satisfactory stability of the pulse output.

Step 4: bacterial population evaluation

After PEF treatment, the bacterial concentration in each sample is evaluated as described in Section 1.1.3. The precision of this procedure depends on the uncertainties introduced by the serial dilutions that are necessary to obtain a readable result on a Petri dish. If we call C the bacterial concentration in the original sample, and N_f the number of bacteria in 1 ml estimated through the Petri dish procedure, we can write

$$C = \frac{N_f}{V_1^{n+1}} \cdot (V_1 + V_2)^n \tag{4.1}$$

if the sample has undergone n dilutions. The volumes V_1 and V_2 are simply the 1 ml and 9 ml volumes of liquid used in any dilution. Usually V_1 and V_2 can be prepared with a precision of $\sim 1\%$, and the error on the measure of the concentration will be

$$\delta C = \Bigg[\Big(N_f\Big[-(n+1)V_1^{-(n+2)}(V_1+V_2)^n + \\ + nV_1^{-(n+1)}(V_1+V_2)^{n-1}\Big]\cdot\delta V_1\Big)^2 + \Big(n\frac{N_f}{V_1^{n+1}}(V_1+V_2)^{n-1}\cdot\delta V_2\Big)^2\Bigg]^{\frac{1}{2}} \tag{4.2}$$

The usual dilution number does not go beyond 4, thus, as seen from fig. 4.7, the precision on the measure of the bacterial concentration can be estimated around 4-6%.

4.2 PEF inactivation experiments

The experimental procedure described in section 4.1.1 can in principle be used to determine the uncertainty σ of the single measure, assuming the errors are arising only from the fluctuations in bacterial concentration due to the dilution procedure. We have seen that the relative value of uncertainties can be estimated in this way to be $\sim 5\%$. There is no reason, if considering only this source of error, to expect a variation of σ with the number of applied pulses. We have seen, anyway, that the experimental practice suggests an increase of σ with the number of pulses, and we also related this behavior to the distribution of average cell dimensions and found the expected values of σ

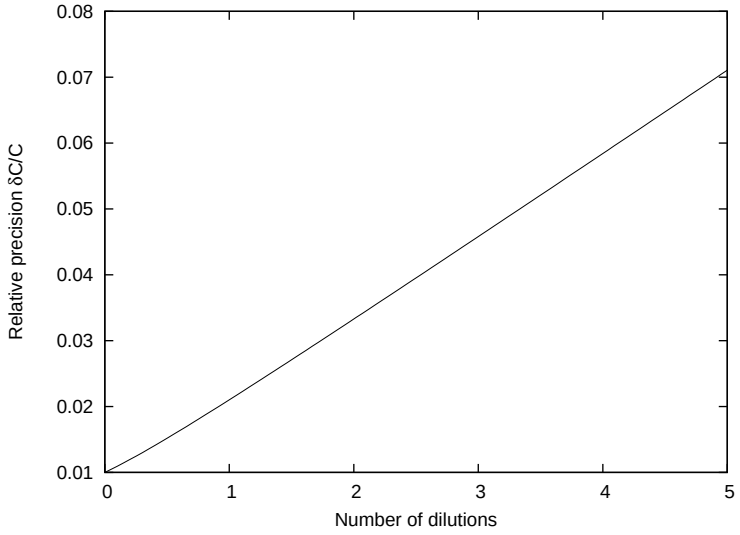

Figure 4.7: Variation of relative precision in estimating bacterial concentrations as a function of dilution number.

by means of a computer simulation. It is clear that if both the factors combine to determine the total σ, the uncertainties arising from the distribution of average cell dimensions dominate even for very small numbers of applied pulses. We tried to estimate the standard deviation by repeating the same condition of number of pulses on each sample, the results are reported in table 4.1. Unfortunately, given the long times required to carry out these measures, we could not investigate more than two conditions. It is therefore impossible to experimentally verify the results of our simulation on the variation of σ. Nevertheless, measures reported in table 4.1 are clearly incompatible with the relative uncertainty $\sigma_x/\mathrm{x} \sim 0.05$ arising from the procedure of counting bacteria alone. We chose therefore to make use of the results of our theoretical simulations in the estimation of experimental uncertainties.

4.2.1 PEF inactivation results

Measures of PEF inactivation on *Escherichia coli* were carried out at 25 kVcm^{-1}, 1 μs, for a pulse repetition rate of 1 Hz. In fig. 4.8-4.13 the ratio between final and initial bacterial concentration (usually referred to as relative inactivation) is plotted as a function of the number of applied pulses and compared to the predictions of computer simulations described in Chapter 3.

Initial measures (fig. 4.8-4.10) were carried out for a number of applied

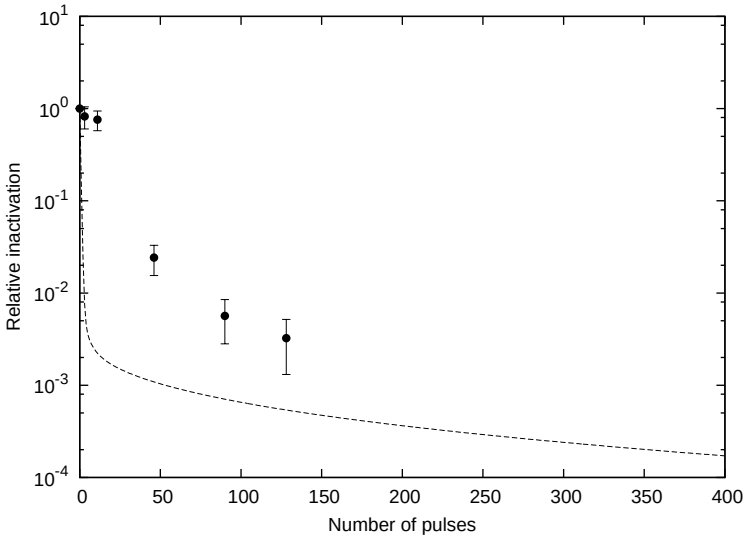

Figure 4.8: Comparison between predicted inactivation and PEF experiments on *Escherichia coli* at 25 kVcm^{-1}. Initial bacterial concentration is (3.1 $\pm$ 0.2) $\times$ 10^8 CFU/ml.

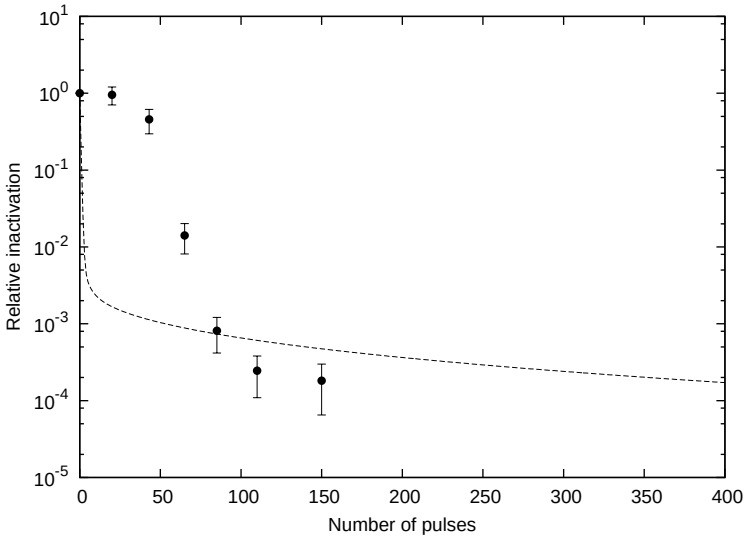

Figure 4.9: Comparison between predicted inactivation and PEF experiments on *Escherichia coli* at 25 kVcm^{-1}. Initial bacterial concentration is (6.1 $\pm$ 0.3) $\times$ 10^9 CFU/ml.

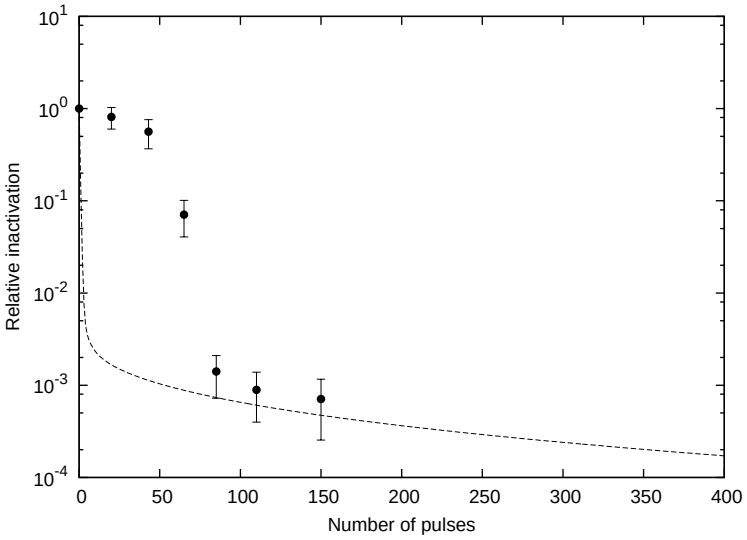

Figure 4.10: Comparison between predicted inactivation and PEF experiments on *Escherichia coli* at 25 kVcm^{-1}. Initial bacterial concentration is $(8.9 \pm 0.4) \times 10^9$ CFU/ml.

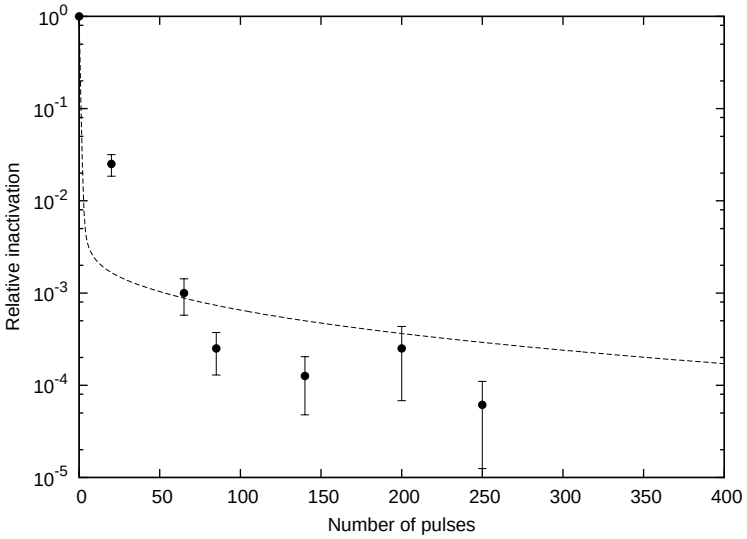

Figure 4.11: Comparison between predicted inactivation and PEF experiments on *Escherichia coli* at 25 kVcm^{-1}. Initial bacterial concentration is $(3.2 \pm 0.2) \times 10^8$ CFU/ml.

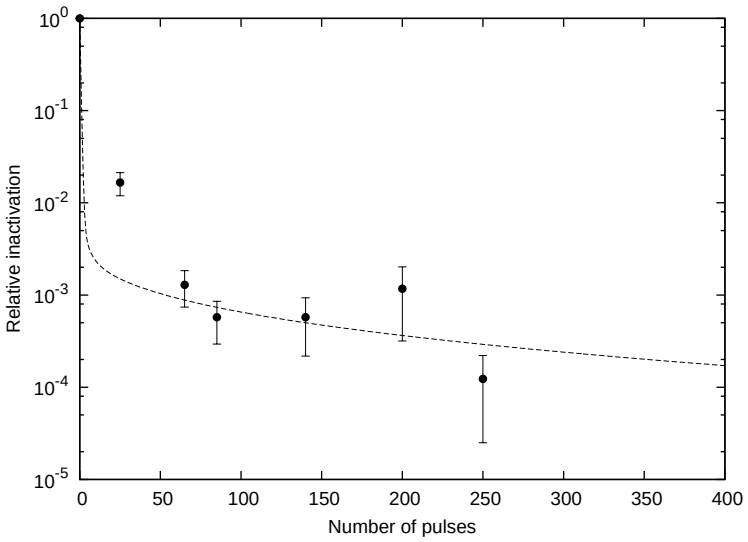

Figure 4.12: Comparison between predicted inactivation and PEF experiments on *Escherichia coli* at 25 kVcm^{-1}. Initial bacterial concentration is $(3.9 \pm 0.2) \times 10^8$ CFU/ml.

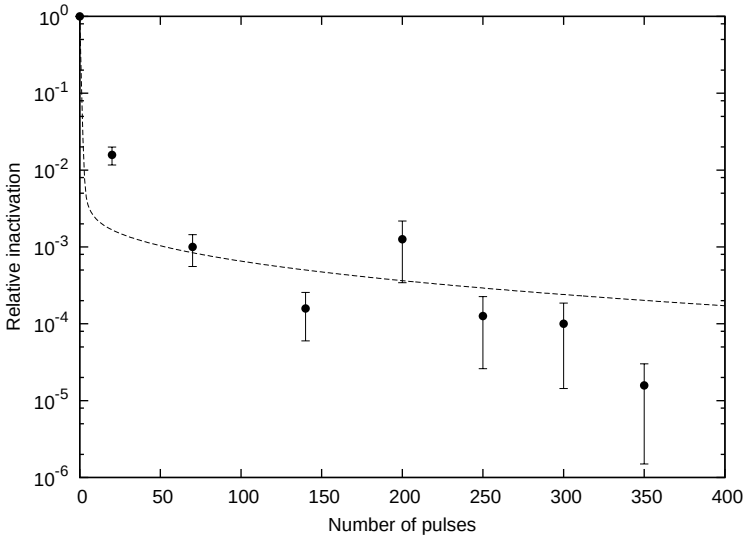

Figure 4.13: Comparison between predicted inactivation and PEF experiments on *Escherichia coli* at 25 kVcm^{-1}. Initial bacterial concentration is $(4.0 \pm 0.2) \times 10^8$ CFU/ml.

Measure N°	50 Pulses	200 Pulses
1	$3.65 \cdot 10^6$	$8.32 \cdot 10^5$
2	$5.60 \cdot 10^6$	$1.07 \cdot 10^6$
3	$7.65 \cdot 10^6$	$1.66 \cdot 10^5$
4	$9.95 \cdot 10^6$	$7.41 \cdot 10^4$
5	$5.30 \cdot 10^6$	$9.55 \cdot 10^5$
6		$9.55 \cdot 10^5$
Measured σ_x/x	0.38 ± 0.13	0.6 ± 0.2
Simulated σ_x/x	0.38 ± 0.05	0.7 ± 0.1

Table 4.1: Microbial concentrations after 50 and 200 at 25 kVcm^{-1} on *E. coli*. Concentrations are expressed in CFU/ml.

pulses N_p lower than 150, and the measured inactivations were clearly different from what expected for $N_p \lesssim 100$. The difference between predictions and measures in this range could have a qualitative explanation in the ability of bacteria to adapt to hostile environments. It is possible that, for a small amount of pulses delivered, the bacterium is able to repair the damages inflicted and possibly activate some mechanism to contrast the effectiveness of PEF. The plasma membrane, in fact, usually maintains a constant transmembrane potential around -70 mV by regulating the concentration of charged ions inside and outside the cell (see Chapter 1). When pulses are applied, this transmembrane potential increases greatly, as we have seen in Chapter 3, as a consequence of charge accumulation. At least initially, the membrane probably tries to compensate this accumulation by acting on the concentration of charged ions, resulting in an inactivation probability smaller than expected. Similar decreased effectiveness of PEF on *E. coli* for a small number of applied pulses has been observed in other studies [112], particularly in relation to the occurrence of sublethal injuries to the cells. A detailed explanation of these possible mechanisms, however, has not been given yet, and its future investigation could be important to gain insight on electroporation at microscopic level.

Subsequently we increased the number of applied pulses (fig. 4.11-4.13), concentrating our investigation on the tail of inactivation curves. For large number of pulses the adaptation mechanisms performed by *E. coli* are overcome by electroporation and the cell populations qualitatively approximate to the curve found in our simulations. The levels of inactivation reached are in the range of 4-5 order of magnitudes. The apparent tail effect is compatible with the predictions of computer simulations, and could therefore be related

to the decreased intensity of electric field near the edges of the electrodes. The saturation effect is only apparent, and in principle it is possible to reach higher levels of inactivations by increasing the number of applied pulses N_p. It is clear, anyway, that the energy efficiency falls dramatically for high N_p. A more quantitative measure of this effect would require a better knowledge of the constants involved in the calculation of survival probability S in eq. 2.38 used in our simulations. Particularly, only the order of magnitude of Γ and γ is known [77], and their variation (especially as regards to γ) has a great influence on the estimation of the apparent saturation level.

The impact of edge effect can be reduced developing different treatment chamber shapes, and adequate designs are therefore necessary for the use of PEF in specific applications, depending on the required inactivation levels, in order to minimize the energy consumption. Finally, increasing the total volume of treatment chambers would also reduce the impact of edge effect. We will discuss the subject of volumes in Chapter 5, where an innovative solution will be proposed.

4.2.2 Variation of effectiveness with initial concentration

The theory of electroporation does not predict any influence of bacterial concentration on survival probability. In principle, anyway, some kind of interaction among bacteria is possible, and could affect PEF inactivation levels. Local distortions of the electric field, due to the presence of bacteria, could play a role as well. Previous works have found contradicting results on this subject both for *E. coli* and other bacterial species [113, 114]. For these reasons we decided to investigate the effectiveness of PEF as a function of the initial bacterial concentration. In this experiment 11 measures where performed with an electric field intensity of 25 $\mathrm{kVcm^{-1}}$, a pulse duration of 1 μs and a repetition rate of 1 Hz. Each measure consisted in the delivery of a different amount of pulses to 7 liquid samples of the same initial bacterial concentration. This concentration was varied among different experiments, from 10^5 to 10^{10} CFU/ml, while the set of applied pulses was kept constant, namely 20, 70, 140, 200, 250, 300, 350. Experimental results are reported in fig. 4.14-4.24.

In order to evaluate the possible change in PEF effectiveness, the relative inactivation levels reached for each given number of applied pulses were compared, as shown in fig 4.25 and 4.26, were a linear and a parabolic regressions are performed. Measures reveal that bacterial inactivation is influenced by the initial sample concentration, being higher when the bacterial concentra-

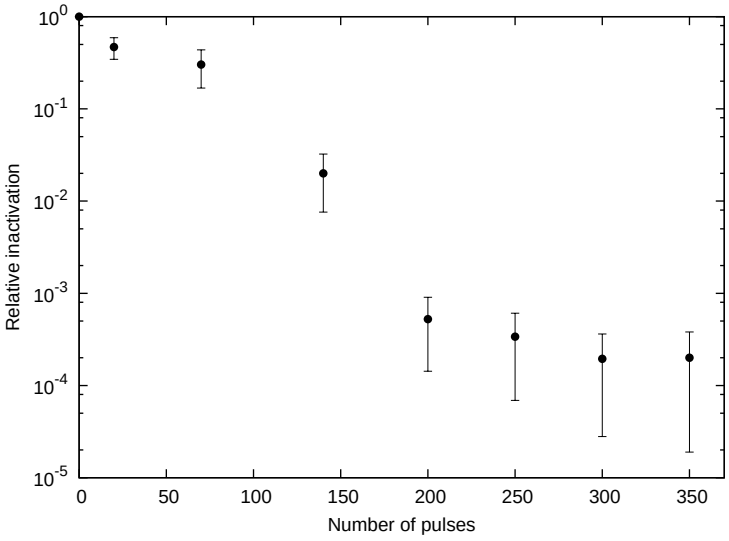

Figure 4.14: Relative bacterial inactivation for an initial population of (6.6 $\pm$ 0.3) $\times$ 10^5 CFU/ml.

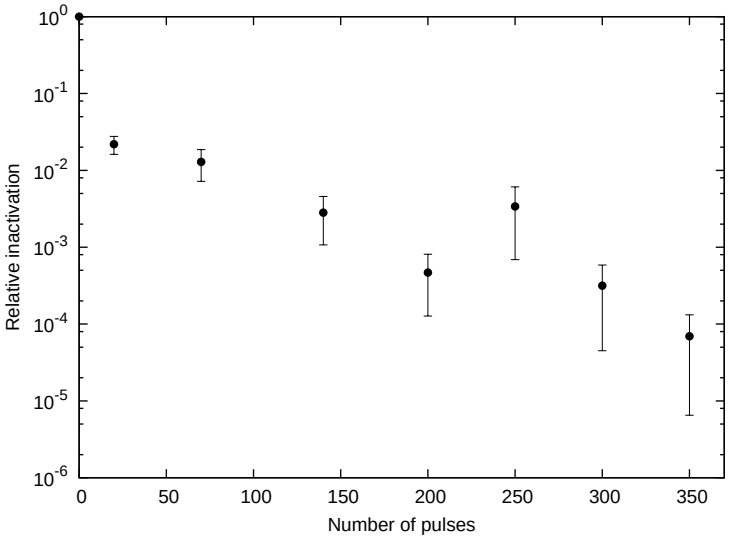

Figure 4.15: Relative bacterial inactivation for an initial population of (2.0 $\pm$ 0.1) $\times$ 10^6 CFU/ml.

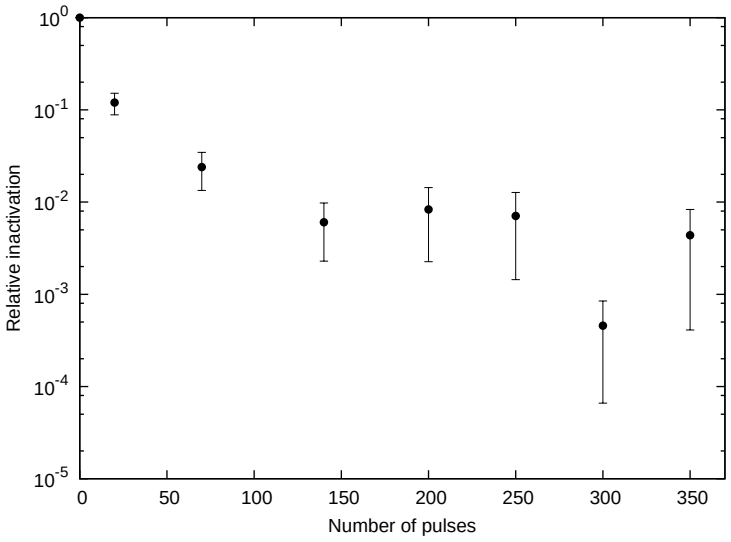

Figure 4.16: Relative bacterial inactivation for an initial population of (6.9 $\pm$ 0.3) $\times$ 10^6 CFU/ml.

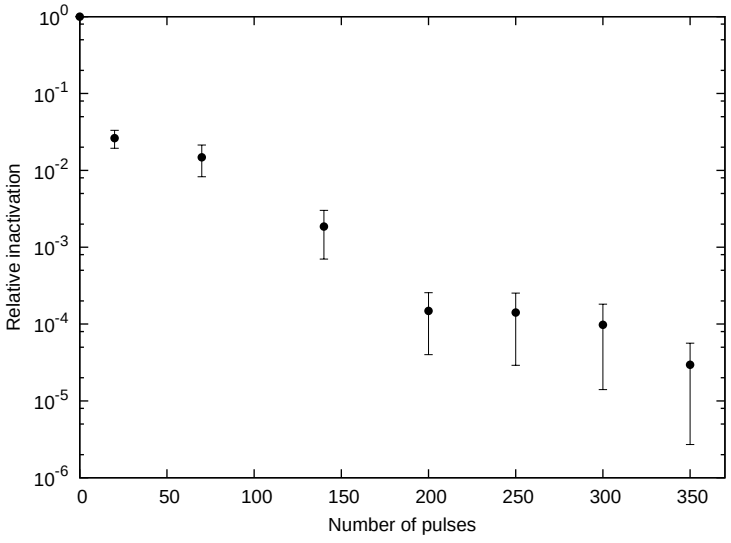

Figure 4.17: Relative bacterial inactivation for an initial population of (3.6 $\pm$ 0.2) $\times$ 10^7 CFU/ml.

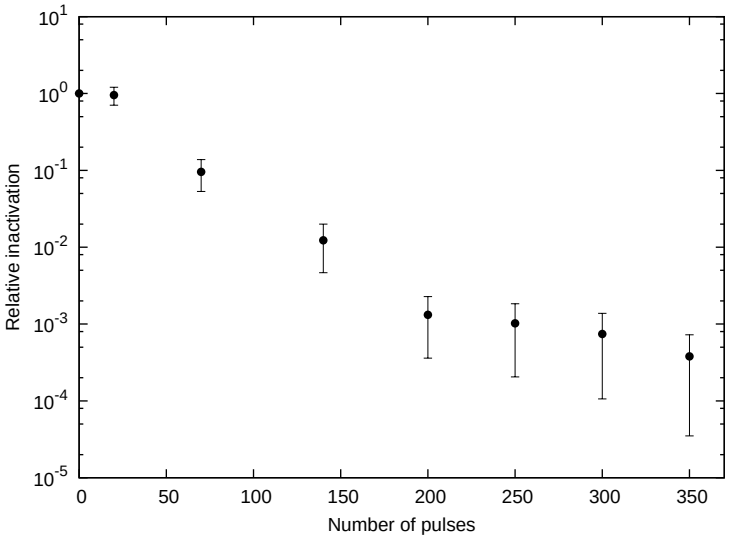

Figure 4.18: Relative bacterial inactivation for an initial population of (7.1 $\pm$ 0.4) $\times$ 10^7 CFU/ml.

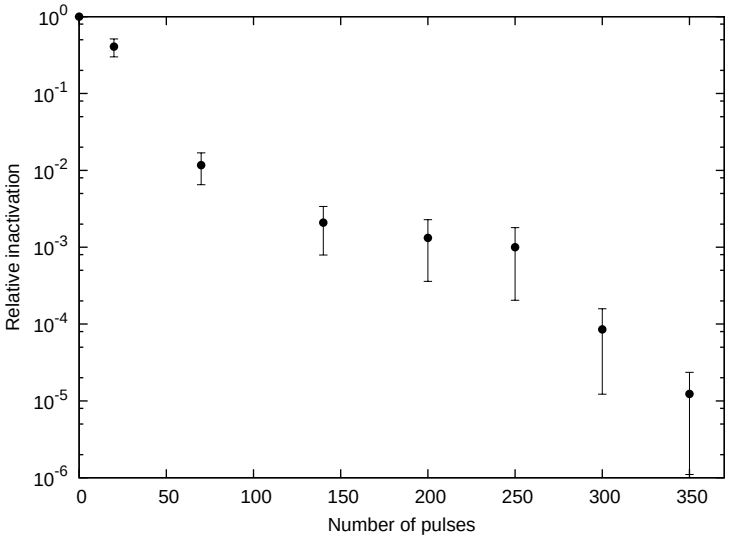

Figure 4.19: Relative bacterial inactivation for an initial population of (3.9 $\pm$ 0.2) $\times$ 10^8 CFU/ml.

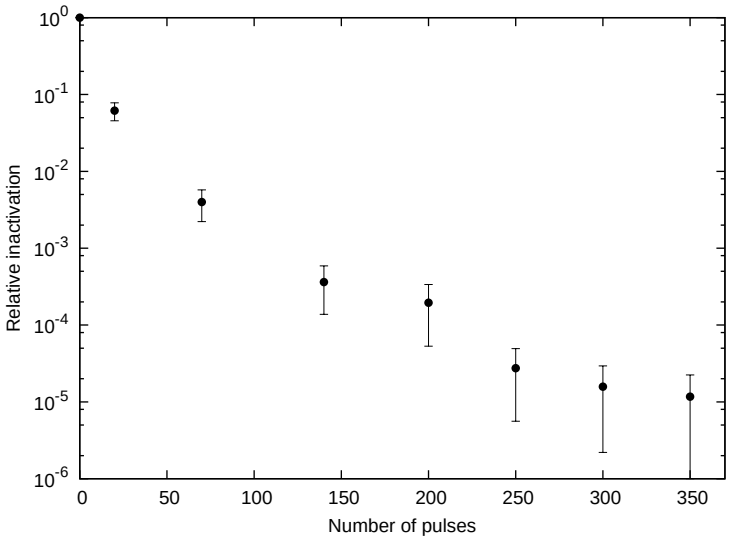

Figure 4.20: Relative bacterial inactivation for an initial population of (3.0 $\pm$ 0.2) $\times$ 10^9 CFU/ml.

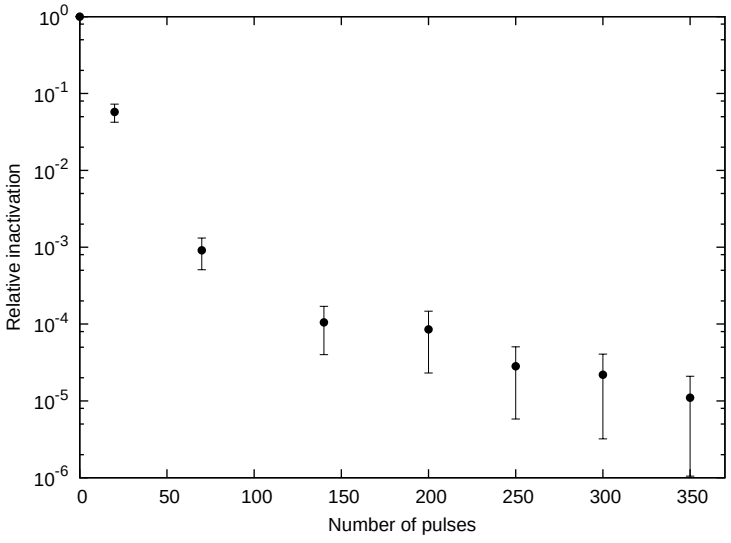

Figure 4.21: Relative bacterial inactivation for an initial population of (5.4 $\pm$ 0.3) $\times$ 10^9 CFU/ml.

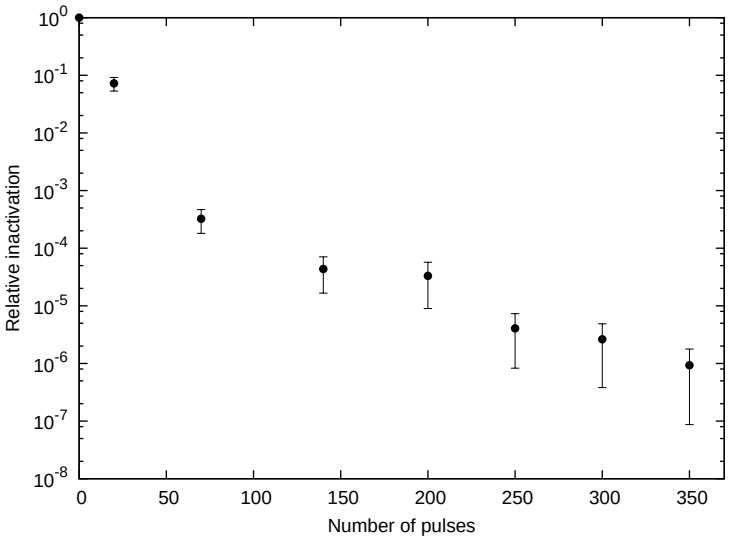

Figure 4.22: Relative bacterial inactivation for an initial population of (1.55 $\pm$ 0.08) $\times$ 10^{10} CFU/ml.

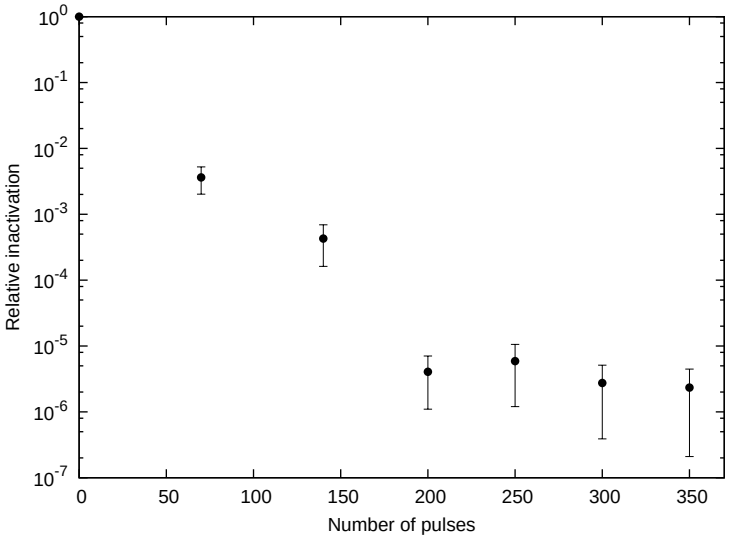

Figure 4.23: Relative bacterial inactivation for an initial population of (4.8 $\pm$ 0.2) $\times$ 10^{10} CFU/ml.

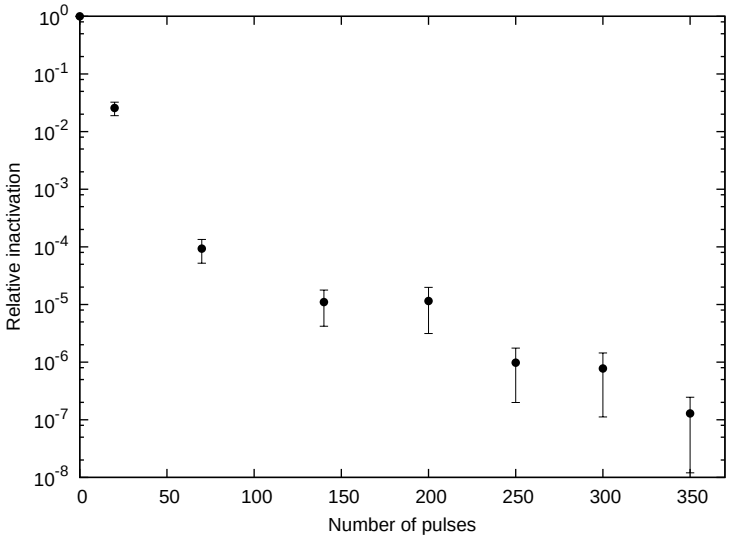

Figure 4.24: Relative bacterial inactivation for an initial population of (5.0 $\pm$ 0.3) $\times$ 10^{10} CFU/ml.

tion is higher. It is difficult to understand what type of correlation relates the experimental data for each amount of applied pulses N_p. For a low number of pulses applied the adaptation mechanism described in previous section affects the spread of measures, resulting in an underestimation of the uncertainties and great values of χ^2/ndf both for a linear and a parabolic fit. The plot at 20 pulses is not shown for this reason, while for the plots at 70 and 140 pulses the poor agreement both with a linear and quadratic fit is evident. The adaptation improves starting from 200 pulses for both the regressions. Since no explanation of this change in effectiveness has been found, there is in principle no reason to prefer a linear or a quadratic regression (or even a more complicated function). From this data, anyway, we can exclude that the effectiveness of PEF remains constant in the range of bacterial concentration from 10^5 to 10^{10} CFU/ml. If we choose to describe this behavior with a straight line in Log-Log scale, it is possible to relate the effectiveness of PEF on *E. coli* to the initial bacterial concentration with

$$R_1^{(N)} = R_0^{(N)} \left(\frac{C_1}{C_0} \right)^m \tag{4.3}$$

where $R_1^{(N)}$ and $R_0^{(N)}$ are the relative final concentrations after N pulses for samples with initial concentration C_1 and C_0, respectively.

A change in effectiveness of PEF could be related either to electrical or biological issues. The inactivation probability is affected by the local E field

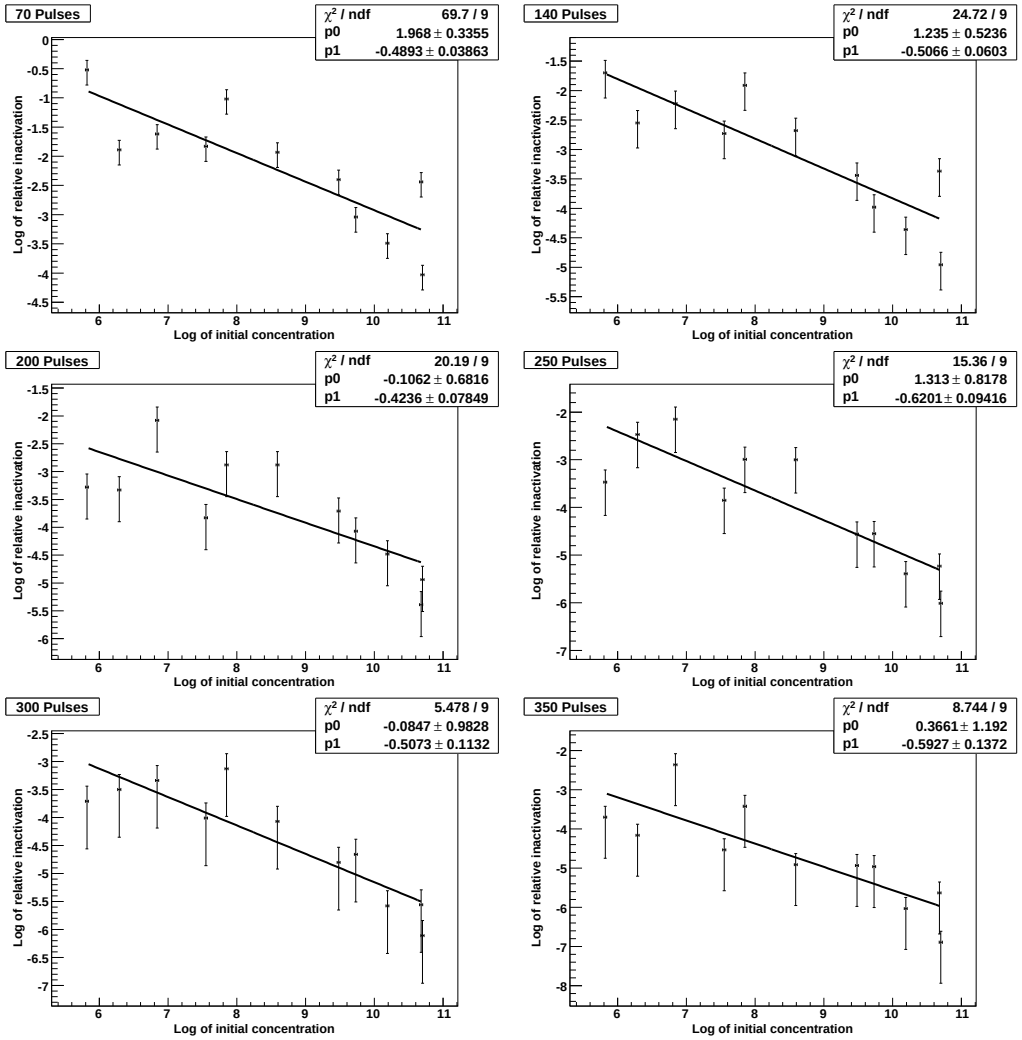

Figure 4.25: Linear regressions for the variation of PEF effectiveness with the initial bacterial concentration.

intensity, and it could be influenced by bacterial concentration. The conductivity of the suspension liquid changes when bacteria are suspended, but this change, experimentally estimated in $\sim 15 - 20\%$, does not affect the charging constants τ_1 and τ_2 discussed in Section 3.2 in such a way to affect the charging process, that can still be considered instantaneous with respect to the pulse duration. Since the electric field is kept constant by adjusting the pulse intensity before and during the experiment, a global electric effect cannot be involved in the explanation of this phenomenon. Locally, instead, the presence of a great density of bacteria could influence the distribution

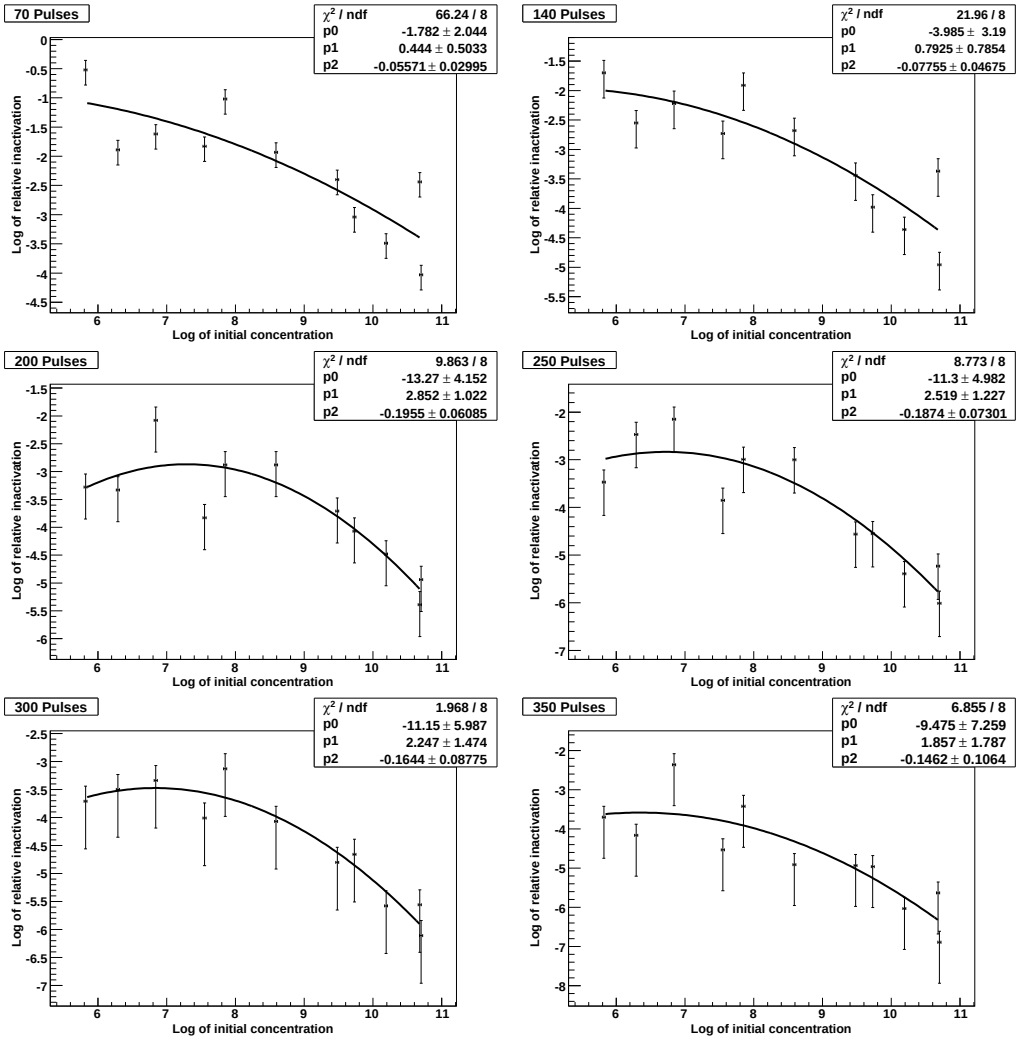

Figure 4.26: Quadratic regressions for the variation of PEF effectiveness with the initial bacterial concentration.

of the electric field, since bacteria are known to aggregate in clusters (see fig. 4.27), and this behavior is enhanced the greater bacterial concentration. The cluster formation leads to a local distortion of the electric field lines, and therefore the individual bacteria experience a non-uniform field. The analysis on transmembrane potential carried out in Chapter 3 is not valid anymore and some particular phenomenon of field enhancement could lead to the greater inactivation levels measured in our experiments. On the other hand, it is well known that adjacent cells can be led to fusion by an external electric field [115]. Usually cells are placed in adjacent position by

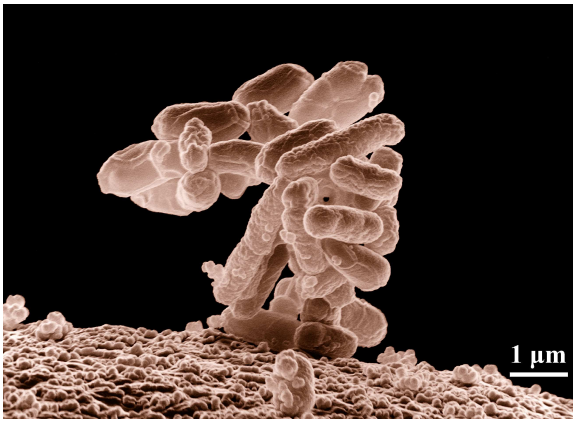

Figure 4.27: A cluster of *Escherichia coli*.

application of a low intensity external electric field, then a breakdown pulse of tens of microseconds and ~ 1 kVcm^{-1} is delivered to reach electrofusion. If the cells are already in favorable position, because of the formation of a cluster, the application of PEF pulses could trigger electrofusion in some spots in the cluster itself. The modifications in plasma membranes caused by this phenomenon could in principle lead to a decreased membrane stability and an enhanced susceptibility to PEF. A support to this explanation comes from the observation [111] that PEF is more effective on bacteria in the exponential phase of growth. This phenomenon is usually related to a diminished resistance to external stresses caused by the modifications to which the plasma membrane is undergoing during the process of cell growth and division. Further research, anyway, will be necessary to precisely understand this change in effectiveness of PEF with bacterial concentrations.

4.3 Conclusions

Pulsed Electric Fields technology has been applied to the treatment of *Escherichia coli* suspended in McIlvane buffer solution. The apparatus was described and the test procedure analyzed in order to achieve a comprehensive evaluation of uncertainties. Results of numerical simulations were used to evaluate the intrinsic fluctuations of PEF measures. Bacterial experiments showed qualitative agreement with the results of simulations developed in Chapter 3, when the number of pulses delivered is greater than 100. Inactivation levels reached were in the order of 4-5 Logs for 350 pulses of 25 kVcm^{-1}, 1 μs at 1 Hz. An effectiveness lower than expected was found

instead for a low number of pulses, probably indicating the activation by bacteria of some adaptation mechanism to contrast the development of the high transmembrane voltages responsible for membrane rupture. The variation of effectiveness of PEF as a function of initial population was studied and higher efficiency was found for greater bacterial concentrations, in contrast with the theoretical absence of variation predicted by the transient aqueous pore model. The high spread of results does not allow to draw conclusions about the relation between initial bacterial concentration and relative inactivation, although the simple linear and quadratic regressions seem to approximate reasonably to the experimental data when the number of pulses delivered is high. For low number of pulses the bacterial tendency to adapt to PEF treatment, observed in previous experiments, increases the variability of results worsening the correlation among measures. A possible biological explanation to this variation of effectiveness was given, in relation to the occurrence of interactions between lipid membranes of adjacent cells in a cluster, but further researches will be necessary to better understand this phenomenon.

Chapter 5

High permittivity ceramic materials in PEF

Among the factors slowing the application of PEF on large scale, an important role is played by chamber volumes and durability of electrodes. Using a transmission line based modulator has the advantage of delivering squared pulses to the treated liquid, which is reckoned to maximize the effectiveness of PEF treatment. On the downside, it requires a degree of impedance matching of the load to the PFN of the generator. This places a limitation on the possible volumes of treatment chambers, as can be seen in a simple rectangular electrodes shape (see fig. 5.1). The total volume v is related to

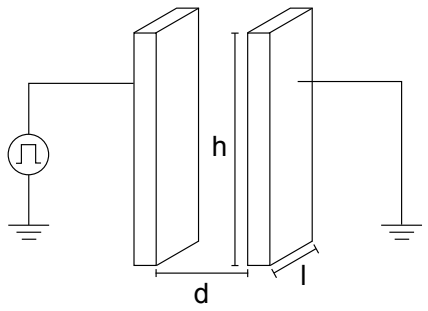

Figure 5.1: A simple rectangular electrode chamber. The surface $s = l \cdot h$ and the distance between electrodes d set the electric characteristics of the chamber.

the electric parameters by

$$v = \frac{1}{\sigma} \frac{V^2}{Z_0 E_0^2} \tag{5.1}$$

where σ is the liquid conductivity, V is the voltage between the electrodes given by the pulser, Z_0 is the characteristic impedance of the PFN and E_0 the desired electric field. The liquids of interest for PEF treatment are all in the range 0.1 - 0.5 Sm^{-1}, and the electric field necessary for bacterial inactivation, from what discussed in Chapter 2, are in the range of $20 - 30$ kVcm^{-1}. Common pulse generators can reach ~ 40 kV without the use of transformers, which results in a maximum volume for treatment chambers of $20 - 30$ ml. Larger volumes would reduce the resistance of the chamber and the voltage experienced between the electrodes. The use of pulse transformers, to increase V, would not affect the value of v as they also modify the characteristic impedance leaving the ratio V^2/Z_0 constant. Although perfect matching is not strictly required, tolerable slight mismatches would not make possible to increase volumes beyond the tens of ml. It is clear that these volumes can be very difficult to adapt to a large scale plant, where the liquid flux must be in the order of 2000 - 5000 L/h. If we consider for example a flux of 3600 L/h, the resident time in a 20 ml chamber is just 20 ms, hence, in order to deliver a typical value of 200 pulses capable of reducing bacterial population of a factor 10^3, the pulse frequency must be 10^4 Hz. But such a high repetition frequency has the double disadvantage of requiring an enormous power consumption and increasing the temperature of the treatment chamber to a point where PEF cannot be considered a non-thermal treatment anymore, unless heat is removed from the electrodes using a cooling system. This, again, would increase the power consumption, and the high repetition frequency could also enhance the possibility of breakdowns both in the treatment chamber and in the modulator itself.

5.1 High permittivity ceramics

A possible way to increase the chamber volumes would be to increase their resistance. As we have seen already, the liquid conductivity varies in a very narrow range, for typical liquid foods, and cannot be exploited for this purpose. If the electrodes are covered with a layer of very resistive ceramic material, instead, the total resistance of the chamber would be increased accordingly (see fig. 5.2). We expect the voltage drop, in such a configuration, to develop only across the very resistive ceramic layer, at least when the steady state is reached. There is anyway the possibility of a transient electric field in the liquid, as it was shown in [116]. The potential inside the dielectric materials and the liquid can be expressed as

$$\varphi_1(z,t) = A_1(t)z + B_1(t)$$

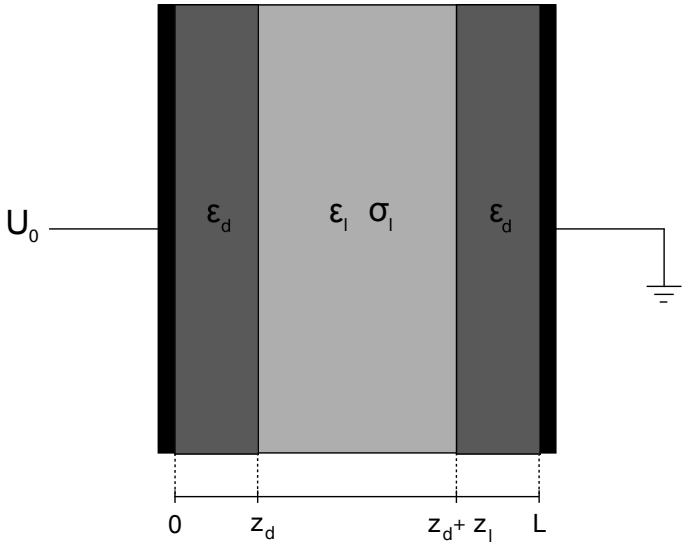

Figure 5.2: A simple parallel plates PEF chamber with dielectric layers.

$$\varphi_2(z,t) = A_2(t)z + B_2(t)$$
$$\varphi_3(z,t) = A_3(t)z + B_3(t) \tag{5.2}$$

where the dielectric layers are described by φ_1 and φ_3, while the liquid by φ_2. The boundary conditions

$$\varphi_1(0,t) = U_0 f(t)$$
$$\varphi_1(z_d,t) = \varphi_2(z_d,t)$$
$$\varphi_2(z_d+z_l,t) = \varphi_3(z_d+z_l,t)$$
$$\varphi_3(L,t) = 0 \tag{5.3}$$

and the equation of continuity allow an analytical solution of the electric field in the liquid

$$E_l(t) = E_0 e^{-\frac{t}{\tau_f}} \tag{5.4}$$

with

$$E_0 = U_0 \left(z_l + 2\frac{\epsilon_l}{\epsilon_d} z_d \right)^{-1} \tag{5.5}$$

and

$$\tau_f = \left(\frac{\epsilon_l}{\epsilon_d} + \frac{z_l}{2z_d} \right) \frac{\epsilon_0 \epsilon_d}{\sigma_l} \tag{5.6}$$

A transient electric field is therefore experienced in the chamber. The intensity E_0 and time constant τ_f depend on the values of the parameters involved, and particularly ϵ_d, the relative permittivity of the ceramic layer. High values of ϵ_d, compared to the relative permittivity of liquid solution, $\epsilon_r = 80$, are required to reach the desired intensity and duration of the transient electric field. The electric field experienced in the dielectric can also be calculated

$$E_d = E_0 \left[\left(\frac{\epsilon_l}{\epsilon_d} + \frac{z_l}{2z_d} \right) \left(1 - e^{-\frac{t}{\tau_f}} \right) + \left(\frac{\epsilon_0}{\epsilon_l} \right) e^{-\frac{t}{\tau_f}} \right] \tag{5.7}$$

Dielectric materials with high relative permittivity in DC current are commonly used to increase the capacitance of electronic components. The most common ones, anyway, like for example Lead Zirconate Titanate (PZT) and Barium Titanate, are highly toxic and thus not suitable for applications in food treatment.

5.2 Non toxic high permittivity materials

A new material, the Sodium Potassium Niobate (KNN) [117, 118], as been recently developed as a non toxic replacement of high permittivity ceramics, with ϵ_r around 1000 and a very high resistivity ($10^8 - 10^9 \Omega m$). This high ρ would force the thickness of a KNN layer to be very small in order to achieve perfect impedance matching to the PFN, thus compromising its duration in time because of the high electric field that would be induced across this layer and because of mechanical frailty. This solution would also be unpractical as very thin layers are extremely difficult and expensive to achieve.

If the thickness of the ceramic, instead, is kept to a reasonable value, the resistance of the chamber would be in principle extremely high, but perfect matching to the generator can still be achieved by simply connecting the chamber in parallel to a power resistor of the desired resistance. In this way the resistance of the treatment chamber is effectively uncoupled to the characteristic impedance of the PFN, and therefore its volume can be chosen arbitrarily. The only dimension of the chamber that has to be taken into account is the distance d between the electrodes, as it determines the electric field in the treatment chamber and also influences the time constant τ_f. But since the matching to the PFN is now reached through a power resistor, pulse transformers can effectively be used to increase the voltages reached between electrodes. To give an example, we can easily set up a 10 L chamber with the parameters in table 5.1, and the resulting electric field in the liquid and in the ceramic layers is reported in fig. 5.3. Clearly the choice of radius R is completely arbitrary, and has been made only to reach

Parameter	Value	Parameter	Value
ϵ_l	80	z_l	4 cm
ϵ_d	1000	z_d	0.25 mm
σ_l	0.2 Sm^{-1}	U_0	130 kV
σ_d	10^{-8} Sm^{-1}	R	28.2 cm

Table 5.1: Parameters of a simple parallel plates chamber. The electrodes are taken to be circular with radius R.

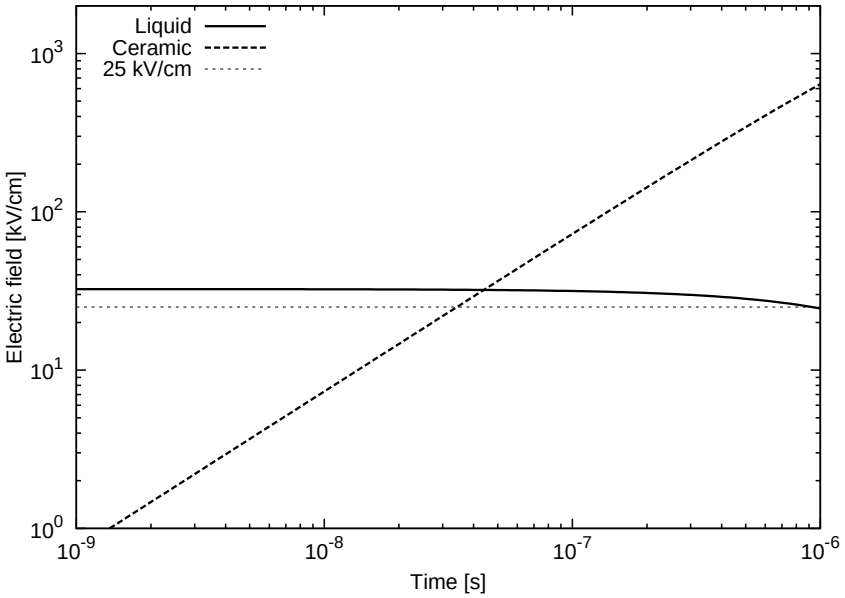

Figure 5.3: Electric field across the liquid and the dielectric layer in a chamber with dimensions in table 5.1.

the 10 L volume. The electric field in the liquid is above 25 kVcm^{-1} for more than 1 μs, thus inactivation should be compatible with the levels reached in our experiments. After 1 μs the electric field experienced in the dielectric is around 600 kVcm^{-1}, a level reported not to affect Sodium Potassium Niobate, although further tests on this subject are required. The presence of this layer of dielectric has also the advantage of improving the duration of the electrodes, often damaged by discharges due to the presence of impurity or air bubbles in the liquid.

Five samples of KNN, circular shape, 1.0 cm diameter, 1.0 mm thickness, have been acquired from Ferroperm Piezoceramics (Kvistgard, DK) in order

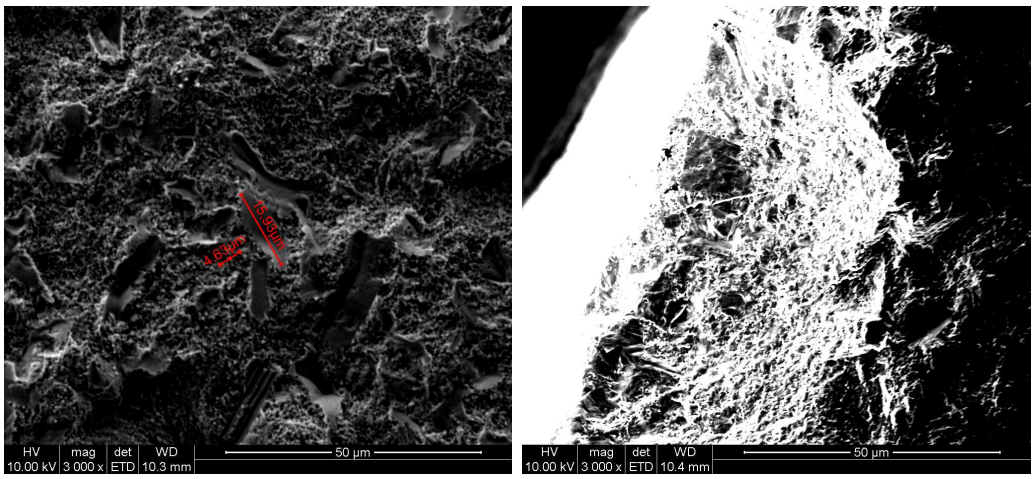

Figure 5.4: SEM images of the surface of a KNN layer.

Parameter	Value	Parameter	Value
ϵ_l	80	z_l	2 mm
ϵ_d	1000	z_d	1 mm
σ_l	5 mSm^{-1}	U_0	7.5 kV
σ_d	10^{-8} Sm^{-1}	R	0.5 cm

Table 5.2: Parameters of the test KNN chamber

to set up a test of this material in PEF treatments. The surface of KNN was studied at the scanning electron microscope, as shown in fig. 5.4. The presence of porosity, with dimensions compatible or larger than bacteria, could represent a possible source of contamination, particularly if the material is used for a long period of time. This will have to be investigated during the tests. Otherwise, from the electrical point of view the surface smoothness seems satisfactory. A test chamber has been set up, as seen in fig. 5.5, by gluing two disks of KNN on the surface of a metallic electrode by means of araldite epoxy resin. The thickness of the layer is 1.0 mm, as manufacturing a thinner layer would be useless for the purpose of a preliminary test. This thickness, anyway, has the advantage of resulting in a lower electric field in the ceramic, reducing the probability of damages to the material.

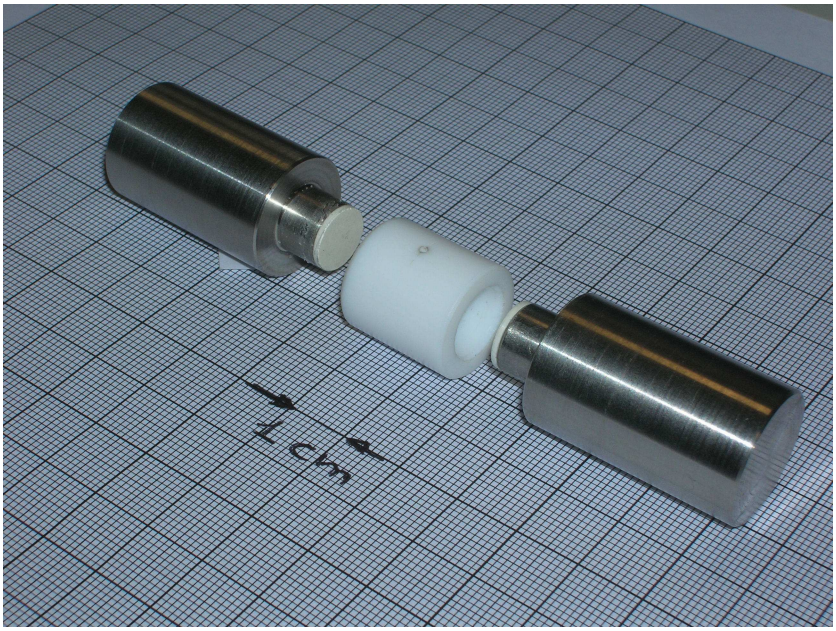

Figure 5.5: The new PEF test cell with KNN ceramic layer.

5.2.1 Estimation of bacterial inactivation

The dimensions and electric parameters of KNN chamber are reported in table 5.2, and in fig. 5.6 the resulting electric fields are plotted. The time constant τ_f is now 1.91 μs. The liquid conductivity has to be taken as low as 5 mSm^{-1} because of the thickness of the dielectrics and the distance between the electrodes, limited by the output of the pulse generator. Although this value is just below the range of drinking water, and it does not represent a particularly eccentric choice of liquid, it has an influence on the membrane charging constants τ_1 and τ_2 discussed in Chapter 3. The value of τ_2, in particular, can be estimated to be around 0.2 - 0.3 μs for average *Escherichia coli* cell, both for the spherical and the cylindrical part. Approximating the cell to a sphere of radius 0.4 μm, the expected inactivation levels in the standard and KNN chamber can be compared. An expression of $U(t)$, the time course of transmembrane potential for a cell subject to an exponential pulse, can be found in [116]. In fig. 5.7 the membrane response to an exponential and a squared pulse is shown. The charging process, therefore, cannot be considered instantaneous in a KNN chamber with respect to the pulse duration. The survival probability has to be computed from eq. 2.38,

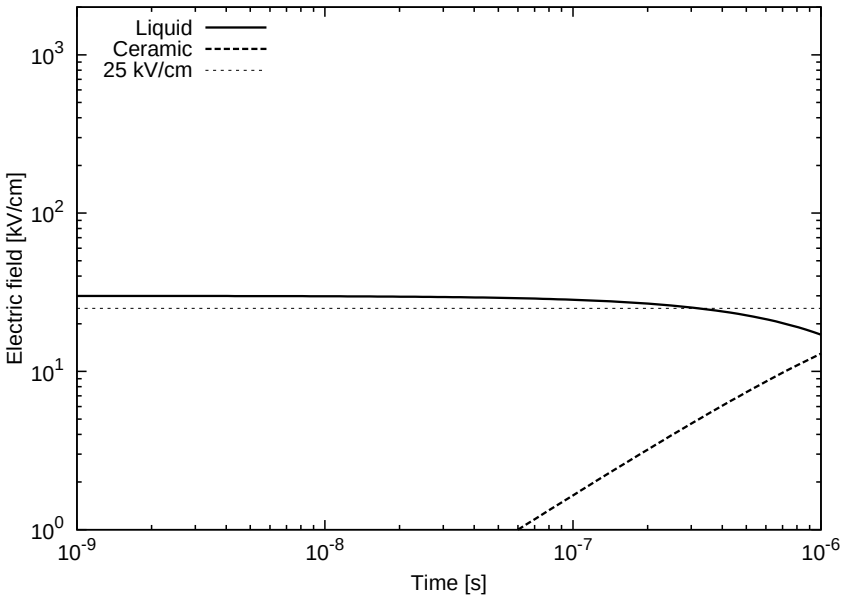

Figure 5.6: Electric field across the liquid and the dielectric layer in the new KNN test chamber.

by integration

$$S(\Delta t) = \exp\left(\frac{\Delta t}{\tau_\infty}\int_0^{\Delta t} e^{-\frac{\Delta F}{1+[\beta U(t)]^2}}\right) \tag{5.8}$$

This integration can be solved by means of a computer simulation both for a constant U, in the case of squared pulse, and for a exponential varying $U(t)$. The ratio between the survival probability in the new KNN chamber S_{KNN} and in the standard chamber S_{ST} is shown in fig 5.8. After 1 μs the survival probability is 28.7 % higher than in a standard chamber, but, even if it is expected that the effectiveness in this configuration will be lower, it should be possible to measure bacterial inactivation by Pulsed Electric Fields in this KNN test chamber.

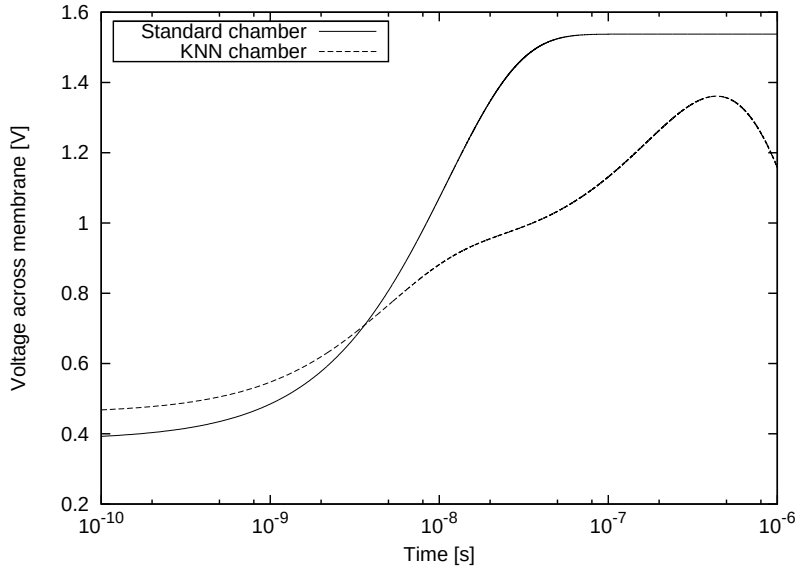

Figure 5.7: Transmembrane voltage for a spherical membrane of radius 0.4 μm in the standard and in the KNN chamber.

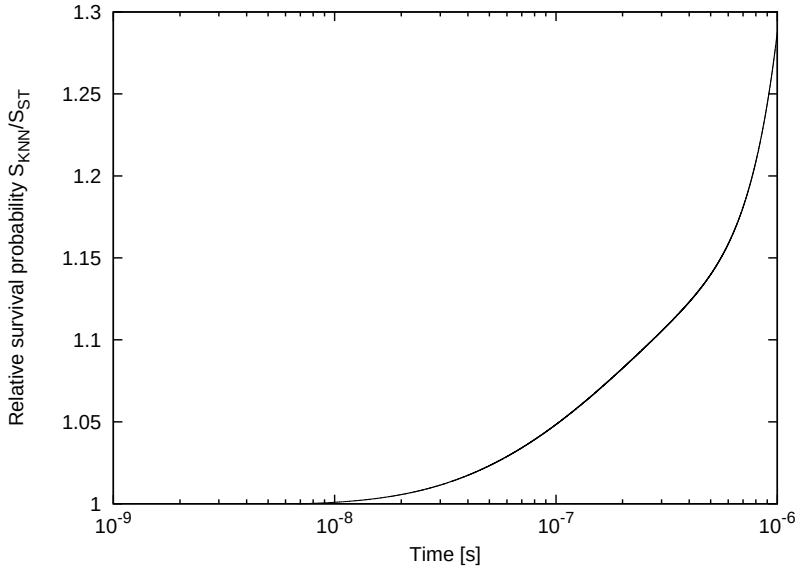

Figure 5.8: Ratio between expected survival probability in KNN and standard chamber as a function of exposure time for a spherical membrane of radius 0.4 μm.

Chapter 6

Conclusions

An extensive investigation on the interaction of Pulsed Electric Fields with cell membranes has been carried out in this thesis. The theoretical models explaining bacterial inactivation were examined and compared, and the most important experimental evidences on this subject described. A theoretical analysis was implemented, taking into account the effects of the different physical parameters involved. The intensity and time course of transmembrane potential for a generic cell shape were related to local membrane curvature and suspension liquid conductivity, and analytical expressions were derived, allowing quantitative evaluation of the expected inactivation levels in any experimental condition. By the use of computer simulations, the apparent saturation of inactivation curves for great amount of pulses delivered was related to edge effects caused by the finite dimensions of electrodes. Experimental measures on *Escherichia coli* qualitatively confirm these results when the number of pulses delivered to the cells is high, while for small numbers the possible interaction of some bacterial protection mechanism reduces the effectiveness of PEF. Investigations on the possible explanation of this mechanism and its influence on PEF applications will be carried out in future research. A model to explain the variability of PEF inactivation results was proposed, and its impact evaluated by means of computer simulations. Although it was not possible, because of the duration of biological measures, to precisely verify the correctness of our assumptions, the model seems to estimate the uncertainties correctly for large amounts of pulses delivered to the treatment chamber, while for small numbers the interaction of other mechanisms, noticed also in previous experiments, increases the spread of results beyond the predictions. The formulation of a valid hypothesis on this bacterial protection mechanism and its inclusion in our simulation is going to be subject of future studies.

Experimental evidence on variations of PEF effectiveness on *Escherichia*

coli over 5 orders of magnitude of initial bacterial concentration was discovered in our tests. A satisfying explanation has yet to be found, and could be related to interactions between the phospholipidic membranes of different cells. This phenomenon could affect the applications of PEF technology in specific areas, depending on the levels of bacterial inactivation required and the typical microorganism population of the liquid substrate involved. Furthermore, this result could be specific for *Escherichia coli* or have a greater or smaller quantitative impact on other microorganisms. For this reason, a careful analysis of the effectiveness of PEF as a function of initial concentration is going to be carried out on other cell species in the future.

An innovative design of PEF treatment chambers has been proposed using high permittivity ceramic materials. The analysis of their application to PEF reveals that they could greatly increase the volumes of chambers while retaining levels of bacterial inactivation comparable to those of standard treatment cells. Furthermore, the use of these materials is believed to greatly reduce the possibility of electric breakdowns, increasing therefore the duration of electrodes. These advantages could be critical to facilitate the wide-scale application of PEF as an alternative to thermal pasteurization. A prototype chamber has been prepared with the use of a non-toxic high permittivity ceramic layer, the Sodium Potassium Niobate, and it is ready to be tested in PEF experiments.

Bibliography

[1] M. T. Madigan and T. D. Brock. Brock biology of microorganisms. *ed. Pearson/Benjamin Cummings*, 2008.

[2] J. E. Dunn and J. S. Pearlman. Methods and apparatus for extending the shelf life of fluid food products. *US Patent 4, 695, 472*, 1987.

[3] B. Qin, U. Pothakamury, H. Vega, O. Martin, G. V. Barbosa-Canovas, and B. Swanson. Food pasteurization using high intensity pulsed electric fields. *Journal of Food Technology*, 49(9):55–60, 1995.

[4] J. Fernandez-Molina, E. Barkstrom, P. Torstensson, G. V. Barbosa-Cnovas, and B. Swanson. Shelf-life extension of raw skim milk by combining heat and pulsed electric fields. *Food Res Int*, 1999.

[5] S. Michalac, V. Alvarez, T. Ji, and Zhang Q. H. Inactivation of selected microorganisms and properties of pulsed electric field processed milk. *Journal of Food Processing Preservation*, 27:137–151, 2003.

[6] H. Hulsheger, J. Pottel, and E. G. Niemann. Electric field effects on bacteria and yeast cells. *Radiat Environ Biophys*, 22:149–162, 1983.

[7] E. E. Oamen, A. P. Hansen, and K. R. Swartzel. Effect of ultrahigh temperature steam injection processing and aseptic storage on labile water-soluble vitamins in milk. *J. Dairy Science*, 72(3):614–619, 1989.

[8] M. L. Calderon-Miranda, G. V. Barbosa-Canovas, and B. G. Swanson. Transmission electron microscopy of listeria innocua treated by pulsed electric elds and nisin in skimmed milk. *International Journal of Food Microbiology*, 51:31–38, 1999.

[9] K. Smith, G. S. Mittal, and M. W. Griffiths. Pasteurization of milk using pulsed electrical field and antimicrobials. *Journal of Food Science*, 67(6):2304–2307, 2002.

[10] V. L. Hughey and E. A. Johnson. Antimicrobial activity of lysozyme against bacteria involved in food spoilage and food-borne disease. *Applied and Environmental Microbiology*, 53:2165–2170, 1987.

[11] I. E. Pol, H. C. Mastwijk, P. V. Bartels, and Smid E. J. Pulsed-electric field treatment enhances the bactericidal action of nisin against bacillus cereus. *Applied and Environmental Microbiology*, 66(1):428–430, 2000.

[12] J. J. Fernandez-Molina, G. V. Barbosa-Canovas, and B. G. Swanson. Pasteurization of skim milk with heat and pulsed electric fields. in: Technical program abstracts. chicago: Institute of food technologist. IFT Annual Meeting, June 2000, Dallas, Tex., U.S.A. 207 p.

[13] H. W. Yeom, G. A. Evrendilek, Z. T. Jin, and Zhang Q. H. Processing of yogurt-based products with pulsed electric fields: microbial, sensory and physical evaluation. *Journal of Food Processing Preservation*, 28:161–178, 2004.

[14] N. Dutreux, S. Notermans, T. Wijtzesa, M. M. Gongora-Nieto, G. V. Barbosa-Canovas, and B. G. Swanson. Pulsed electric fields inactivation of attached and free-living escherichia coli and listeria innocua under several conditions. *International Journal of Food Microbiology*, 54(1-2):91–98, 2000.

[15] G. A. Evrendilek and Q. H. Zhang. Effects of pulse polarity and pulse delaying time on pulsed electric fields-induced pasteurization on escherichia coli. *Journal of Food Engineering*, 68:271–276, 2005.

[16] N. Dutreux, S. Notermans, and M. M. Gongora-Nieto B. G. Swanson. Effects of combined exposure of micrococcus luteus to nisin and pulsed electric fields. *International Journal of Food Microbiology*, 60:147–162, 2000.

[17] I. Sensoy, Q. H. Zhang, and S. K. Sastry. Inactivation kinetics of salmonella dublin by pulsed electric field. *Journal of Food Process Engineering*, 20:367–381, 1997.

[18] S. Michalac. Inactivation of selected microorganisms and properties of pulsed electric field processed milk. *Journal of Food Processing and Preservation*, 27:137–151, 2003.

[19] M. L. Calderon-Miranda, G. V. Barbosa-Canovas, and B. G. Swanson. Transmission electron microscopy of listeria innocua treated by pulsed

electric fields and nisin skimmed milk. *International Journal of Food Microbiology*, 51:31–38, 1999.

[20] M. Amiali, M. O. Ngadi, J. P. Smith, and V. G. S. Raghavan. Inactivation of salmonella enteritidis in liquid egg products using pulsed electric field (pef). *CSAE/SCGR 2005 Meeting Winnipeg, Manitoba*, 2005.

[21] L. D. Reina, Z. T. Jin, A. E. Youcef, and Q. H. Zhang. Inactivation of listeria monocytogenes in milk by pulsed electric fields. *Journal of Food Protection*, 61(9):1203–1206, 1998.

[22] G. J. Fleischman, S. Ravishankar, and V. M. Balasubramaniam. The inactivation of listeria monocytogenes by pulsed electric field (pef) treatment in static chamber. *Food Microbiology*, 21:91–95, 2004.

[23] B. L. Qin, G. V. Barbosa-Canovas, B. G. Swanson, and P. D. Pedrow. Inactivating microorganisms using a pulsed electric field continuous treatment system. *IEEE Transaction Industrial Application*, 34(1):43–49, 1998.

[24] G. A. Evrendilek, W. R. Dantzer, C. B. Streaker, P. Ratanatriwong, and Q. H. Zhang. Shelf life evaluation of liquid foods treated by pilot plant pulsed electric field system. *Journal of Food Processing and Preservation*, 25:283–297, 2001.

[25] K. Smith, G. S. Mittal, and M. W. Griffiths. Pasteurization of milk using pulsed electrical field and antimicrobials. *Food Microbiology and Safety*, 67(6):2304–2308, 2002.

[26] C. S. Chen, P. E. Shaw, and M. E. Parish. Orange and tangerine juices. *Fruit juice processing technology. Ed. Agscience. Auburndale, FL*, pages 110–165, 1993.

[27] R. J. Braddock. Single strength orange juices and concentrate. *in Handbook of Citrus By-products and Processing Technologies. Ed. Wiley, New York.*, pages 53–83, 1999.

[28] B. Sen Gupta, F. Masterson, and T. R. A. Magee. Inactivation of e. coli k12 in apple juice by high voltage pulsed electric field. *Eur Food Res Technol*, 217:434437, 2003.

[29] B. L. Qin, G. V. Barbosa-Canovas, B. G. Swanson, and P. D. Pedrow. Inactivation of microorganisms by pulsed electric field of different voltage waveforms. *IEEE Transactions on Dielectrics and Electrical Insulation*, 1(6):1047–1057, 1994.

[30] H. W. Yeom, C. B. Streaker, Q. H. Zhang, and D. B. Min. Effects of pulsed electric fields on the quality of orange juice and comparison with heat pasteurization. *Journal of Agricultural and Food Chemistry*, 48:4597–4605, 2000.

[31] V. Heinz, S. Toepfl, and D. Knorr. Impact of temperature on lethality and energy efficiency of apple juice pasteurization by pulsed electric fields treatment. *Innovative Food Science and Emerging Technologies*, 4:167–175, 2003.

[32] M. V. Simpson, G. V. Barbosa-Canovas, and B. G. Swanson. The combined inhibitory effect of lysozyme and high voltage pulsed electric fields on the growth of bacillus subtilis spores. *IFT Annual Meeting: Book of Abstracts*, 267, 1995.

[33] C. J. McDonald, S. W. Lloyd, M. A. Vitale, K. Petersson, and E. Innings. Effects of pulsed electric fields on microorganisms in orange juice using electric field strengths of 30 and 50 kv cm-1. *Journal of Food Science*, 65(6):984–989, 2000.

[34] M. V. Selma, P. S. Fernandez, M. Valero, and M. C. Salmeron. Control of enterobacter aerogenes by high-intensity, pulsed electric fields in horchata, a spanish low-acid vegetable beverage. *Food Microbiology*, 20:105–110, 2003.

[35] D. Rodrigo, G. V. Barbosa-Canovas, A. Martinez, and M. Rodrigo. Weibull distribution function based on empirical mathematical model for inactivation of escherichia coli by pulsed electric fields. *Journal of Food Protection*, 66(6):1007–1012, 2003.

[36] B. S. Gupta, F. Masterson, and T. R. A. Magee. Inactivation of escherichia coli k12 in apple juice by high voltage pulsed electric field. *European Food Research and Technology*, 217:434–437, 2003.

[37] J. Iu, G. S. Mittal, and M. W. Griffiths. Reduction in levels of escherichia coli o157:h7 in apple cider by pulsed electric fields. *Journal of Food Protection*, 64(7):964–969, 2001.

[38] G. A. Evrendilek, Q. H. Zhang, and E. R. Richter. Inactivation of escherichia coli o157:h7 and escherichia coli 8739 in apple juice by pulsed electric fields. *Journal of Food Processing*, 62(7):793–796, 1999.

[39] M. V. Selma, M. C. Salmeron, M. Valero, and P. S. Fernandez. Control of lactobacillus plantarum and escherichia coli by pulsed electric fields in mrs broth, nutrient broth and orange-carrot juice. *Food Microbiology*, 21:519–525, 2004.

[40] Zs. Cserhalmi, I. Vidacs, J. Beczner, and B. Czukor. Inactivation of saccharomyces cerevisea and bacillus cereus by pulsed electric fields technology. *Innovative Food Science and Emerging Technologies*, 3:41–45, 2002.

[41] J. Raso, M. L. Calderon, M. M. Gongora-Nieto, and G. V. Barbosa-Canovas. Inactivation of zygosaccharomyces bailii in fruit juices by heat, hydrostatic pressure and pulsed electric fields. *Journal of Food Science*, 63(6):1042–1044, 1998.

[42] C. Poppe. Epidemiology of salmonella enterica serovar enteritidis. *in Salmonella enterica Serovar Enteritidis in Humans and Animals, Epidemiology, Pathogenesis, and Control*, Iowa State University Press, Ames, Iowa:3–19.

[43] N. Hermawan, G. A. Evrendilek, W. R. Dantzer, Q. H. Zhang, and E. R. Ritcher. Pulsed electric field treatment of liquid whole egg inoculated with salmonella enteritidis. *Journal of Food Safety*, 24:71–85, 2004.

[44] O. Martin-Belloso, H. Vega-Mercado, B. L. Qin, F. J. Chang, G. V. Barbosa-Canovas, and B. G. Swanson. Inactivation of escherichia coli suspended in liquid egg using pulsed electric fields. *Journal of Food Processing and Preservation*, 21:193–208, 1997.

[45] M. L. Calderon-Miranda, G. V. Barbosa-Canovas, B. G. Swanson, and F. J. Chang. Inactivation of listeria innocua in liquid whole egg by pulsed electric elds and nisin. *International Journal of Food Microbiology*, 51:7–17, 1999.

[46] R. Jeantet, F. Baron, F. Nau, M. Roignant, and G. Brulé. High intensity pulsed electric fields applied to egg white: Effect on salmonella enteritidis inactivation and protein denaturation. *Journal of Food Protection*, 62(12):1381–1386, 1999.

[47] O. Martin-Belloso, H. Vega-Mercado, B. L. Qin, F. J. Chang, G. V. Barbosa-Canovas, and B. G. Swanson. Inactivation of escherichia coli suspended in liquid egg using pulsed electric fields. *Journal of Food Processing and Preservation*, 21:193–208, 1997.

[48] M. I. Bazhal, M. O. Ngadi, J. P. Smith, and V. G. S. Raghavan. Kinetics of escherichia coli in liquid whole egg using combined pef and thermal treatments. *Lebensmittel-Wissenschaft und Technologie*, 2005.

[49] G. A. Hermawan, W. R. Evrendilek, Q. H. Zhang, and E. R. Richter. Pulsed electric field treatment of liquid whole egg inoculated with salmonella enteritidis. *Journal of Food Safety*, 24:1–85, 2004.

[50] M. L. Calderon-Miranda, G. V. Barbosa-Canovas, and B. G. Swanson. Inactivation of listeria innocua in liquid whole egg by pulsed electric fields and nisin. *International Journal of Food Microbiology*, 51:7–17, 1999.

[51] J. Mankovski and M. Kritiansen. A review of short pulse generator technology. *IEEE Transaction on Plasma Science*, 8(1):102–108, 2000.

[52] M. Kristiansen A. Guenther and T. Martin (Editors). Opening switches. *Plenum Press, New York*, 1987.

[53] I. Vitkovsky. High power switching. *Van Nostrand Reinhold Press, New York, Chapter 2*, 1989.

[54] S. Ravishankar, H. Zhang, and M. L. Kempes. Pulsed electric fields. *Food Science and Technology International*, 14(5):429–432, 2008.

[55] R. Stampfli. Reversible electrical breakdown of the excitable membrane of a ranvier node. *Am. Acad. Brasil. Ciens.*, pages 57–63, 1958.

[56] A. J. Sale and W. A. Hamilton. Effects of high electric fields on microorganisms: I. killing of bacteria and yeasts. *Biochimica et Biophysica Acta*, 148:781–788, 1967.

[57] H. P. Schwan. Electrical properties of tissue and cell suspensions. *In: J. H. Lawrence, A. Tobias (Eds.), Advances in biological and medical physics, Academic Press, New York*, 5:147–209, 1957.

[58] A. Parsegian. Energy of an ion crossing a low dielectric membrane: solutions to four relevant electrostatic problems. *Nature*, 221:844–846, March 1969.

[59] A. Parsegian. Ion-membrane interactions as structural forces. *Ann. N. Y. Acad. Sci.*, 264:161–174, 1975.

[60] A. Finkelstein. Discussion paper. *Ann. N. Y. Acad. Sci.*, 264:244–245, 1975.

[61] D. G. Levitt. Electrostatic calculations for an ion channel. *Biophys. J.*, 22:209–219, 1978.

[62] I. G. Abidor, L. V. Arakelyan, L. V. Chernomordik, Yu. A. Chizmadzhev, V. F. Pastushenko, and M. R. Tarasevich. Electric breakdown of bilayer membranes: The main experimental facts and their qualitative discussion. *Bioelectrochem. Bioenerg.*, 6:37–52, 1979.

[63] D. Wobshall. Voltage dependence of bilayer membrane capacitance. *J. Colloid. Interface. Sci.*, 40:417–423, 1972.

[64] R. Benz and K. Janko. Voltage-induced capacitance relaxation of lipid bilayer membranes. effects of membrane composition. *Biochim. Biophys. Acta*, 455:721–725, 1976.

[65] A. V. Babakov and L. N. Ermishkin. Influence of electric field on the capacity of phospholipid membranes. *Nature*, 210:953–955, 1966.

[66] O. Alvarez and R. Latorre. Voltage-dependent capacitance in lipid bilayers made from monolayers. *Biophys. J.*, 21:1–17, 1978.

[67] M. Montal and P. Mueller. Formation of biomolecular membranes from lipid monolayers and a study of their electrical properties. *Proc. Nat. Acad. Sci. USA*, 69:3561–3566, 1972.

[68] J. M. Crowley. Electrical breakdown of biomolecular lipid membranes as an electromechanical instability. *Biophysical Journal*, 13:711–724, 1973.

[69] G. I. Taylor and D. H. Michael. On making holes in a sheet of fluid. *J. Fluid. Mech.*, 58:625–639, 1973.

[70] B. V. Deryagin and A. V. Prokhorov. On the theory of the rupture of black films. *J. Colloid. Interface Sci.*, 81:108–115, 1981.

[71] R. Becker and W. Doring. Kinetic treatment of grain-formation in super-saturated vapors. *Ann. Physik.*, 24:719–725, 1935.

[72] H. V. Kramers. Brownian motion in a field of force and the diffusion model of chemical reactions. *Physica*, 7:284–302, 1940.

[73] J. B. Zeldovich. To the theory of new phase formation. cavitation. *J. Exp. Theor. Phys.*, 12:53–62, 1942.

[74] B. V. Deryagin and Yu. V. Gutop. Theory of the breakdown (rupture) of free films. *Kolloidn Zh.*, 24:370–374, 1962.

[75] J. D. Litster. Stability of lipid bilayers and red blood cell membranes. *Phys. Lett.*, 53A:193–194, 1975.

[76] C. Taupin, M. Dvolaitzky, and C. Sauterey. Osmotic pressure induced pores in phospholipid visicles. *Biochem.*, 14:4771–4775, 1975.

[77] J. C. Weaver and Yu. A. Chizmadzhev. Theory of electroporation: A review. *Bioelectrochemistry and Bioenergetics*, 41:135–160, 1996.

[78] J. C. Weaver and R. A. Mintzer. Decreased bilayer stability due to transmembrane potentials. *Phys. Lett A*, 86:57–59, 1981.

[79] J. S. Langer and J. D. Reppy. Progress in low temperature physics. *ed. G. J. Gorter (North Holland)*, Vol. 6:p. 1, 1970.

[80] R. W. Glaser, S. L. Leikin, L. V. Chernomordik, V. F. Pastushenko, and A. I. Soriko. Reversible electrical breakdown of lipid bilayers: formation and evolution of pores. *Biochimica et Biophysica Acta*, 940:275–287, 1988.

[81] A. G. Petrov, M. D. Mitov, and A. I. Derzhnansky. Advances in liquid crystal research and applications. *Oxford/Budapest*, pages 695–737, 1980.

[82] J. N. Israelachvili and R. M. Pashley. Measurement of the hydrophobic interaction between two hydrophobic surfaces in aqueous electrolyte solutions. *J. Coll. Interface Sci.*, 98:500–514, 1984.

[83] S. Marcelja. Structural contribution to solute-solute interaction. *Croat. Chem. Acta*, 49:348–357, 1977.

[84] R. P. Rand. Interacting phospholipid bilayers: Measured forces and induced structural changes. *Annu. Rev. Biophys. Bioeng.*, 10:277–314, 1981.

[85] S. E. Feller and R. W. Pastor. Effect of electrostatic force truncation on interfacial and transport properties of water. *Journal of Physical Chemistry*, 100:17011–17020, 1996.

[86] S. I. Sukharev, P. Blount, B. Martinac, F. R. Blattner, and C. Kung. A large-conductance mechanosensitive channel in e. coli encoded by mscl alone. *Nature*, 368:265–268, 1994.

[87] T. Benachir and M. Lafleur. Osmotic and ph transmembrane gradients control the lytic power of melittin. *Biophys. J.*, 70:831–840, 1996.

[88] S. R. James, R. A. Demel, and C. P. Downes. Interfacial hydrolysis of phosphatidylinositol 4-phosphate a-nd phosphatidylinositol 4,5-bisphosphate by turkey erythrocyte phospholipase c. *Biochem. J.*, 298:499–506, 1994.

[89] H. Isambert. Understanding the electroporation of cells and artificial bilayer membranes. *Phys. Rev. Lett.*, 780:3404–3407, 1998.

[90] R. P. Joshi, Q. Hu, Schoenbach K. H., and H. P. Hjalmarson. Improved energy model for membrane electroporation in biological cells subjected to electrical pulses. *Physical Review E*, 65, 041920:1–7, 2002.

[91] J. Israelachvili. Intermolecular and surface forces. *2nd ed. (Academic, London, 1992).*

[92] J. C. Neu and W. Krassowska. Asymptotic model of electroporation. *Phys. Rev. E*, 59:3471–3482, 1999.

[93] V. F. Pastushenko and Yu. A. Chhizmadzhev. *Biofizika*, 28:1036, 1983.

[94] A. Barnett and J. C. Weaver. Electroporation: a unified, quantitative theory of reversible electrical breakdown and mechanical rupture in artificial planar bilayer membranes. *Bioelectrochem. Bioenerg.*, 25:163–182, 1991.

[95] E. M. Renkin. Filtrion, diffusion, and molecular sieving through porous cellulose membranes. *The Journal of General Physiology*, 38:225–243, 1954.

[96] S. I. Sukharev, V. B. Arakelyan, I. G. Abidor, L. V. Chernomordik, and V. F. Pastushenko. Rupture of planar blm under influence of electric field. *Biophysica*, 28:756–760, 1983.

[97] K. T. Powell and J. C. Weaver. Transient acqueous pores in bilayer membranes: a statistical theory. *Bioelectrochem. Bioenerg.*, 15:221–227, 1986.

[98] R.E. Bruhn, P.D. Pedrow, R.G. Olsen, G.V. Barbosa-Canovas, and B.G. Swanson. Electrical environment surrounding microbes exposed to pulsed electric fields. *Dielectrics and Electrical Insulation, IEEE Transactions on*, 4(6):806–812, Dec 1997.

[99] Tadej Kotnik, Damijan Miklavcic, and Tomaz Slivnik. Time course of transmembrane voltage induced by time-varying electric fields–a method for theoretical analysis and its application. *Bioelectrochemistry and Bioenergetics*, 45(1):3 – 16, 1998.

[100] M. Hibino, H. Itoh, and K. Kinosita Jr. Time courses of cell electroporation as revealed by submicrosecond imaging of transmembrane potential. *Biophysical Journal*, 64(6):1789 – 1800, 1993.

[101] W. Krassowska and P. D. Filev. Modelling electroporation in a single cell. *Biophysical Journal*, 92(2):404–417, 2007.

[102] M. Winterhalter and W. Helfrich. Effect of voltage on pore membranes. *Physical Review A*, 36(12):5874–5876, 1987.

[103] C. Wilhelm, M. Winterhalter, U. Zimmermann, and R. Benz. Kinetics of pore size during irreversible electrical breakdown of lipid bilayer membranes. *Biophysical Journal*, 64(1):121 – 128, 1993.

[104] I. V Timoshkin. Private comunication.

[105] T.B. Jones. Dielectrophoretic force calculation. *Journal of Electrostatics*, 6(1):69 – 82, 1979.

[106] P. M. Morse and H. Feshbach. Methods of theoretical physics, part i. *McGraw-Hill, New York*, pages 656 – 666, 1953.

[107] Tadej Kotnik and Damijan Miklavcic. Analytical description of transmembrane voltage induced by electric fields on spheroidal cells. *Biophysical Journal*, 79(2):670 – 679, 2000.

[108] G. Bryant and J. Wolfe. Electromechanical stresses produced in the plasma membranes of suspended cells by applied electric fields. *Journal of Membrane Biology*, 96:129–139, 1987.

[109] J. Wolfe, M. F. Dowgert, and P. L. Steponkus. Mechanical study of the deformation and rupture of the plasma membranes of protoplasts during osmotic expansions. *Journal of Membrane Biology*, 93:63–74, 1986.

[110] O. Pierucci. Dimensions of escherichia coli at various growth rates: model for envelope growth. *Journal of bacteriology*, 135:559–574, 1978.

[111] G. Cebrin, N. Sagarzazu, R. Pagn, S. Condn, and P. Maas. Heat and pulsed electric field resistance of pigmented and non-pigmented enterotoxigenic strains of staphylococcus aureus in exponential and stationary phase of growth. *International Journal of Food Microbiology*, 118(3):304 – 311, 2007.

[112] S. Perni, P. R. Chalise, G. Shama, and M. G. Kong. Bacterial cells exposed to nanoseconds pulsed electric fields show lethal and sublethal effects. *International Journal of Food Microbiology*, 120:311–314, 2007.

[113] G. V. Barborsa-Canovas, M. M. Gongora-Nieto, V. R. Pothakamury, and B. G. Swanson. Preservation of food with pulsed electric fields. *London: Academic Press*, 1999.

[114] P. Molinari, A. M. R. Pilosof, and R. J. Jagus. Effect of growth phase and inoculum size on the inactivation of saccharomyces cerevisiae in fruit juices, by pulsed electric fields. *Food Research International*, 37(8):793 – 798, 2004.

[115] U. Zimmermann. Electric field-mediated fusion and related electrical phenomena. *Biochimica et Biophysica Acta, 694 (1982) 2 2 7 - 2 7 7*, 694:227 – 277, 1982.

[116] I. V. Timoshkin, S. J. MacGregor, R. A. Fouracre, B. H. Crichton, and J. G. Anderson. Transient electrical field across cellular membranes: pulsed electric fields treatment of microbial cells. *J. Phys. D: Appl. Phys.*, 39:596–603, 2006.

[117] G. Feuillard et al. *2003 IEEE Symposium on Ultrasonics*, 2:1995–1998, 2003.

[118] S. Lanfredi M. A. L. Nobre. *Catalysis Today*, 78:529538, 2003.

Acknowledgments

I would like to express my gratitude to my tutor, Professor Marco Paganoni, for the invaluable advice, support and enthusiasm shown during my doctorate work.

My sincere thanks also go to Professor Giuseppe Dellacasa and Professor Elisabetta Carraro for giving me the opportunity to carry out the experimental research activity in the laboratories of the Department of Science and Advanced Technology and of the Department of Environmental and Life Science at the University of Piemonte Orientale in Alessandria. I am also grateful to Dr. Silvia Bonetta, Dr. Francesca Motta, Dr. Roberto Gemme and Dr. Pietro Cortese for their collaboration.

I am indebted to Professor Scott J. MacGregor and Professor John G. Anderson of the Strathclyde University of Glasgow for the time I spent in ROLEST laboratory. I would also like to thank Dr. Joseph Beveridge, Dr. Igor Timoshkin and all the ROLEST staff.

A special acknowledgment goes to my family for all the understanding and support they provided me through the course of my studies. Finally, I would like to thank Francesca for being at my side during these three years of doctorate work.